

EQUATIONS AND CHARTS
FOR THE EVALUATION OF THE
HYPERSONIC AERODYNAMIC CHARACTERISTICS
OF LIFTING CONFIGURATIONS
BY THE NEWTONIAN THEORY

By

E. L. Clark and L. L. Trimmer
von Kármán Gas Dynamics Facility
ARO, Inc.
a subsidiary of Sverdrup and Parcel, Inc.

March 1964

ARO Project No. VT8002

FOREWORD

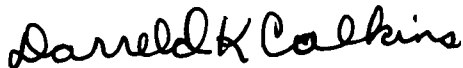
The authors wish to express their appreciation to Mrs. P. Trenchi for her help with the preparation of this report.

ABSTRACT

The pressure distribution predicted by the modified Newtonian theory is used to develop equations for the aerodynamic forces, moments, and stability derivatives for components of hypersonic lifting configurations. In conjunction with the equations, a set of charts is presented to enable simple determination of the aerodynamic characteristics of swept cylinders, swept wedges, spherical segments, and cone frustums at zero sideslip and angles of attack from 0 to 180 deg. This method allows evaluation of most delta wing-body combinations without the need for numerical or graphical integration. As an example of the procedure, the theoretical characteristics of a blunt, 75-deg swept delta wing are calculated and compared with experimental results.

PUBLICATION REVIEW

This report has been reviewed and publication is approved.



Darreld K. Calkins
Major, USAF
AF Representative, VKF
DCS/Test



Jean A. Jack
Colonel, USAF
DCS/Test

CONTENTS

| | <u>Page</u> |
|---|-------------|
| ABSTRACT | v |
| NOMENCLATURE | ix |
| 1.0 INTRODUCTION | 1 |
| 2.0 DEVELOPMENT OF EQUATIONS | |
| 2.1 Delta-Wing Components | 5 |
| 2.2 Body Components | 22 |
| 2.3 Composite Configurations | 35 |
| REFERENCES | 36 |
| APPENDIX - Application of Method to a Typical Delta Wing | 39 |

ILLUSTRATIONS

Figure

| | |
|---|----|
| 1. Axis and Coefficient Nomenclature | 41 |
| 2. Aerodynamic Characteristics of Spherical-Wedge Noses | |
| a. Normal Force | 42 |
| b. Axial Force | 43 |
| c. Side-Force Derivative, $\beta = 0$ | 44 |
| 3. Aerodynamic Characteristics of Flat-Topped Spherical-Wedge Noses | |
| a. Normal Force | 45 |
| b. Axial Force | 46 |
| c. Side-Force Derivative, $\beta = 0$ | 47 |
| 4. Aerodynamic Characteristics of Swept-Cylinder Leading Edges ($\phi' = \pi/2$) | |
| a. Normal Force | 48 |
| b. Axial Force | 49 |
| c. Side-Force Derivative, $\beta = 0$ | 50 |
| d. Rolling-Moment Derivative, $\beta = 0$ | 51 |
| 5. Aerodynamic Characteristics of Flat-Topped Swept-Cylinder Leading Edges ($\phi' = \pi/2$) | |
| a. Normal Force | 52 |
| b. Axial Force | 53 |
| c. Side-Force Derivative, $\beta = 0$ | 54 |
| d. Rolling-Moment Derivative, $\beta = 0$ | 55 |

AEDC-TDR-64-25

| <u>Figure</u> | <u>Page</u> |
|---|-------------|
| 6. Aerodynamic Characteristics of Spherical Segments | |
| a. Normal Force, $\delta = 0$ to 45 deg | 56 |
| b. Normal Force, $\delta = 45$ to 70 deg | 57 |
| c. Axial Force | 58 |
| d. Side-Force Derivative ($\beta = 0$), $\delta = 0$ to 45 deg | 59 |
| e. Side-Force Derivative ($\beta = 0$), $\delta = 45$ to 70 deg | 60 |
| 7. Aerodynamic Characteristics of Flat-Topped Spherical Segments | |
| a. Normal Force, $\delta = 0$ to 45 deg | 61 |
| b. Normal Force, $\delta = 45$ to 70 deg | 62 |
| c. Axial Force | 63 |
| d. Side-Force Derivative ($\beta = 0$), $\delta = 0$ to 45 deg | 64 |
| e. Side-Force Derivative ($\beta = 0$), $\delta = 45$ to 70 deg | 65 |
| 8. Aerodynamic Characteristics of Cone Frustums | |
| a. Normal Force | 66 |
| b. Axial Force, $\delta = 5$ to 25 deg | 67 |
| c. Axial Force, $\delta = 25$ to 40 deg | 68 |
| d. Side-Force Derivative, $\beta = 0$ | 69 |
| 9. Aerodynamic Characteristics of Flat-Topped Cone Frustums | |
| a. Normal Force | 70 |
| b. Axial Force | 71 |
| c. Side-Force Derivative, $\beta = 0$ | 72 |
| 10. Details of 75-deg Swept Delta Wing. | 73 |
| 11. Aerodynamic Characteristics of a 75-deg Delta Wing | |
| a. Normal Force | 74 |
| b. Axial Force | 75 |
| c. Pitching Moment, Referenced to $0.6 L_D$ | 76 |
| d. Lift | 77 |
| e. Drag | 78 |
| f. Lift-to-Drag Ratio | 79 |
| g. Side-Force Derivative, $\beta = 0$ | 80 |
| h. Yawing-Moment Derivative, $\beta = 0$, Referenced to $0.6 L_D$ | 81 |
| i. Rolling-Moment Derivative, $\beta = 0$ | 82 |

NOMENCLATURE

| | |
|-----------------------------|--|
| A | Body surface area |
| A_b | Base area of swept-wedge wing half |
| A_p | Planform area of swept-wedge wing half |
| A_s | Side area of swept-wedge wing half |
| b | Half-span of swept-wedge wing |
| C_A | Axial-force coefficient, $F_A/q_\infty S$ |
| C_D | Drag coefficient, $\text{drag}/q_\infty S$ |
| C_L | Lift coefficient, $\text{lift}/q_\infty S$ |
| C_ℓ | Rolling-moment coefficient, $M_x/q_\infty S \ell$ |
| $C_\ell\beta$ | Rolling-moment coefficient derivative, $\partial C_\ell/\partial \beta$ at $\beta = 0$, 1/radian |
| C_m | Pitching-moment coefficient, $M_Y/q_\infty S \ell$ |
| C_N | Normal-force coefficient, $F_N/q_\infty S$ |
| C_n | Yawing-moment coefficient, $M_Z/q_\infty S \ell$ |
| $C_n\beta$ | Yawing-moment coefficient derivative, $\partial C_n/\partial \beta$ at $\beta = 0$, 1/radian |
| C_p | Pressure coefficient, $(p - p_\infty)/q_\infty$ |
| $C_{p_{\max}}$ | Pressure coefficient at stagnation point |
| $C_{p_{\text{nose}}}$ | Pressure coefficient at nose of pointed body |
| C_Y | Side-force coefficient, $F_Y/q_\infty S$ |
| $C_Y\beta$ | Side-force coefficient derivative, $\partial C_Y/\partial \beta$ at $\beta = 0$, 1/radian |
| c | Chord of swept-wedge wing |
| F | Function defining body surface |
| F_A | Axial force |
| F_N | Normal force |
| F_Y | Side force |
| h | Vertical displacement of swept-wedge wing half from wing centerline |
| $\bar{i}, \bar{j}, \bar{k}$ | Unit vectors directed along the X-, Y-, and Z- axes, respectively |

AEDC-TDR-64-25

| | |
|--------------------------|--|
| K | Proportionality constant used in the modified Newtonian theory |
| L | Body length |
| L_D | Delta-wing length, measured from theoretical apex |
| L/D | Lift-to-drag ratio |
| ℓ | Moment coefficient reference length |
| M_X | Rolling moment |
| M_Y | Pitching moment |
| M_Z | Yawing moment |
| M_∞ | Free-stream Mach number |
| $(n, x), (n, y), (n, z)$ | Angles between unit normal vector, \bar{n} , and the positive X-, Y-, and Z-axes, respectively |
| \bar{n} | Inward directed unit vector normal to the body surface |
| p | Surface static pressure |
| P_{t_2} | Stagnation pressure behind normal shock |
| p_∞ | Free-stream static pressure |
| q_∞ | Free-stream dynamic pressure |
| R | Radius of curvature |
| R_b | Base radius of cone frustum |
| R_n | Nose radius of cone frustum |
| r | Local body radius on cone frustum |
| S | Reference area |
| t | Thickness of swept-wedge wing half |
| V_∞ | Free-stream velocity |
| X, Y, Z | Orthogonal body axes |
| X_T, Z_T | Moment transfer lengths |
| x, y, z | Coordinates along X-, Y-, and Z - axes |
| α | Angle of attack |
| α_0 | Angle of attack where $\phi_0 = -\phi'$ on swept-cylinder leading edge |
| α' | Angle between body X- axis and free-stream velocity vector |

| | |
|------------------------|--|
| β | Angle of sideslip |
| Γ | Dihedral angle of swept-wedge wing |
| γ | Ratio of specific heats and wedge angle normal to leading edge of swept-wedge wing |
| δ | Half-angle of cone frustum and base tangent angle of spherical segment |
| δ_{nose} | Nose half-angle of pointed body |
| ϵ | Centerline angle of swept-wedge wing measured in X, Z- plane |
| η | Angle between surface unit inner normal vector and free-stream velocity vector |
| θ | Angular coordinate which defines cross-sectional planes |
| θ_b | Angle defining base location of spherical segment |
| Λ | Sweepback angle and base angle of spherical wedge |
| ξ | Cone frustum bluntness ratio, R_n/R_b |
| Φ | Angle of body roll measured in Y, Z- plane |
| ϕ | Angular coordinate which defines circumferential position in a cross-sectional plane |
| ϕ_o | Angle defining circumferential position where surface becomes shielded from the flow |
| ϕ' | Angle defining circumferential extent of swept-cylinder leading edge |

SUBSCRIPTS

| | |
|---|--------------------------------|
| L | Lower half of swept-wedge wing |
| U | Upper half of swept-wedge wing |

1.0 INTRODUCTION

In the design and testing of lifting re-entry configurations, there is often the need for a simple, approximate method of predicting the pressures and forces acting on the vehicle at hypersonic speeds. The Newtonian theory has proven very useful for this purpose. A number of studies have shown the accuracy of this simple theory in predicting the pressures and forces on such configurations as sharp and blunted cones (Refs. 1 through 5), circular cylinders (Refs. 6 and 7), hemispheres (Ref. 7), and delta wings (Ref. 8). Although the Newtonian theory is easily applied to the calculation of pressure distribution, integration of the pressure over the body surface to obtain total forces and moments can be difficult and time consuming. Hence, the theory is not always used to full advantage. Design charts which simplify the evaluation of body loads have been developed for complete and partial bodies of revolution (Refs. 5 and 9 through 13), elliptic cones (Refs. 5, 14, and 15), delta-wing components (Ref. 13), and three-dimensional bodies (Ref. 16). The charts of Refs. 5, 9, 11, 13, 14, and 15 provide total loads and derivatives for selected bodies, while the methods of Refs. 10, 12, and 16 apply to arbitrary bodies but require numerical or graphical integration.

The purpose of the present report is to extend the scope of the previous design charts by providing additional aerodynamic characteristics and an increased angle-of-attack range. To avoid a requirement of numerical integration, only selected configurations consisting of typical delta-wing and body components are considered. Equations are derived for the pressure distribution on each component, and this distribution is then integrated over the surface area in closed form to obtain total forces and moments. Equations and charts are given for the longitudinal stability and performance coefficients (C_N , C_A , C_m) and the directional and lateral stability derivatives ($C_{Y\beta}$, $C_{n\beta}$, $C_{l\beta}$) for an angle-of-attack range of 0 to 180 deg at zero sideslip.

An example of the use of the charts is given in the appendix, where the aerodynamic characteristics of a blunt, 75-deg swept delta wing are computed and compared with experimental results.

2.0 DEVELOPMENT OF EQUATIONS

The Newtonian theory has been discussed in a number of references, and only a brief summary will be given here. A thorough analysis of this theoretical method is given by Hayes and Probstein in Ref. 17.

Manuscript received January 1964.

AEDC-TDR-64-25

Newton calculated the force on a body by assuming that the impact of fluid particles was completely inelastic for the normal component of momentum and was frictionless. Thus, the normal component of momentum is converted to a pressure force on the body while the tangential component remains unchanged. The analysis based on these assumptions gives the surface pressure coefficient, C_p , as

$$C_p = 2 \cos^2 \eta \quad (1)$$

where η is the angle between the free-stream velocity vector and the inward directed unit vector normal to the surface.

At high Mach numbers the disturbed region in front of a body becomes very limited in extent. The bow shock wave has approximately the same inclination as the body and is separated from the body surface by a very thin, practically inviscid, shock layer. With this flow geometry, the normal momentum of impinging molecules is lost inelastically and the tangential component of momentum is conserved. Hence, Newton's analysis is realistic for this type of flow, and the validity of the analysis increases as the shock-layer thickness decreases. For the shock wave to approach the inclination of the body, the gas dynamic equations show that the ratio of the density ahead of the shock to that behind the shock must approach zero. The equations further show that for the density ratio to approach zero, the Mach number must approach infinity and the ratio of specific heats must approach unity. If these Newtonian conditions ($M_\infty \rightarrow \infty$, $\gamma \rightarrow 1$) are satisfied, the Newtonian pressure coefficient, Eq. (1), is identical to that given by the oblique shock relations for the pressure immediately behind the shock wave.

In Newton's analysis, the impinging molecules leave the body surface along an unaccelerated path. However, in the case of a curved body with a thin shock layer, the particles are constrained in the shock layer and must follow an accelerated path. Therefore, for a correct analysis Eq. (1) must be modified to allow for the pressure gradient resulting from the centrifugal forces acting on the particles. This correction was first obtained by Busemann (Ref. 18), and the rational theory including the correction has been called the Newton-Busemann theory in Ref. 17. However, despite the theoretical correctness of the Newton-Busemann relation, the simple Newtonian theory has been found to agree much better with experimental data (e. g., Ref. 7), and the equations given in the present paper have not been corrected for centrifugal effects.

Equation (1) has been modified by a number of investigators to provide a better correlation with experimental data for several classes of bodies. The modified forms of the equation have the general relation,

$$C_p = K \cos^2 \eta \quad (2)$$

where K is a multiplicative factor which is used to match certain limiting conditions. For a flat plate with attached shock (i. e., at low angles of attack), Love (Ref. 19) suggested that $K = \gamma + 1$ provides better agreement with the exact oblique shock solution. For a slender pointed body with attached shock, best agreement with exact theory is obtained by using either the simple Newtonian value of $K = 2$ or the value suggested in Ref. 19 of $K = \frac{C_{p_{nose}}}{\sin^2 \delta_{nose}}$, where δ_{nose} is the surface angle at the nose and $C_{p_{nose}}$ is the exact value of pressure coefficient for this angle. Lees (Ref. 20) suggested that for a blunt body with detached shock wave the Newtonian theory could be modified to match conditions at the stagnation point by letting $K = C_{p_{max}} = \frac{p_{t_2} - p_{\infty}}{q_{\infty}}$, which is closely approximated by $K = \gamma + 3/\gamma + 1$ for large Mach numbers. In the present derivations, the modified form of the Newtonian approximation as given in Eq. (2) will be used with an arbitrary value of K .

The angle, η , between the velocity vector \bar{V}_{∞} and the surface unit inner normal vector \bar{n} is determined by the scalar product of the two vectors. The velocity vector (Fig. 1) is

$$\bar{V}_{\infty} = -V_{\infty} (\bar{i} \cos \alpha \cos \beta + \bar{j} \sin \beta + \bar{k} \sin \alpha \cos \beta) \quad (3)$$

where \bar{i} , \bar{j} , and \bar{k} are unit vectors directed along the X-, Y-, and Z-axes. The body surface may be described by the equation $F(x, y, z) = 0$. Then the inward directed unit vector normal to the body surface is

$$\bar{n} = \bar{i} \cos(n, x) + \bar{j} \cos(n, y) + \bar{k} \cos(n, z) \quad (4a)$$

where (n, x) , (n, y) , and (n, z) are the angles between \bar{n} and the positive X-, Y-, and Z-axes, respectively, and their cosines are given by

$$\left. \begin{aligned} \cos(n, x) &= - \frac{\partial F / \partial x}{\sqrt{(\partial F / \partial x)^2 + (\partial F / \partial y)^2 + (\partial F / \partial z)^2}} \\ \cos(n, y) &= - \frac{\partial F / \partial y}{\sqrt{(\partial F / \partial x)^2 + (\partial F / \partial y)^2 + (\partial F / \partial z)^2}} \\ \cos(n, z) &= - \frac{\partial F / \partial z}{\sqrt{(\partial F / \partial x)^2 + (\partial F / \partial y)^2 + (\partial F / \partial z)^2}} \end{aligned} \right\} \quad (4b)$$

Thus,

$$\begin{aligned} \cos \eta &= \frac{\bar{V}_{\infty} \cdot \bar{n}}{V_{\infty}} \\ &= - \left[\cos \alpha \cos \beta \cos(n, x) + \sin \beta \cos(n, y) + \sin \alpha \cos \beta \cos(n, z) \right] \end{aligned} \quad (5)$$

AEDC-TDR-64-25

The Newtonian theory predicts pressures only on surfaces which face the flow. For surfaces which are shielded from the flow, it is assumed that the surface pressure is equal to the free-stream static pressure and $C_p = 0$. Therefore, Eqs. (1) and (2) are applicable only for $\cos \eta \geq 0$.

Force and moment coefficient nomenclature utilized in the derivation is shown in Fig. 1. The coefficients are non-dimensionalized by an arbitrary reference area, S , and, in the case of moment coefficients, by an arbitrary reference length, ℓ . The moment reference point of each component is given in the corresponding figure. The coefficients are obtained by integrating the Newtonian pressure distribution over the body surface area, A , as indicated in the following general equations where the moment reference point is at the origin of the axes:

$$C_N = \frac{F_N}{q_\infty S} = - \frac{K}{S} \iint_A \cos^2 \eta \cos(n, z) dA \quad (6)$$

$$C_A = \frac{F_A}{q_\infty S} = - \frac{K}{S} \iint_A \cos^2 \eta \cos(n, x) dA \quad (7)$$

$$C_m = \frac{M_Y}{q_\infty S \ell} = - \frac{K}{S \ell} \left[\iint_A x \cos^2 \eta \cos(n, z) dA - \iint_A z \cos^2 \eta \cos(n, x) dA \right] \quad (8)$$

$$C_Y = \frac{F_Y}{q_\infty S} = \frac{K}{S} \iint_A \cos^2 \eta \cos(n, y) dA \quad (9)$$

$$C_n = \frac{M_Z}{q_\infty S \ell} = \frac{K}{S \ell} \left[\iint_A x \cos^2 \eta \cos(n, y) dA - \iint_A y \cos^2 \eta \cos(n, x) dA \right] \quad (10)$$

$$C_\ell = \frac{M_X}{q_\infty S \ell} = \frac{K}{S \ell} \left[\iint_A y \cos^2 \eta \cos(n, z) dA - \iint_A z \cos^2 \eta \cos(n, y) dA \right] \quad (11)$$

In the integration over the surface area, it is assumed that $C_p = 0$ on all surfaces shielded from the flow and on all flat surfaces (except in the case of the swept wedge) because these surfaces are usually concealed by other body components. Equations and charts are given for components having vertical symmetry and for the corresponding flat-topped components. For flat-bottomed components, the loads may be determined by taking the difference between the loads acting on the complete component and those acting on the flat-topped component and adding the pressure load of the flat lower surface to the normal force and pitching moment.

2.1 DELTA-WING COMPONENTS

The basic components of a delta wing are the nose, leading edge, and wing. The loads on these components are computed in the following sections. The method of combining the components to give a complete wing is described in Section 2.3.

2.1.1 Spherical-Wedge Nose

The nose of a delta wing is usually a spherical wedge. If the wing centerline angle ϵ (see Fig. F) is not zero, the nose is not exactly spherical, but the error in force coefficients will be negligible when ϵ is small. The nomenclature used in the derivation is shown in Fig. A.

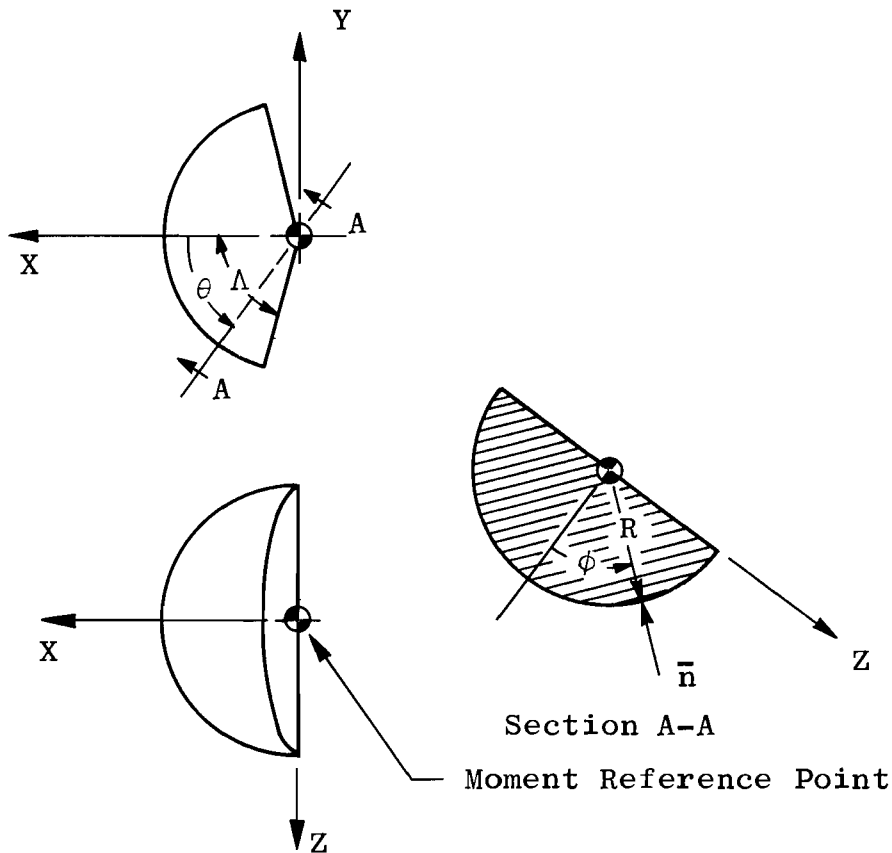


Fig. A Spherical-Wedge Nose

The direction cosines of the inward directed unit normal vector, \bar{n} , as obtained from Eq. (4b) or by analytic geometry are

$$\left. \begin{aligned} \cos(n, x) &= -\cos \phi \cos \theta \\ \cos(n, y) &= \cos \phi \sin \theta \\ \cos(n, z) &= -\sin \phi \end{aligned} \right\} \quad (12)$$

AEDC-TDR-64-25

The angle η between the free-stream velocity and the normal vector is obtained from Eq. (5) which gives

$$\cos \eta = \cos \beta (\cos a \cos \phi \cos \theta + \sin a \sin \phi) - \sin \beta \cos \phi \sin \theta \quad (13)$$

The pressure distribution over the nose is given by Eq. (2) as

$$C_p = K \cos^2 \eta$$

The value of ϕ at which the surface becomes shielded from the flow is designated as ϕ_o and is defined by $C_p = 0$ or $\cos \eta = 0$, thus

$$\tan \phi_o = \frac{\sin \beta \sin \theta - \cos \beta \cos a \cos \theta}{\cos \beta \sin a} \quad (14)$$

and at $\beta = 0$

$$\phi_o = -\tan^{-1} \left(\frac{\cos \theta}{\tan a} \right) \quad (14a)$$

The elemental surface area is given by

$$dA = R^2 \cos \phi \, d\phi \, d\theta \quad (15)$$

As was mentioned previously, it is assumed that $C_p = 0$ on the flat base surfaces even at angles of attack where these surfaces are not shielded from the flow. All coefficients and derivatives are evaluated at $\beta = 0$.

2.1.1.1 Normal-Force Coefficient

The normal-force coefficient is given by Eq. (6):

$$C_N = -\frac{K}{S} \iint_A \cos^2 \eta \cos(n, z) \, dA$$

Since the body has lateral symmetry, this equation may be integrated over the left side and the results multiplied by 2. Then, for $0 \leq a \leq \pi$,

$$C_N = \frac{2KR^2}{S} \int_0^\Lambda \int_{\phi_o}^{\pi/2} \cos^2 \eta \sin \phi \cos \phi \, d\phi \, d\theta \quad (16)$$

Substituting the value for $\cos \eta$ at $\beta = 0$ from Eq. (13) and performing the indicated integrations gives the normal-force coefficient as a function of a and Λ . Note that the equation must be evaluated by integrating first between $\phi = \phi_o$ and $\phi = \pi/2$ and then integrating the resulting function between $\theta = 0$ and $\theta = \Lambda$ since ϕ_o is a function of θ .

Then,

$$C_N \frac{S}{KR^2} = \frac{\sin a}{2} \left[\cos a \sin \Lambda \left(\frac{\pi}{2} + \tan^{-1} \frac{\cos \Lambda}{\tan a} \right) + \tan^{-1} (\sin a \tan \Lambda) \right] \quad (17)$$

Equation (17) was evaluated for $\alpha = 0$ to 180 deg and $\Lambda = 60$ to 90 deg and the results are presented in Fig. 2a.

2.1.1.2 Axial-Force Coefficient

The axial-force coefficient is given by Eq. (7):

$$C_A = - \frac{K}{S} \iint_A \cos^2 \eta \cos(n, x) dA$$

Then, for $0 \leq \alpha \leq \pi$,

$$C_A = - \frac{2KR^2}{S} \int_0^\Lambda \int_{\phi_0}^{\pi/2} \cos^2 \eta \cos^2 \phi \cos \theta d\phi d\theta \quad (18)$$

Integration of Eq. (18) gives

$$C_A \frac{S}{KR^2} = \frac{1}{4} \left[(\sin^2 \alpha \sin \Lambda + 3 \cos^2 \alpha \sin \Lambda - \cos^2 \alpha \sin^3 \Lambda) \left(\frac{\pi}{2} + \tan^{-1} \frac{\cos \Lambda}{\tan \alpha} \right) + 2 \cos \alpha \tan^{-1} (\sin \alpha \tan \Lambda) + \sin \alpha \cos \alpha \sin \Lambda \cos \Lambda \right] \quad (19)$$

The numerical evaluation of Eq. (19) is presented in Fig. 2b.

2.1.1.3 Pitching-Moment Coefficient

Since the force on any element of surface is directed toward the center of curvature, the resultant force acts through the center, and the moment about the reference point is zero.

2.1.1.4 Side-Force Coefficient Derivative

The side-force coefficient is given by Eq. (9):

$$C_Y = \frac{K}{S} \iint_A \cos^2 \eta \cos(n, y) dA$$

For either side of the nose, at $0 \leq \alpha \leq \pi$,

$$C_Y = \pm \frac{KR^2}{S} \int_0^{\pm\Lambda} \int_{\phi_0(\beta)}^{\pi/2} \cos^2 \eta \cos^2 \phi \sin \theta d\phi d\theta \quad (20)$$

where the upper sign corresponds to the left side of the nose and the lower sign corresponds to the right side. The derivative of the side-force coefficient with respect to β is

$$C_{Y\beta} = \pm \frac{KR^2}{S} \int_0^{\pm\Lambda} \sin \theta \frac{\partial}{\partial \beta} \int_{\phi_0(\beta)}^{\pi/2} \cos^2 \eta \cos^2 \phi d\phi d\theta \quad (21)$$

AEDC-TDR-64-25

Since the lower limit, ϕ_o , is a function of β , the Liebnitz rule is used to obtain the derivative

$$\frac{\partial}{\partial \beta} \int_{\phi_o(\beta)}^{\pi/2} \cos^2 \eta \cos^2 \phi \, d\phi = -\cos^2 \eta(\phi_o) \cos^2 \phi_o \frac{\partial \phi_o}{\partial \beta} + \int_{\phi_o(\beta)}^{\pi/2} \frac{\partial \cos^2 \eta}{\partial \beta} \cos^2 \phi \, d\phi$$

By definition, $\cos^2 \eta(\phi_o) = 0$, and $\partial \phi_o / \partial \beta$ is finite, so the first term is zero. Thus

$$C_{Y\beta} = \pm \frac{KR^2}{S} \int_0^{\pm \Lambda} \int_{\phi_o(\beta)}^{\pi/2} \frac{\partial \cos^2 \eta}{\partial \beta} \cos^2 \phi \sin \theta \, d\phi \, d\theta \quad (22)$$

Since ϕ and θ are independent of β , the derivative at $\beta = 0$ is

$$\left(C_{Y\beta} \right)_{\beta=0} = \pm \frac{KR^2}{S} \int_0^{\pm \Lambda} \int_{\phi_o(\beta=0)}^{\pi/2} \left(\frac{\partial \cos^2 \eta}{\partial \beta} \right)_{\beta=0} \cos^2 \phi \sin \theta \, d\phi \, d\theta \quad (23)$$

From Eq. (13)

$$\left(\frac{\partial \cos^2 \eta}{\partial \beta} \right)_{\beta=0} = -2 \cos \phi \sin \theta (\cos a \cos \phi \cos \theta + \sin a \sin \phi) \quad (24)$$

Substituting Eq. (24) in Eq. (23) shows that $C_{Y\beta}$ is the same for both sides of the nose. Then, multiplying Eq. (23) by 2 and performing the integration gives

$$C_{Y\beta} \frac{S}{KR^2} = -\frac{1}{2} \left[\cos a \sin^3 \Lambda \left(\frac{\pi}{2} + \tan^{-1} \frac{\cos \Lambda}{\tan a} \right) + \tan^{-1} (\sin a \tan \Lambda) - \sin a \sin \Lambda \cos \Lambda \right] \quad (25)$$

The numerical evaluation of Eq. (25) is presented in Fig. 2c.

2.1.1.5 Yawing-Moment and Rolling-Moment Coefficient Derivatives

As was the case with pitching moment, the yawing-moment and rolling-moment coefficients and their derivatives are zero about the reference point.

2.1.2 Flat-Topped Spherical-Wedge Nose

The geometry of the flat-topped spherical wedge is shown in Fig. B.

The direction cosines, pressure coefficient, and elemental area are the same as for the complete spherical wedge. For $0 \leq a \leq \pi/2$ no

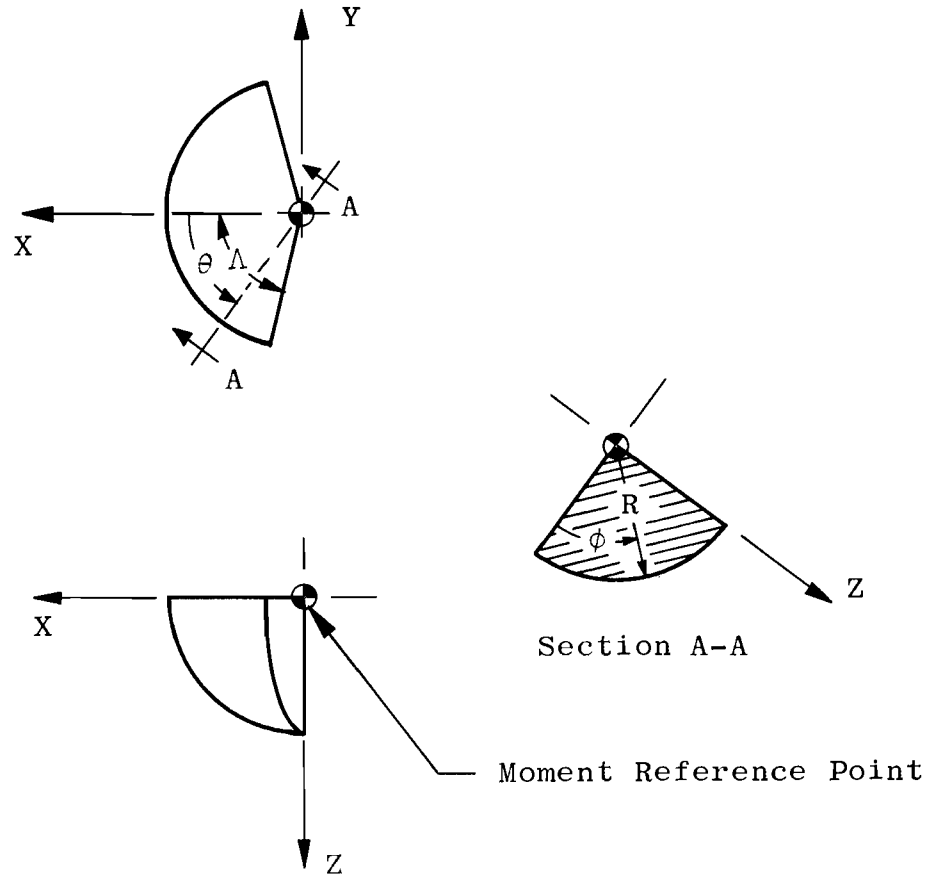


Fig. B Flat-Topped Spherical-Wedge Nose

part of the curved surface is shielded from the flow, so the limits of integration on ϕ become 0 to $\pi/2$. Then, Eqs. (16), (18), and (23) give the following results:

$$C_N \frac{S}{KR^2} = \frac{1}{4} \left[\pi \sin a \cos a \sin \Lambda + \cos^2 a \sin \Lambda \cos \Lambda + \Lambda (1 + \sin^2 a) \right] \quad (26)$$

$$C_A \frac{S}{KR^2} = \frac{1}{4} \left[\frac{3\pi}{2} \cos^2 a \left(\sin \Lambda - \frac{\sin^3 \Lambda}{3} \right) + \frac{\pi}{2} \sin^2 a \sin \Lambda \right. \\ \left. + 2 \cos a \sin a (\Lambda + \sin \Lambda \cos \Lambda) \right] \quad (27)$$

$$C_{Y\beta} \frac{S}{KR^2} = - \frac{1}{4} \left[\pi \cos a \sin^3 \Lambda + 2 \sin a (\Lambda - \sin \Lambda \cos \Lambda) \right] \quad (28)$$

where Λ is in radians. The moment coefficients and their derivatives are zero for the indicated reference point. For $a \geq \pi/2$ the equations for the complete spherical wedge also apply to the flat-topped spherical wedge.

AEDC-TDR-64-25

The characteristics of the flat-topped spherical wedge are presented in Fig. 3.

2.1.3 Swept-Cylinder Leading Edge

The delta-wing leading edge which is analyzed in this section consists of two symmetrically swept circular cylinders. The nomenclature used in the derivation is shown in Fig. C.

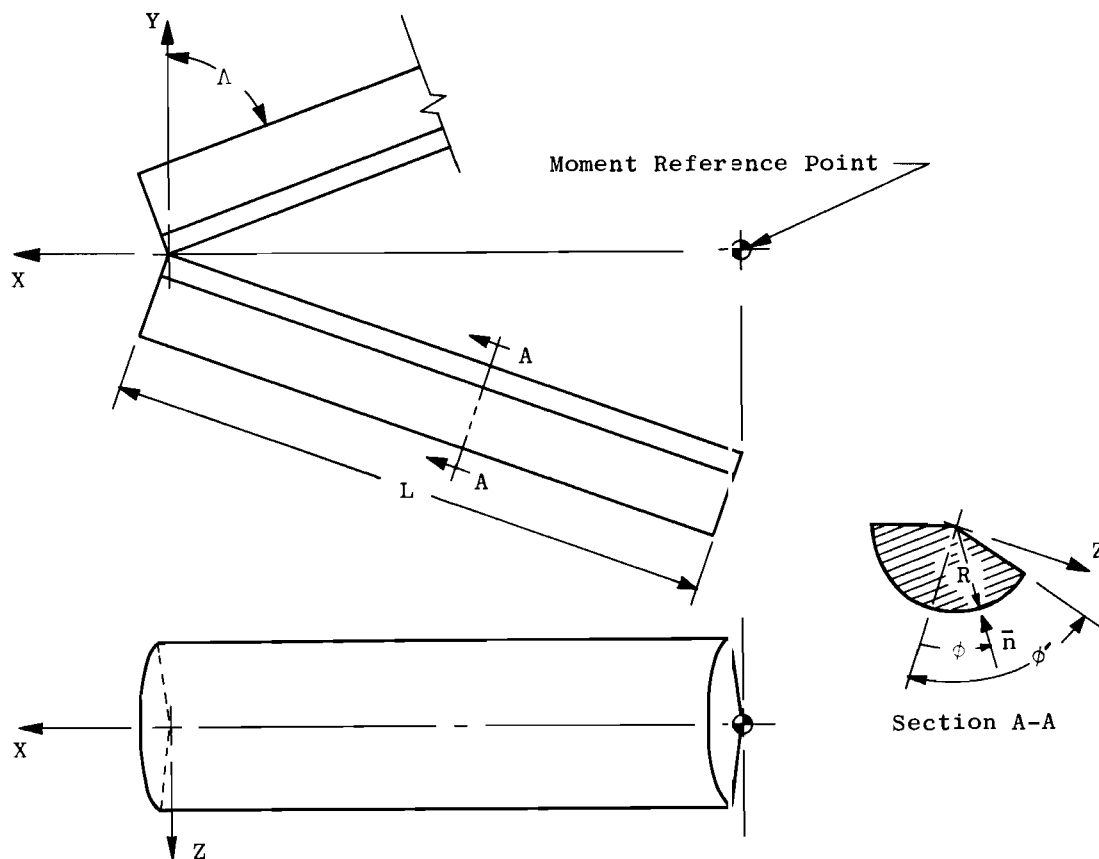


Fig. C Swept-Cylinder Leading Edge

The two sides are treated as a unit in the analysis, and the sweepback angle Λ is taken as positive in the equations for the leading-edge coefficients. Where the two sides must be considered separately, as in Eqs. (29) and (30), the sign convention is $\Lambda > 0$ for the right side and $\Lambda < 0$ for the left side.

The direction cosines of the inward directed unit normal vector are

$$\left. \begin{aligned} \cos(n, x) &= -\cos\phi \cos\Lambda \\ \cos(n, y) &= -\cos\phi \sin\Lambda \\ \cos(n, z) &= -\sin\phi \end{aligned} \right\} \quad (29)$$

Then, from Eq. (5)

$$\cos\eta = \cos\beta (\cos\alpha \cos\phi \cos\Lambda + \sin\alpha \sin\phi) + \sin\beta \cos\phi \sin\Lambda \quad (30)$$

At $\beta = 0$ the surface becomes shielded from the flow along a line defined by $\phi = \phi_0$, where

$$\phi_0 = -\tan^{-1} \left(\frac{\cos\Lambda}{\tan\alpha} \right) \quad (31)$$

The elemental surface area is

$$dA = 2LR \, d\phi \quad (32)$$

The integration of the pressure distribution over the surface has as its limit the geometric angle ϕ' , which is always positive. For a leading edge which is tangent to the wing surface, ϕ' is determined by the wing sweepback and dihedral angles Λ and Γ , as shown in Fig. D.

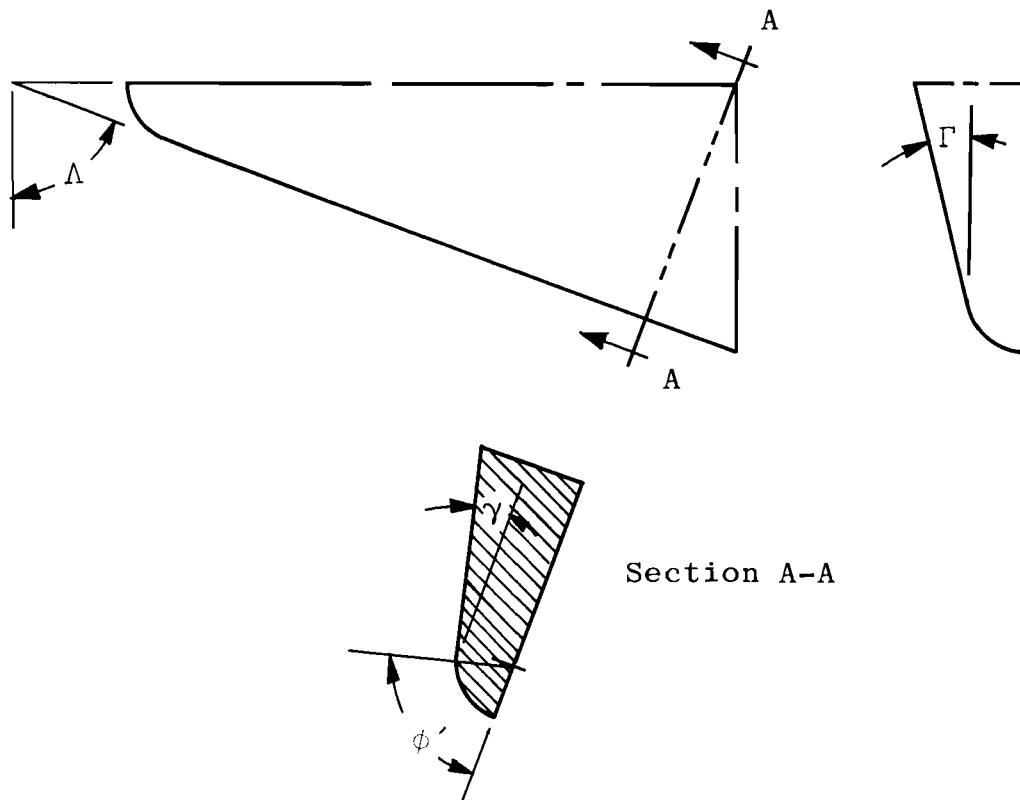


Fig. D Leading Edge and Wing Geometry

AEDC-TDR-64-25

Thus,

$$\phi' = \frac{\pi}{2} - \gamma \quad (33a)$$

and

$$\gamma = \tan^{-1} \left(\frac{\tan \Gamma}{\sin \Lambda} \right) \quad (33b)$$

Therefore

$$\phi' = \tan^{-1} \left(\frac{\sin \Lambda}{\tan \Gamma} \right) \quad (33c)$$

For a leading edge which is not tangent to the wing surface, Eq. (33) is not valid and ϕ' must be determined from the leading-edge geometry. It is assumed that $C_p = 0$ on all flat surfaces, and the coefficients and their derivatives are evaluated at $\beta = 0$.

2.1.3.1 Normal-Force Coefficient

The normal-force coefficient is given by

$$C_N = \frac{2 K L R}{S} \int_{\phi_0 \text{ (or } -\phi')}^{\phi'} \cos^2 \eta \sin \phi \, d\phi \quad (34)$$

If $\phi' < |\phi_0|$, the lower limit of integration is $\phi = -\phi'$. The limit changes to $\phi = \phi_0$ at $\phi_0 = -\phi'$ or at $a = a_0$, where

$$a_0 = \tan^{-1} \left(\frac{\tan \Gamma}{\tan \Lambda} \right) \quad (35)$$

Evaluating Eq. (34) for $0 \leq a \leq a_0$ with the lower limit $-\phi'$,

$$C_N \frac{S}{K L R} = \frac{8}{3} \sin a \cos a \cos \Lambda \sin^3 \phi' \quad (36)$$

and for $a_0 \leq a \leq (\pi - a_0)$ with the lower limit ϕ_0 ,

$$C_N \frac{S}{K L R} = \frac{2}{3} \left[(\sin^2 a - \cos^2 a \cos^2 \Lambda) (\cos^3 \phi' - \cos^3 \phi_0) \right. \\ \left. - 3 \sin^2 a (\cos \phi' - \cos \phi_0) + 2 \sin a \cos a \cos \Lambda (\sin^3 \phi' - \sin^3 \phi_0) \right] \quad (37)$$

where ϕ_0 and ϕ' are given by Eqs. (31) and (33c), respectively. If the wing dihedral, Γ , is small, the leading edge will be closely approximated by a complete hemicylinder ($\phi' = \pi/2$). Then, from Eqs. (31) and (37) for $0 \leq a \leq \pi$

$$C_N \frac{S}{K L R} = \frac{4}{3} \sin a \left(\cos a \cos \Lambda + \sqrt{1 - \sin^2 \Lambda \cos^2 a} \right) \quad (38)$$

Equation (38) was evaluated for $a = 0$ to 180 deg and $\Lambda = 60$ to 90 deg, and the results are presented in Fig. 4a.

2.1.3.2 Axial-Force Coefficient

The axial-force coefficient is given by

$$C_A = \frac{2 \text{KLR}}{S} \int_{\phi_o}^{\phi'} \cos^2 \eta \cos \phi \cos \Lambda d\phi \quad (39)$$

Then, for $0 \leq a \leq a_o$

$$C_A \frac{S}{\text{KLR}} = \frac{4 \cos \Lambda}{3} \left[(\sin^2 a - \cos^2 a \cos^2 \Lambda) \sin^3 \phi' + 3 \cos^2 a \cos^2 \Lambda \sin \phi' \right] \quad (40)$$

and for $a_o \leq a \leq (\pi - a_o)$

$$C_A \frac{S}{\text{KLR}} = \frac{2 \cos \Lambda}{3} \left[(\sin^2 a - \cos^2 a \cos^2 \Lambda) (\sin^3 \phi' - \sin^3 \phi_o) \right. \\ \left. + 3 \cos^2 a \cos^2 \Lambda (\sin \phi' - \sin \phi_o) \right. \\ \left. - 2 \sin a \cos a \cos \Lambda (\cos^3 \phi' - \cos^3 \phi_o) \right] \quad (41)$$

For the hemicylinder ($\phi' = \pi/2$),

$$C_A \frac{S}{\text{KLR}} = \frac{4 \cos \Lambda}{3} \left(\frac{\sin^2 a}{2} + \cos^2 a \cos^2 \Lambda + \cos a \cos \Lambda \sqrt{1 - \sin^2 \Lambda \cos^2 a} \right) \quad (42)$$

The numerical evaluation of Eq. (42) is presented in Fig. 4b.

2.1.3.3 Pitching-Moment Coefficient

The resultant force acts through the center of curvature at a point midway between the ends. Thus,

$$C_m = C_N \frac{L \sin \Lambda}{2 \ell} \quad (43)$$

2.1.3.4 Side-Force Coefficient Derivative

The side-force coefficient for either side (with proper sign convention on Λ) is

$$C_Y = - \frac{\text{KLR}}{S} \int_{\phi_o}^{\phi'} \cos^2 \eta \cos \phi \sin \Lambda d\phi \quad (44)$$

Using the same procedure as was used with the spherical-wedge nose,

$$C_{Y\beta} = - \frac{\text{KLR}}{S} \int_{\phi_o}^{\phi'} \left(\frac{\partial \cos^2 \eta}{\partial \beta} \right)_{\beta=0} \cos \phi \sin \Lambda d\phi \quad (45)$$

AEDC-TDR-64-25

where

$$\left(\frac{\partial \cos^2 \eta}{\partial \beta} \right)_{\beta=0} = 2 \cos \phi \sin \Lambda (\cos a \cos \phi \cos \Lambda + \sin a \sin \phi) \quad (46)$$

Substituting Eq. (46) in Eq. (45) shows that $C_{Y\beta}$ is the same for both sides. Then, multiplying Eq. (45) by 2 and performing the integration gives for $0 \leq a \leq a_0$

$$C_{Y\beta} \frac{S}{KLR} = -8 \cos a \cos \Lambda \sin^2 \Lambda \left(\sin \phi' - \frac{\sin^3 \phi'}{3} \right) \quad (47)$$

and for $a_0 \leq a \leq (\pi - a_0)$

$$C_{Y\beta} \frac{S}{KLR} = -\frac{4}{3} \sin^2 \Lambda \left[\cos a \cos \Lambda (3 \sin \phi' - 3 \sin \phi_0 - \sin^3 \phi' + \sin^3 \phi_0) \right. \\ \left. - \sin a (\cos^3 \phi' - \cos^3 \phi_0) \right] \quad (48)$$

For the hemicylinder ($\phi' = \pi/2$),

$$C_{Y\beta} \frac{S}{KLR} = -\frac{4}{3} \sin^2 \Lambda \left[2 \cos a \cos \Lambda + \frac{\sin^2 a + 2 \cos^2 a \cos^2 \Lambda}{\sqrt{1 - \sin^2 \Lambda \cos^2 a}} \right] \quad (49)$$

The numerical evaluation of Eq. (49) is presented in Fig. 4c.

2.1.3.5 Yawing-Moment Coefficient Derivative

The yawing-moment coefficient is given by Eq. (10):

$$C_n = \frac{K}{S \ell} \left[\iint_A x \cos^2 \eta \cos(n, y) dA - \iint_A y \cos^2 \eta \cos(n, x) dA \right]$$

From Fig. C, $x = \pm \frac{L}{2} \sin \Lambda$ and $y = \pm \frac{L}{2} \cos \Lambda$, where the upper sign applies to the right side and the lower sign applies to the left side. Since x and y are not functions of ϕ , the yawing-moment coefficient for either side is

$$C_n = \pm \frac{L}{2 \ell} (C_Y \sin \Lambda + C_A \cos \Lambda)$$

Comparing Eq. (39) and Eq. (44) gives

$$C_A = \frac{-C_Y}{\tan \Lambda}$$

Then,

$$C_n = \pm C_Y \frac{L}{2 \ell} \left(\frac{2 \sin^2 \Lambda - 1}{\sin \Lambda} \right)$$

The total yawing-moment coefficient for both sides is

$$C_n = (C_{Y_{\text{right}}} + C_{Y_{\text{left}}}) \frac{L}{2 \ell} \left(\frac{2 \sin^2 \Lambda - 1}{\sin \Lambda} \right)$$

and the derivative is

$$C_{n\beta} = \left(C_{Y\beta_{\text{right}}} + C_{Y\beta_{\text{left}}} \right) \frac{L}{2l} \left(\frac{2 \sin^2 \Lambda - 1}{\sin \Lambda} \right)$$

$$\text{But, } C_{Y\beta_{\text{right}}} = C_{Y\beta_{\text{left}}} = \frac{C_{Y\beta}}{2}$$

Therefore

$$C_{n\beta} = C_{Y\beta} \frac{L}{2l} \left(\frac{2 \sin^2 \Lambda - 1}{\sin \Lambda} \right) \quad (50)$$

2.1.3.6 Rolling-Moment Coefficient Derivative

The rolling-moment coefficient is given by Eq. (11):

$$C_l = \frac{K}{S l} \left[\iint_A y \cos^2 \eta \cos(n, z) dA - \iint_A z \cos^2 \eta \cos(n, y) dA \right]$$

From Fig. C, $y = \pm \frac{L}{2} \cos \Lambda$ and $Z = 0$, where the upper sign applies to the right side and the lower sign applies to the left side. Since y is not a function of ϕ , the rolling-moment coefficient for either side is

$$C_l = \pm \frac{L \cos \Lambda}{2l} (-C_N)$$

The total rolling-moment coefficient for both sides is

$$C_l = \frac{L \cos \Lambda}{2l} (C_{N_{\text{left}}} - C_{N_{\text{right}}})$$

and the derivative is

$$C_{l\beta} = \frac{L \cos \Lambda}{2l} (C_{N\beta_{\text{left}}} - C_{N\beta_{\text{right}}})$$

For either side, Eq. (34) gives

$$C_{N\beta} = \frac{KLR}{S} \int_{\phi_0}^{\phi'} \left(\frac{\partial \cos^2 \eta}{\partial \beta} \right)_{\beta=0} \sin \phi d\phi$$

Integrating gives

$$C_{N\beta} = \frac{2KLR}{3S} \sin \Lambda \left[\sin a \sin^3 \phi - \cos a \cos \Lambda \cos^3 \phi \right]_{\phi_0}^{\phi'} \quad (51)$$

Thus,

$$C_{N\beta_{\text{left}}} = -C_{N\beta_{\text{right}}}$$

and

$$C_{l\beta} = \frac{-2KL^2R \cos \Lambda \sin \Lambda}{3Sl} \left[\sin a \sin^3 \phi - \cos a \cos \Lambda \cos^3 \phi \right]_{\phi_0}^{\phi'} \quad (52)$$

AEDC-TDR-64-25

For $0 \leq a \leq a_0$

$$C_{l\beta} \frac{S l}{K L^2 R} = - \frac{4}{3} \sin a \cos \Lambda \sin \Lambda \sin^3 \phi' \tag{53}$$

and for $a_0 \leq a \leq (\pi - a_0)$

$$C_{l\beta} \frac{S l}{K L^2 R} = - \frac{2}{3} \cos \Lambda \sin \Lambda \left[\sin a (\sin^3 \phi' - \sin^3 \phi_0) - \cos a \cos \Lambda (\cos^3 \phi' - \cos^3 \phi_0) \right] \tag{54}$$

For the hemicylinder ($\phi' = \pi/2$)

$$C_{l\beta} \frac{S l}{K L^2 R} = - \frac{2}{3} \cos \Lambda \sin \Lambda \sin a \left(1 + \frac{\cos a \cos \Lambda}{\sqrt{1 - \sin^2 \Lambda \cos^2 a}} \right) \tag{55}$$

The numerical evaluation of Eq. (55) is presented in Fig. 4d.

2.1.4 Flat-Topped Swept-Cylinder Leading Edge

The geometry of the flat-topped swept-cylinder leading edge is shown in Fig. E.

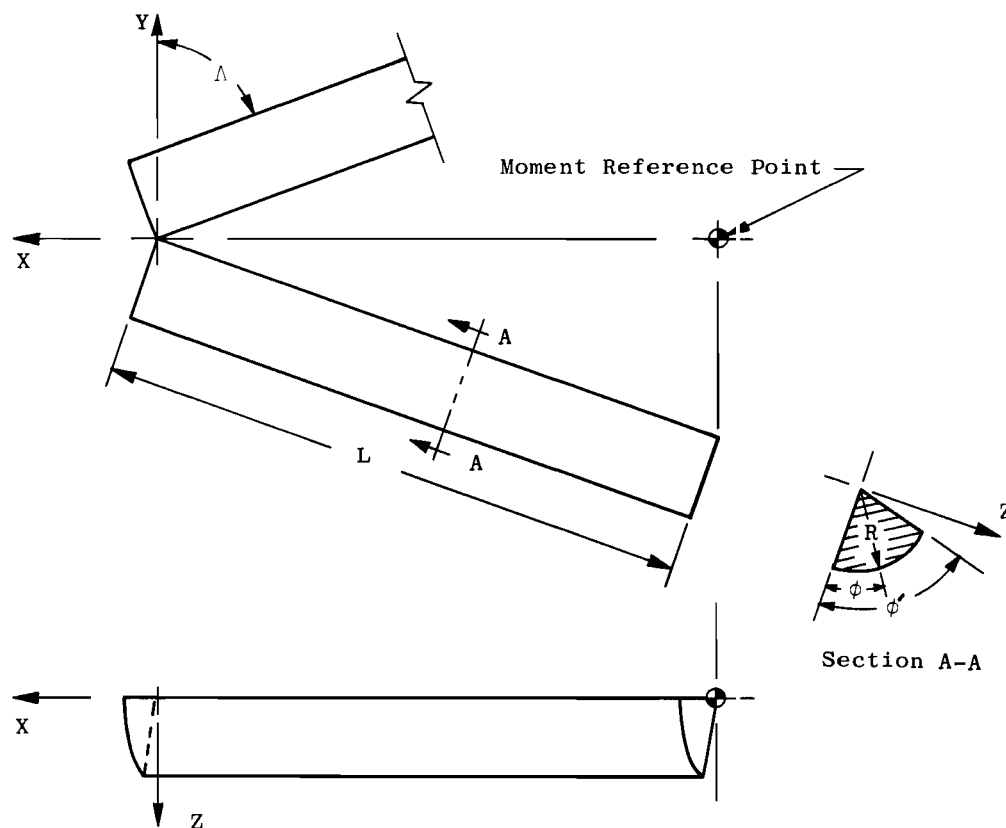


Fig. E Flat-Topped Swept-Cylinder Leading Edge

The directional cosines, pressure coefficient, and elemental area are the same as for the complete cylindrical leading edge. For $0 \leq a \leq \pi/2$, the limits of integration on ϕ are from 0 to ϕ' . Then Eqs. (34), (39), (45), and (52) give

$$C_N \frac{S}{KLR} = \frac{2}{3} \left[(\sin^2 a - \cos^2 a \cos^2 \Lambda) (\cos^3 \phi' - 1) - 3 \sin^2 a (\cos \phi' - 1) + 2 \sin a \cos a \cos \Lambda \sin^3 \phi' \right] \quad (56)$$

$$C_A \frac{S}{KLR} = \frac{2}{3} \cos \Lambda \left[(\sin^2 a - \cos^2 a \cos^2 \Lambda) \sin^3 \phi' + 3 \cos^2 a \cos^2 \Lambda \sin \phi' - 2 \sin a \cos a \cos \Lambda (\cos^3 \phi' - 1) \right] \quad (57)$$

$$C_{Y\beta} \frac{S}{KLR} = -\frac{4}{3} \sin^2 \Lambda \left[\cos a \cos \Lambda (3 \sin \phi' - \sin^3 \phi') - \sin a (\cos^3 \phi' - 1) \right] \quad (58)$$

$$C_{l\beta} \frac{S}{KL^2R} = -\frac{2}{3} \cos \Lambda \sin \Lambda \left[\sin a \sin^3 \phi' - \cos a \cos \Lambda (\cos^3 \phi' - 1) \right] \quad (59)$$

For the hemicylinder with $\phi' = \pi/2$,

$$C_N \frac{S}{KLR} = \frac{4}{3} \left(\sin^2 a + \sin a \cos a \cos \Lambda + \frac{\cos^2 a \cos^2 \Lambda}{2} \right) \quad (60)$$

$$C_A \frac{S}{KLR} = \frac{4}{3} \cos \Lambda \left(\frac{\sin^2 a}{2} + \sin a \cos a \cos \Lambda + \cos^2 a \cos^2 \Lambda \right) \quad (61)$$

$$C_{Y\beta} \frac{S}{KLR} = -\frac{4}{3} \sin^2 \Lambda (\sin a + 2 \cos a \cos \Lambda) \quad (62)$$

$$C_{l\beta} \frac{S l}{KL^2R} = -\frac{2}{3} \cos \Lambda \sin \Lambda (\sin a + \cos a \cos \Lambda) \quad (63)$$

The pitching-moment coefficient and yawing-moment coefficient derivative are given by Eqs. (43) and (50), respectively, with C_N and $C_{Y\beta}$ determined from Eqs. (56) and (58) or (60) and (62). For $a \geq \pi/2$, the equations for the complete leading edge also apply to the flat-topped leading edge.

The characteristics of the flat-topped swept-cylinder with $\phi' = \pi/2$ are given in Fig. 5.

AEDC-TDR-64-25

2.1.5 Swept-Wedge Wing

A planar wing having sweepback and dihedral is analyzed in this section. The nomenclature used in the derivation is shown in Fig. F.

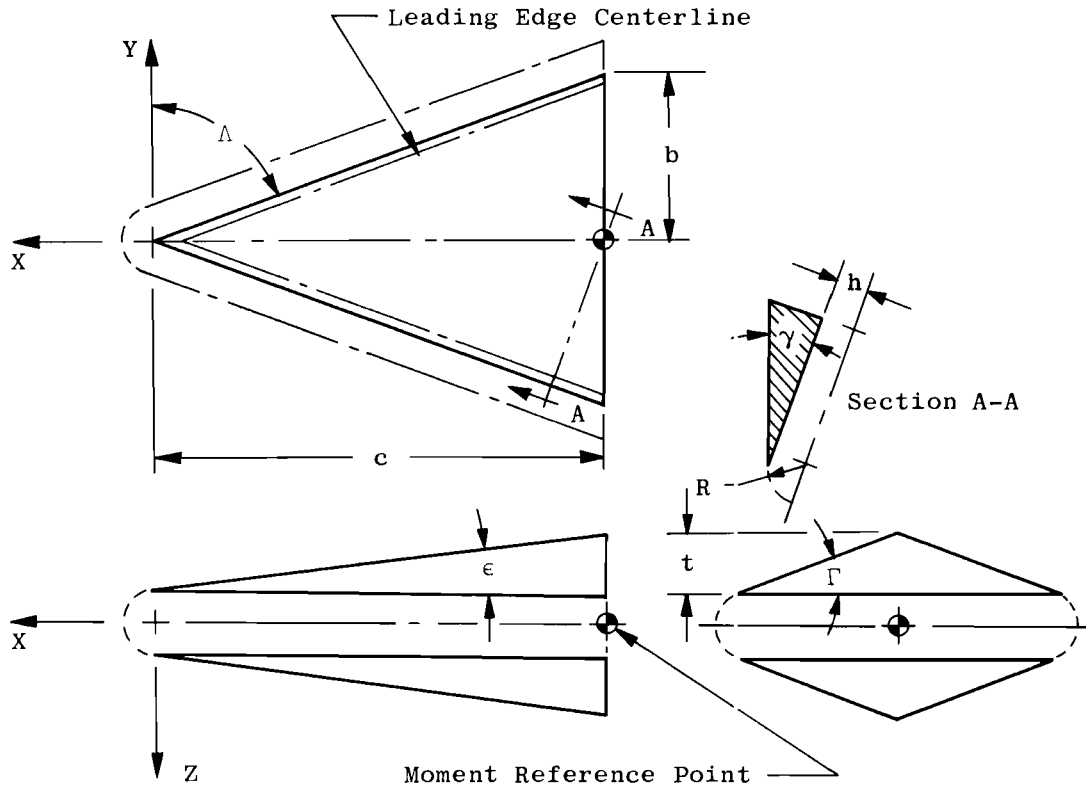


Fig. F Swept-Wedge Wing

The sweepback angle, Λ , is taken as positive in the equations for the coefficients of the entire wing. Where the sides must be considered separately, as in Eqs. (65) and (66), the sign convention is $\Lambda > 0$ for the right side and $\Lambda < 0$ for the left side. The centerline angle, ϵ , is always positive and is related to the dihedral angle, Γ , and the sweepback angle, Λ , by

$$\epsilon = \tan^{-1} \left(\frac{\tan \Gamma}{\tan \Lambda} \right) \tag{64}$$

The direction cosines of the inward directed unit normal vector are

$$\left. \begin{aligned} \cos(n, x) &= \frac{-\sin \epsilon}{\sqrt{1 + \tan^2 \Lambda \sin^2 \epsilon}} \\ \cos(n, y) &= \frac{-\tan \Lambda \sin \epsilon}{\sqrt{1 + \tan^2 \Lambda \sin^2 \epsilon}} \\ \cos(n, z) &= \frac{\pm \cos \epsilon}{\sqrt{1 + \tan^2 \Lambda \sin^2 \epsilon}} \end{aligned} \right\} \tag{65}$$

where the upper sign applies to the upper surface and the lower sign applies to the lower surface. Then, from Eq. (5)

$$\cos \eta = \frac{\cos \beta \sin (\epsilon \pm a) + \sin \beta \tan \Lambda \sin \epsilon}{\sqrt{1 + \tan^2 \Lambda \sin^2 \epsilon}} \quad (66)$$

where $(\epsilon + a)$ is used for the lower surface and $(\epsilon - a)$ is used for the upper surface. At $\beta = 0$, the upper surface becomes shielded from the flow at $a = \epsilon$, and the lower surface is shielded at $a = \pi - \epsilon$. Equation (66) is valid only within these limits.

Since the pressure coefficient is constant over each of the wedge surfaces it is not necessary to integrate to obtain total loads. The force and moment coefficients are most easily calculated by using the projected planform, base, and side areas. The total planform area, A_p , is

$$A_p = bc \quad (67)$$

The base area, A_b , for either half of wing is

$$A_b = bt \quad (68)$$

The side area, A_s , for either half of wing is

$$A_s = \frac{ct}{2} \quad (69)$$

In the following derivations it is assumed that $C_p = 0$ on the base of the wing and that the wing is at $\beta = 0$. Separate equations are given for the lower and upper halves, and the total wing loads may be obtained by combining the two halves. No graphical results are presented because of the simplicity of the equations.

2.1.5.1 Normal-Force Coefficient

For the lower half of the wing at $0 \leq a \leq (\pi - \epsilon)$ the pressure coefficient is

$$C_{p_L} = K \cos^2 \eta = \frac{K \sin^2 (\epsilon + a)}{1 + \tan^2 \Lambda \sin^2 \epsilon} \quad (70)$$

and the normal-force coefficient is

$$C_{N_L} = C_{p_L} \frac{A_p}{S} \quad (71)$$

at $(\pi - \epsilon) \leq a \leq \pi$, $C_{N_L} = 0$

For the upper half of the wing at $0 \leq a \leq \epsilon$, the pressure coefficient is

$$C_{p_U} = \frac{K \sin^2 (\epsilon - a)}{1 + \tan^2 \Lambda \sin^2 \epsilon} \quad (72)$$

AEDC-TDR-64-25

and the normal-force coefficient is

$$C_{N_U} = -C_{P_U} \frac{A_p}{S} \quad (73)$$

At $\epsilon \leq \alpha \leq \pi$, $C_{N_U} = 0$.

2.1.5.2 Axial-Force Coefficient

For the lower half of the wing at $0 \leq \alpha \leq (\pi - \epsilon)$

$$C_{A_L} = C_{P_L} \frac{A_b}{S} \quad (74)$$

For the upper half at $0 \leq \alpha \leq \epsilon$

$$C_{A_U} = C_{P_U} \frac{A_b}{S} \quad (75)$$

where C_{P_L} and C_{P_U} are given in Eqs. (70) and (72)

2.1.5.3 Pitching-Moment Coefficient

For the lower half of the wing at $0 \leq \alpha \leq (\pi - \epsilon)$

$$C_{m_L} = C_{N_L} \frac{c}{3l} - C_{A_L} \frac{1}{l} \left(\frac{t}{3} + h \right)$$

or from Eqs. (71) and (74)

$$C_{m_L} = \frac{C_{N_L}}{l} \left[\frac{c}{3} - \tan \epsilon \left(\frac{t}{3} + h \right) \right] \quad (76)$$

For the upper half at $0 \leq \alpha \leq \epsilon$

$$C_{m_U} = \frac{C_{N_U}}{l} \left[\frac{c}{3} - \tan \epsilon \left(\frac{t}{3} + h \right) \right] \quad (77)$$

If the leading edge is tangent to the wing surface, h is given by

$$h = R \cos \gamma \quad (78)$$

where R is the leading edge radius and γ is given by Eq (33b). If the leading edge is not tangent to the wing, Eq. (78) is not valid and h must be determined from the leading edge geometry.

2.1.5.4 Side-Force Coefficient Derivative

For the lower half of the wing at $0 \leq \alpha \leq (\pi - \epsilon)$

$$C_{Y_L} = \Delta C_{P_L} \frac{A_s}{S} \quad (79)$$

where, by definition

$$\Delta C_{pL} = (C_{p_{left}} - C_{p_{right}})_L \quad (80)$$

and from Eq. (66)

$$\Delta C_{pL} = \frac{-4 K \cos \beta \sin \beta \tan \Lambda \sin \epsilon \sin (\epsilon + \alpha)}{1 + \tan^2 \Lambda \sin^2 \epsilon} \quad (81)$$

Then,

$$(C_{Y\beta})_L = \left(\frac{\partial \Delta C_{pL}}{\partial \beta} \right)_{\beta=0} \frac{A_s}{S}$$

and

$$(C_{Y\beta})_L = - \frac{4 K A_s}{S} \frac{\tan \Lambda \sin \epsilon \sin (\epsilon + \alpha)}{1 + \tan^2 \Lambda \sin^2 \epsilon} \quad (82)$$

For the upper half at $0 \leq \alpha \leq \epsilon$

$$(C_{Y\beta})_U = - \frac{4 K A_s}{S} \frac{\tan \Lambda \sin \epsilon \sin (\epsilon - \alpha)}{1 + \tan^2 \Lambda \sin^2 \epsilon} \quad (83)$$

2.1.5.5 Yawing-Moment Coefficient Derivative

For the lower half of the wing at $0 \leq \alpha \leq (\pi - \epsilon)$

$$(C_n)_L = \frac{1}{l} \left[\frac{c}{3} C_{YL} + \frac{b}{3} (C_{A_{right}} - C_{A_{left}})_L \right] \quad (84)$$

From Eqs. (74), (79), and (80)

$$(C_{A_{right}} - C_{A_{left}})_L = - C_{YL} \frac{A_b}{A_s}$$

and

$$(C_{n\beta})_L = (C_{Y\beta})_L \frac{c}{3l} \left(1 - \frac{1}{\tan^2 \Lambda} \right) \quad (85)$$

For the upper half at $0 \leq \alpha \leq \epsilon$

$$(C_{n\beta})_U = (C_{Y\beta})_U \frac{c}{3l} \left(1 - \frac{1}{\tan^2 \Lambda} \right) \quad (86)$$

2.1.5.6 Rolling-Moment Coefficient Derivative

For the lower half of the wing at $0 \leq \alpha \leq (\pi - \epsilon)$

$$(C_l)_L = \frac{1}{l} \left[- C_{YL} \left(\frac{t}{3} + h \right) + \frac{b}{3} (C_{N_{left}} - C_{N_{right}})_L \right] \quad (87)$$

AEDC-TDR-64-25

From Eqs. (71), (79), and (80)

$$\left(C_{N_{left}} - C_{N_{right}} \right)_L = \frac{C_{Y_L}}{2} \frac{A_p}{A_s}$$

and

$$\left(C_{l_\beta} \right)_L = \left(C_{Y_\beta} \right)_L \frac{1}{l} \left[\frac{t}{3} \left(\frac{1}{\tan^2 \Gamma} - 1 \right) - h \right] \tag{88}$$

For the upper half at $0 \leq a \leq \epsilon$

$$\left(C_{l_\beta} \right)_U = - \left(C_{Y_\beta} \right)_U \frac{1}{l} \left[\frac{t}{3} \left(\frac{1}{\tan^2 \Gamma} - 1 \right) - h \right] \tag{89}$$

2.2 BODY COMPONENTS

Body components typical of lifting re-entry configurations are the spherical segment, cone frustum, and circular cylinder. The loads on these components are computed in the following sections. The method of combining components to give a complete configuration is described in Section 2.3.

2.2.1 Spherical Segment

The spherical segment is a basic nose for bodies of revolution. The nomenclature used in the derivation is shown in Fig. G.

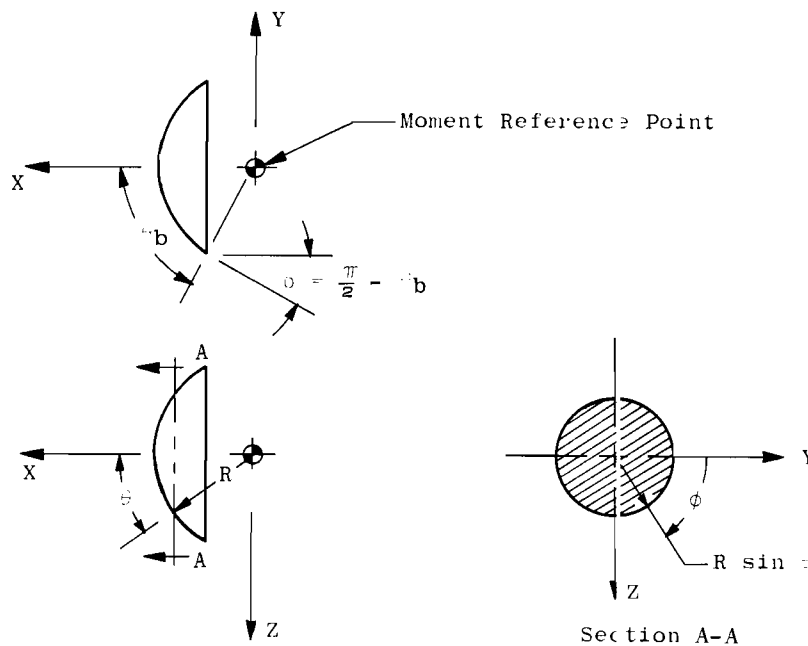


Fig. G Spherical Segment

The direction cosines of the inward directed unit normal vector are

$$\left. \begin{aligned} \cos(n, x) &= -\cos \theta \\ \cos(n, y) &= -\sin \theta \cos \phi \\ \cos(n, z) &= -\sin \theta \sin \phi \end{aligned} \right\} \quad (90)$$

Then, from Eq. (5)

$$\cos \eta = \cos \beta (\cos a \cos \theta + \sin a \sin \theta \sin \phi) + \sin \beta \sin \theta \cos \phi \quad (91)$$

At $\beta = 0$ the surface becomes shielded from the flow along a curve defined by $\phi = \phi_0$, where

$$\phi_0 = -\sin^{-1} \left(\frac{1}{\tan a \tan \theta} \right) \quad (92)$$

This equation is valid only for $\theta \geq (\pi/2 - a)$, since no shielding occurs for $\theta \leq (\pi/2 - a)$. The elemental surface area is

$$dA = R^2 \sin \theta d\theta d\phi \quad (93)$$

It is assumed that $C_p = 0$ on the base at all angles of attack, and the coefficients and their derivatives are evaluated at $\beta = 0$.

2.2.1.1 Normal-Force Coefficient

The normal-force coefficient is given by

$$C_N = \frac{KR^2}{S} \iint_A \cos^2 \eta \sin^2 \theta \sin \phi d\phi d\theta \quad (94)$$

Because of the limitations on the shielding equation, the evaluation of Eq. (94) must be treated as three separate cases. In each case, the integration is taken over the right side of the body and the result is multiplied by 2.

$$(I) \quad 0 \leq a \leq (\pi/2 - \theta_b)$$

$$C_N = \frac{2KR^2}{S} \int_0^{\theta_b} \int_{-\pi/2}^{\pi/2} \cos^2 \eta \sin^2 \theta \sin \phi d\phi d\theta \quad (95)$$

which gives

$$C_N \frac{S}{KR^2} = \frac{\pi}{2} \cos a \sin a \sin^4 \theta_b \quad (96)$$

$$(II) \quad (\pi/2 - \theta_b) \leq a \leq \pi/2$$

$$C_N = \frac{2KR^2}{S} \left[\int_0^{\pi/2 - a} \int_{-\pi/2}^{\pi/2} \cos^2 \eta \sin^2 \theta \sin \phi d\phi d\theta + \int_{\pi/2 - a}^{\theta_b} \int_{\phi_0}^{\pi/2} \cos^2 \eta \sin^2 \theta \sin \phi d\phi d\theta \right] \quad (97)$$

AEDC-TDR-64-25

then

$$C_N \frac{S}{KR^2} = \frac{\sin a}{2} \left\{ \cos^{-1} \left(\frac{\cos \theta_b}{\sin a} \right) + \cos a \sin^4 \theta_b \left[\frac{\pi}{2} + \sin^{-1} \left(\frac{1}{\tan a \tan \theta_b} \right) \right] \right. \\ \left. + \frac{\cos \theta_b}{3} \left[\cos^2 \theta_b \left(3 - \frac{1}{\sin^2 a} \right) - 5 \right] \sqrt{\sin^2 a - \cos^2 \theta_b} \right\} \quad (98)$$

$$(III) \quad \pi/2 \leq a \leq (\pi/2 + \theta_b)$$

$$C_N = \frac{2KR^2}{S} \int_{a-\pi/2}^{\theta_b} \int_{\phi_0}^{\pi/2} \cos^2 \eta \sin^2 \theta \sin \phi \, d\phi \, d\theta \quad (99)$$

This equation reduces to Eq. (98).

To make the spherical segment compatible with the cone frustum, let $\theta_b = \pi/2 - \delta$. Then from Eqs. (96) and (98), for $0 \leq a \leq \delta$,

$$C_N \frac{S}{KR^2} = \frac{\pi}{2} \cos a \sin a \cos^4 \delta \quad (100)$$

and for $\delta \leq a \leq (\pi - \delta)$

$$C_N \frac{S}{KR^2} = \frac{\sin a}{2} \left\{ \cos^{-1} \left(\frac{\sin \delta}{\sin a} \right) + \cos a \cos^4 \delta \left[\frac{\pi}{2} + \sin^{-1} \left(\frac{\tan \delta}{\tan a} \right) \right] \right. \\ \left. + \frac{\sin \delta}{3} \left[\sin^2 \delta \left(3 - \frac{1}{\sin^2 a} \right) - 5 \right] \sqrt{\sin^2 a - \sin^2 \delta} \right\} \quad (101)$$

For $(\pi - \delta) \leq a \leq \pi$, $C_N = 0$.

Equations (100) and (101) were evaluated for $a = 0$ to 180 deg and $\delta = 0$ to 70 deg, and the results are presented in Figs. 6a and b.

2.2.1.2 Axial-Force Coefficient

The axial-force coefficient is given by

$$C_A = \frac{KR^2}{S} \iint_A \cos^2 \eta \cos \theta \sin \theta \, d\phi \, d\theta \quad (102)$$

Evaluating Eq. (102) for the three cases:

$$(I) \quad 0 \leq a \leq (\pi/2 - \theta_b)$$

$$C_A = \frac{2KR^2}{S} \int_0^{\theta_b} \int_{-\pi/2}^{\pi/2} \cos^2 \eta \cos \theta \sin \theta \, d\phi \, d\theta \quad (103)$$

so

$$C_A \frac{S}{KR^2} = \frac{\pi}{2} \left(\frac{\sin^2 a \sin^4 \theta_b}{2} - \cos^2 a \cos^4 \theta_b + \cos^2 a \right) \quad (104)$$

$$(II) \quad (\pi/2 - \theta_b) \leq a \leq \pi/2$$

$$C_A = \frac{2KR^2}{S} \left[\int_0^{\pi/2-a} \int_{-\pi/2}^{\pi/2} \cos^2 \eta \cos \theta \sin \theta \, d\phi \, d\theta \right. \\ \left. + \int_{\pi/2-a}^{\theta_b} \int_{\phi_0}^{\pi/2} \cos^2 \eta \cos \theta \sin \theta \, d\phi \, d\theta \right] \quad (105)$$

then

$$C_A \frac{S}{KR^2} = \frac{1}{2} \left\{ \cos a \cos^{-1} \left(\frac{\cos \theta_b}{\sin a} \right) + \left(\frac{\sin^2 a \sin^4 \theta_b}{2} \right. \right. \\ \left. \left. - \cos^2 a \cos^4 \theta_b + \cos^2 a \right) \left[\frac{\pi}{2} + \sin^{-1} \left(\frac{1}{\tan a \tan \theta_b} \right) \right] \right. \\ \left. + \frac{\cos a \cos \theta_b}{2} (1 - 3 \cos^2 \theta_b) \sqrt{\sin^2 a - \cos^2 \theta_b} \right\} \quad (106)$$

$$(III) \quad \pi/2 \leq a \leq (\pi/2 + \theta_b)$$

The equation for this case reduces to Eq. (106). Letting $\theta_b = \pi/2 - \delta$, Eqs. (104) and (106) give for $0 \leq a \leq \delta$.

$$C_A \frac{S}{KR^2} = \frac{\pi}{2} \left(\frac{\sin^2 a \cos^4 \delta}{2} - \cos^2 a \sin^4 \delta + \cos^2 a \right) \quad (107)$$

and for $\delta \leq a \leq (\pi - \delta)$

$$C_A \frac{S}{KR^2} = \frac{1}{2} \left\{ \cos a \cos^{-1} \left(\frac{\sin \delta}{\sin a} \right) \right. \\ \left. + \left(\frac{\sin^2 a \cos^4 \delta}{2} - \cos^2 a \sin^4 \delta + \cos^2 a \right) \left[\frac{\pi}{2} + \sin^{-1} \left(\frac{\tan \delta}{\tan a} \right) \right] \right. \\ \left. + \frac{\cos a \sin \delta}{2} (1 - 3 \sin^2 \delta) \sqrt{\sin^2 a - \sin^2 \delta} \right\} \quad (108)$$

For $(\pi - \delta) \leq a \leq \pi$, $C_A = 0$.

The numerical evaluation of Eqs. (107) and (108) is presented in Fig. 6c.

2.2.1.3 Pitching-Moment Coefficient

The resultant force acts through the center of curvature, and the pitching moment about the reference point is zero.

2.2.1.4 Side-Force Coefficient Derivative

A general relation for the side-force coefficient derivative for all bodies of revolution can be obtained. Consider an axisymmetric body

AEDC-TDR-64-25

which is pitched through an angle α' relative to the free-stream velocity and is then rolled through an angle Φ about the X-axis as shown in Fig. H.

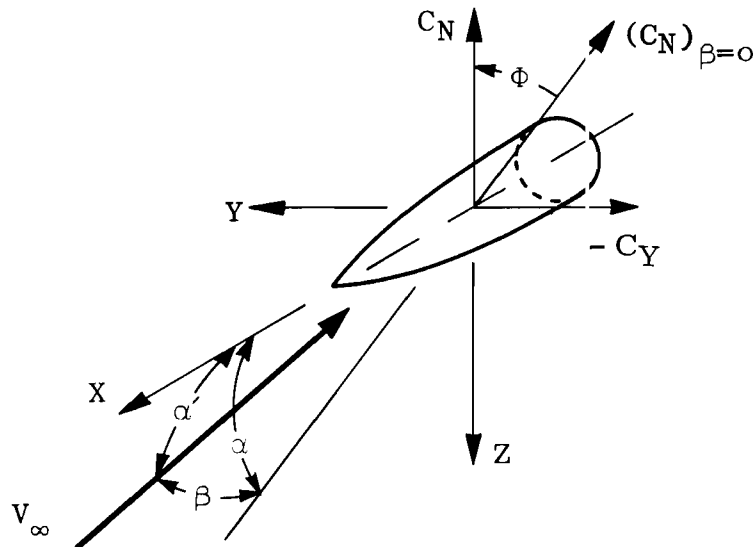


Fig. H Force Coefficients on Body of Revolution at Combined Angles of Attack and Sideslip

The force acting normal to the X-axis in the X, V_∞ -plane is defined, in coefficient form, as $(C_N)_{\beta=0}$ and remains constant as the body is rolled. Then

$$C_Y = - (C_N)_{\beta=0} \sin \Phi \quad (109)$$

By resolving the velocity vector \bar{V}_∞ along the body X-, Y-, and Z- axes, it can be shown that

$$\tan \Phi = \frac{\tan \beta}{\sin \alpha} \quad (110)$$

or

$$\sin \Phi = \frac{\tan \beta}{\sqrt{\tan^2 \beta + \sin^2 \alpha}} \quad (110a)$$

Then,

$$C_Y = - (C_N)_{\beta=0} \frac{\tan \beta}{\sqrt{\tan^2 \beta + \sin^2 \alpha}} \quad (111)$$

Differentiating with respect to β and then letting $\beta = 0$ gives

$$\left(C_{Y\beta} \right)_{\beta=0} = \frac{-C_N}{\sin \alpha} \quad (112)$$

Thus, $C_{Y\beta}$ may be obtained from Eqs. (100) and (101). At $\alpha = 0$, $C_{Y\beta}$ is determined by substituting Eq. (100) into Eq. (112) and then letting $\alpha = 0$. Thus,

$$(C_{Y\beta})_{\alpha=0} = \frac{-\pi KR^2 \cos^4 \delta}{2S} \tag{113}$$

The numerical evaluation of Eqs. (112) and (113) is presented in Figs. 6d and e.

2.2.1.5 Yawing- and Rolling-Moment Coefficient Derivatives

As was the case with pitching moment, the yawing- and rolling-moment coefficients and their derivatives are zero at the moment reference point.

2.2.2 Flat-Topped Spherical Segment

The geometry of the flat-topped spherical segment is shown in Fig. I.

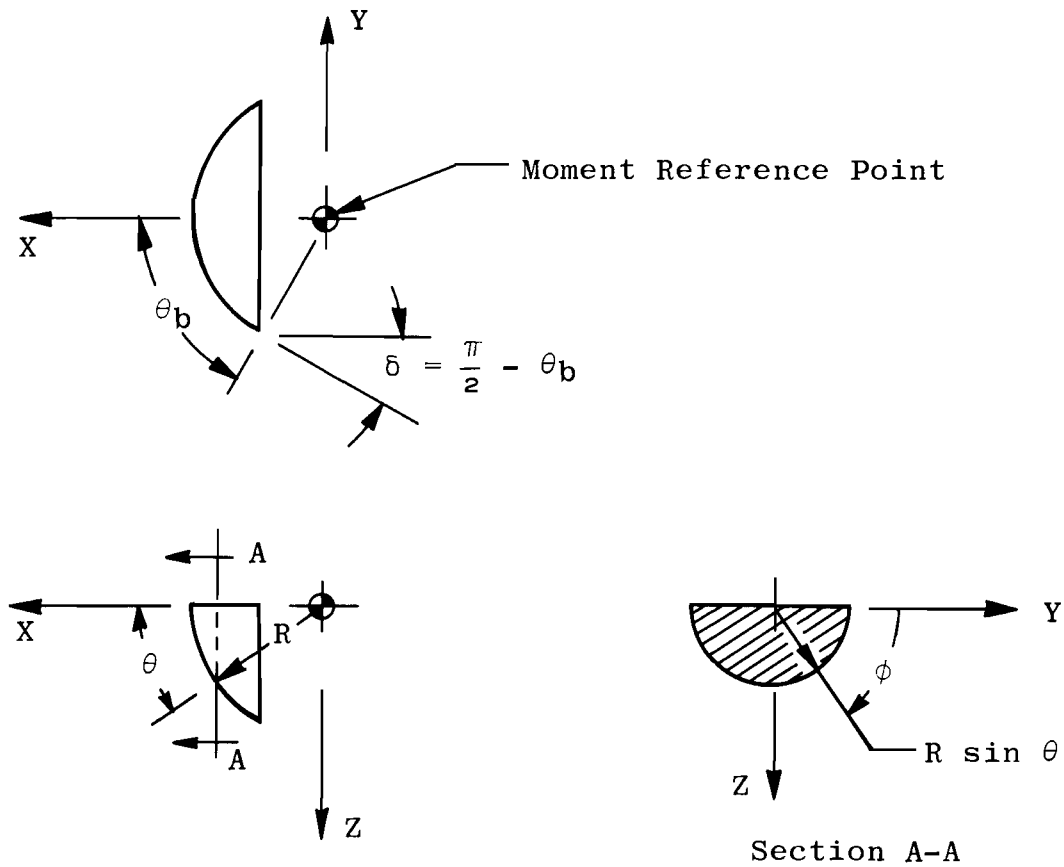


Fig. I Flat-Topped Spherical Segment

AEDC-TDR-64-25

The direction cosines, pressure coefficient, and elemental area are the same as for the complete spherical segment. For $0 \leq a \leq \pi/2$ the limits of integration on ϕ are from 0 to $\pi/2$ and the limits on θ are from 0 to θ_b . Then, from Eqs. (94) and (102), with $\theta_b = (\pi/2 - \delta)$,

$$C_N \frac{S}{KR^2} = \frac{1}{2} \left[\left(\frac{1 + \sin^2 a}{2} \right) \left(\frac{\pi}{2} - \delta \right) + \frac{\pi}{2} \cos a \sin a \cos^4 \delta \right. \\ \left. + \frac{\sin \delta \cos \delta}{2} \left(2 \cos^2 \delta - 1 - \sin^2 a - \frac{10}{3} \sin^2 a \cos^2 \delta \right) \right] \quad (114)$$

$$C_A \frac{S}{KR^2} = \frac{1}{2} \left[\frac{\pi}{2} \cos^2 a (1 - \sin^4 \delta) + \frac{\pi}{4} \sin^2 a \cos^4 \delta \right. \\ \left. + \cos a \sin a \left(\frac{\pi}{2} - \delta - \sin \delta \cos \delta + 2 \sin \delta \cos^3 \delta \right) \right] \quad (115)$$

where δ is in radians.

Equations (112) and (113) apply only to complete bodies of revolution, and $C_{Y\beta}$ for the flat-topped spherical segment must be obtained from Eq. (9) which gives

$$C_Y = - \frac{KR^2}{S} \iint_A \cos^2 \eta \sin^2 \theta \cos \phi \, d\phi \, d\theta \quad (116)$$

For the right side of the segment

$$C_{Y\beta} = - \frac{KR^2}{S} \int_0^{\theta_b} \int_0^{\pi/2} \left(\frac{\partial \cos^2 \eta}{\partial \beta} \right)_{\beta=0} \sin^2 \theta \cos \phi \, d\phi \, d\theta \quad (117)$$

where

$$\left(\frac{\partial \cos^2 \eta}{\partial \beta} \right)_{\beta=0} = 2 \cos \phi \sin \theta (\cos a \cos \theta + \sin a \sin \theta \sin \phi) \quad (118)$$

Substituting Eq. (118) in Eq. (117) shows that $C_{Y\beta}$ is the same for both sides of the segment. Then, multiplying Eq. (117) by 2 and performing the integrations, with $\theta_b = (\pi/2 - \delta)$,

$$C_{Y\beta} \frac{S}{KR^2} = - \frac{1}{2} \left[\frac{\pi}{2} \cos a \cos^4 \delta + \sin a \left(\frac{\pi}{2} - \delta - \sin \delta \cos \delta - \frac{2}{3} \sin \delta \cos^3 \delta \right) \right] \quad (119)$$

The moment coefficients and their derivatives are zero for the indicated reference point. For $a \geq \pi/2$ the equations for the complete spherical segment also apply to the flat-topped spherical segment. The characteristics of the flat-topped spherical segment are presented in Fig. 7.

2.2.3 Hemisphere

Although the hemisphere is a limiting case of either the spherical wedge ($\Lambda = 90$ deg) or the spherical segment ($\delta = 0$ deg), the body is of

enough interest to warrant a presentation of the equations. Letting $\delta = 0$ in Eqs. (101), (108), and (112) gives, for $0 \leq a \leq \pi$,

$$C_N \frac{S}{K R^2} = \frac{\pi}{4} \sin a (1 + \cos a) \tag{120}$$

$$C_A \frac{S}{K R^2} = \frac{\pi}{8} (1 + \cos a)^2 \tag{121}$$

$$C_{Y\beta} \frac{S}{K R^2} = - \frac{\pi}{4} (1 + \cos a) \tag{122}$$

The moment coefficients and their derivatives are zero for a moment reference point at the center of curvature. The characteristics of the hemisphere are presented in Figs. 2 and 6.

2.2.4 Flat-Topped Hemisphere

For $0 \leq a \leq \pi/2$ and $\delta = 0$, Eqs. (114), (115), and (119) give

$$C_N \frac{S}{K R^2} = \frac{\pi}{8} (1 + 2 \cos a \sin a + \sin^2 a) \tag{123}$$

$$C_A \frac{S}{K R^2} = \frac{\pi}{8} (1 + 2 \cos a \sin a + \cos^2 a) \tag{124}$$

$$C_{Y\beta} \frac{S}{K R^2} = - \frac{\pi}{4} (\cos a + \sin a) \tag{125}$$

The moment coefficients and their derivatives are zero for a moment reference point at the center of curvature. For $a \geq \pi/2$ the equations for the full hemisphere apply. The characteristics of the flat-topped hemisphere are presented in Figs. 3 and 7.

2.2.5 Cone Frustum

The cone frustum is frequently used as a nose or flare section of lifting bodies. The nomenclature used in the derivation is shown in Fig. J

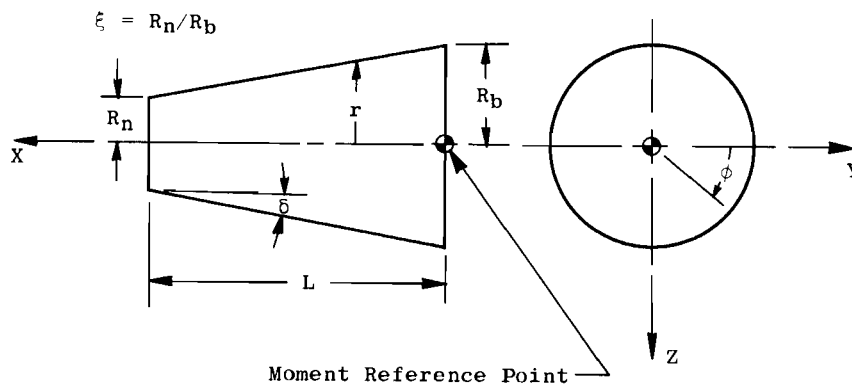


Fig. J Cone Frustum

AEDC-TDR-64-25

The direction cosines of the inward directed unit normal vector are

$$\left. \begin{aligned} \cos(n, x) &= -\sin \delta \\ \cos(n, y) &= -\cos \delta \cos \phi \\ \cos(n, z) &= -\cos \delta \sin \phi \end{aligned} \right\} \quad (126)$$

Then, from Eq. (5)

$$\cos \eta = \cos \beta (\cos \alpha \sin \delta + \sin \alpha \cos \delta \sin \phi) + \sin \beta \cos \delta \cos \phi \quad (127)$$

At $\beta = 0$ the surface becomes shielded from the flow along a line defined by $\phi = \phi_0$, where

$$\phi_0 = -\sin^{-1} \left(\frac{\tan \delta}{\tan \alpha} \right) \quad (128)$$

This equation is valid only for $\alpha \geq \delta$, since there is no shielding of the surface for $\alpha \leq \delta$. The elemental surface area is

$$dA = \frac{r \, d\phi \, dr}{\sin \delta} \quad (129)$$

It is assumed that $C_p = 0$ on the flat surfaces, and the coefficients and their derivatives are evaluated at $\beta = 0$.

2.2.5.1 Normal-Force Coefficient

The normal-force coefficient is given by

$$C_N = \frac{K}{S \tan \delta} \int_{\phi} \int_{R_n}^{R_b} r \cos^2 \eta \sin \phi \, dr \, d\phi \quad (130)$$

Since ϕ_0 is not a function of r , the first integral may be evaluated to give

$$C_N = \frac{K L R_b (1 + \xi)}{2 S} \int_{\phi} \cos^2 \eta \sin \phi \, d\phi \quad (131)$$

where $\xi = R_n/R_b$.

Because of the limitations on the shielding equation, the integration of Eq. (131) must be treated as two separate cases. In each case, the integration is taken over the right side of the body and the result is multiplied by 2.

(I) $0 \leq \alpha \leq \delta$

$$C_N = \frac{K L R_b (1 + \xi)}{S} \int_{-\pi/2}^{\pi/2} \cos^2 \eta \sin \phi \, d\phi \quad (132)$$

which gives

$$C_N \frac{S}{K L R_b (1 + \xi)} = \pi \cos \alpha \sin \alpha \sin \delta \cos \delta \quad (133)$$

$$(II) \quad \delta \leq \alpha \leq (\pi - \delta)$$

$$C_N = \frac{K L R_b (1 + \xi)}{S} \int_{\phi_0}^{\pi/2} \cos^2 \eta \sin \phi \, d\phi \quad (134)$$

which gives

$$C_N \frac{S}{K L R_b (1 + \xi)} = \cos \alpha \sin \alpha \sin \delta \cos \delta \left[\frac{\pi}{2} + \sin^{-1} \left(\frac{\tan \delta}{\tan \alpha} \right) \right] \\ + \left(\frac{2 \sin^2 \alpha \cos^2 \delta + \sin^2 \delta \cos^2 \alpha}{3 \sin \alpha \cos \delta} \right) \sqrt{\sin^2 \alpha - \sin^2 \delta} \quad (135)$$

At $(\pi - \delta) \leq \alpha \leq \pi$, $C_N = 0$. Equations (133) and (135) were evaluated for $\alpha = 0$ to 180 deg and $\delta = 0$ to 40 deg, and the results are presented in Fig. 8a.

2.2.5.2 Axial-Force Coefficient

The axial-force coefficient is given by

$$C_A = \frac{K}{S} \int_{\phi} \int_{R_n}^{R_b} r \cos^2 \eta \, dr \, d\phi \quad (136)$$

Integrating over r ,

$$C_A = \frac{K L R_b (1 + \xi)}{2 S} \tan \delta \int_{\phi} \cos^2 \eta \, d\phi \quad (137)$$

Evaluating Eq. (137) for the two cases:

$$(I) \quad 0 \leq \alpha \leq \delta$$

$$C_A = \frac{K L R_b (1 + \xi)}{S} \tan \delta \int_{-\pi/2}^{\pi/2} \cos^2 \eta \, d\phi \quad (138)$$

which gives

$$C_A \frac{S}{K L R_b (1 + \xi)} = \frac{\pi \tan \delta}{2} (2 \cos^2 \alpha \sin^2 \delta + \sin^2 \alpha \cos^2 \delta) \quad (139)$$

$$(II) \quad \delta \leq \alpha \leq (\pi - \delta)$$

$$C_A = \frac{K L R_b (1 + \xi)}{S} \tan \delta \int_{\phi_0}^{\pi/2} \cos^2 \eta \, d\phi \quad (140)$$

which gives

$$C_A \frac{S}{K L R_b (1 + \xi)} = \frac{\tan \delta}{2} \left\{ (2 \cos^2 \alpha \sin^2 \delta + \sin^2 \alpha \cos^2 \delta) \left[\frac{\pi}{2} + \sin^{-1} \left(\frac{\tan \delta}{\tan \alpha} \right) \right] \right. \\ \left. + 3 \cos \alpha \sin \delta \sqrt{\sin^2 \alpha - \sin^2 \delta} \right\} \quad (141)$$

AEDC-TDR-64-25

At $(\pi - \delta) \leq \alpha \leq \pi$, $C_A = 0$. The numerical evaluation of Eqs. (139) and (141) are presented in Figs. 8b and c.

2.2.5.3 Pitching-Moment Coefficient

The pitching-moment coefficient is given by

$$C_m = \frac{K}{S l} \left[\int_{\phi} \int_{R_n}^{R_b} \frac{r (R_b - r) \cos^2 \eta \sin \phi}{\tan^2 \delta} dr d\phi - \int_{\phi} \int_{R_n}^{R_b} r^2 \cos^2 \eta \sin \phi dr d\phi \right] \quad (142)$$

Integrating over r ,

$$C_m = \frac{K}{S l} \left[\frac{1}{\tan^2 \delta} \left(\frac{r^2 R_b}{2} - \frac{r^3}{3} \right) - \frac{r^3}{3} \right]_{R_n}^{R_b} \int_{\phi} \cos^2 \eta \sin \phi d\phi \quad (143)$$

Substituting Eq. (131) into Eq. (143) gives

$$C_m = C_N \frac{R_b}{l \tan \delta} \left[1 - \frac{2}{3 \cos^2 \delta} \frac{(1 - \xi^3)}{(1 - \xi^2)} \right] \quad (144)$$

Since the limits of integration on ϕ do not enter into this derivation, Eq. (144) is valid for $0 \leq \alpha \leq \pi$.

2.2.5.4 Side-Force Coefficient Derivative

The side-force coefficient derivative is given by Eq. (112),

$$C_{Y\beta} = - \frac{C_N}{\sin \alpha} \quad (145)$$

and $C_{Y\beta}$ may be obtained from Eqs. (133) and (135). For $\alpha = 0$, substituting Eq. (133) into Eq. (145) gives

$$\left(C_{Y\beta} \right)_{\alpha=0} = \frac{S}{K L R_b (1 + \xi)} = - \pi \sin \delta \cos \delta \quad (146)$$

The numerical evaluation of Eqs. (145) and (146) is presented in Fig. 8d.

2.2.5.5 Yawing-Moment Coefficient Derivative

It is obvious from Eq. (145) that a general relation for all bodies of revolution is

$$C_{n\beta} = - \frac{C_m}{\sin \alpha} \quad (147)$$

Substituting Eqs. (144) and (145) in Eq. (147) gives

$$C_{n\beta} = C_{Y\beta} \frac{R_b}{l \tan \delta} \left[1 - \frac{2}{3 \cos^2 \delta} \frac{(1 - \xi^3)}{(1 - \xi^2)} \right] \quad (148)$$

Like Eq. (144), this equation is valid for $0 \leq a \leq \pi$.

2.2.5.6 Rolling-Moment Coefficient Derivative

The resultant force acts through the center of the cone, and there is no rolling moment about the indicated reference point. Therefore, $C_{\ell\beta} = 0$.

2.2.6 Flat-Topped Cone Frustum

The geometry of the flat-topped cone frustum is shown in Fig. K.

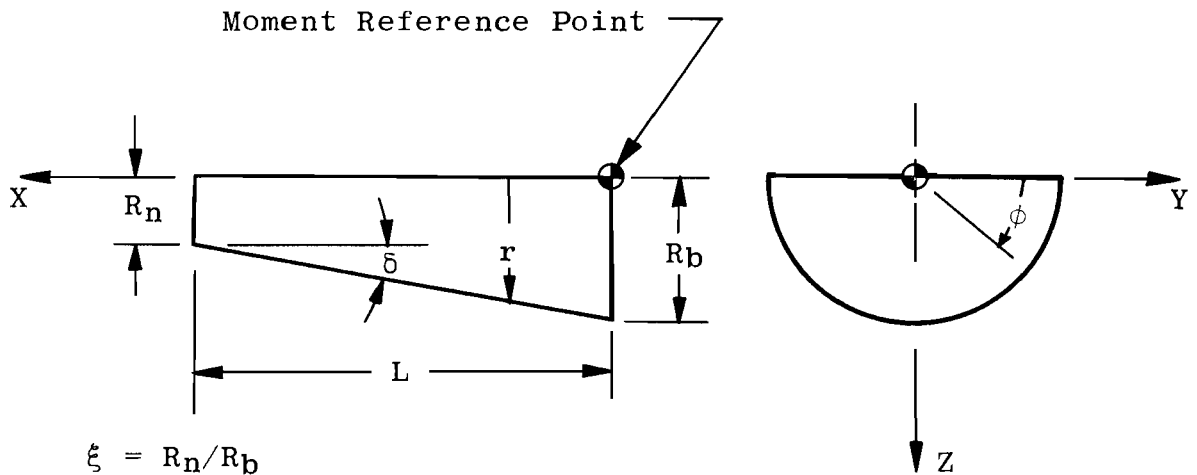


Fig. K Flat-Topped Cone Frustum

The direction cosines, pressure coefficient, and elemental area are the same as for the complete cone frustum. For $0 \leq a \leq \pi/2$, the limits of integration on ϕ are from 0 to $\pi/2$. Then, from Eq. (131) and (137)

$$C_N \frac{S}{K L R_b (1 + \xi)} = \frac{\pi}{2} \cos a \sin a \sin \delta \cos \delta + \cos^2 a \sin^2 \delta + \frac{2}{3} \sin^2 a \cos^2 \delta \quad (149)$$

and

$$C_A \frac{S}{K L R_b (1 + \xi)} = \tan \delta \left[2 \cos a \sin a \sin \delta \cos \delta + \frac{\pi}{2} \left(\cos^2 a \sin^2 \delta + \frac{\sin^2 a \cos^2 \delta}{2} \right) \right] \quad (150)$$

Equations (145) and (146) apply only to the complete cone frustum, and $C_{Y\beta}$ for the flat-topped cone frustum must be obtained from Eq. (9).

AEDC-TDR-64-25

For the right side of the cone frustum,

$$C_Y = - \frac{K}{S \tan \delta} \int_0^{\pi/2} \int_{R_n}^{R_b} r \cos^i \eta \cos \phi \, dr \, d\phi \quad (151)$$

and

$$C_{Y\beta} = - \frac{K L R_b (1 + \xi)}{2 S} \int_0^{\pi/2} \left(\frac{\partial \cos^2 \eta}{\partial \beta} \right)_{\beta=0} \cos \phi \, d\phi \quad (152)$$

where

$$\left(\frac{\partial \cos^2 \eta}{\partial \beta} \right)_{\beta=0} = 2 \cos \delta \cos \phi (\cos \alpha \sin \delta + \sin \alpha \cos \delta \sin \phi) \quad (153)$$

Since $C_{Y\beta}$ is the same for both sides of the cone frustum, Eq. (152) is multiplied by 2 and integrated to give

$$C_{Y\beta} \frac{S}{K L R_b (1 + \xi)} = - \frac{\pi}{2} \cos \alpha \sin \delta \cos \delta - \frac{2}{3} \sin \alpha \cos^2 \delta \quad (154)$$

The pitching-moment coefficient and yawing-moment coefficient derivative are given by Eqs. (144) and (148), respectively, with C_N and $C_{Y\beta}$ determined from Eqs. (149) and (154). The rolling-moment coefficient derivative is zero. For $\alpha \geq \pi/2$ the equations for the complete cone frustum apply to the flat-topped cone frustum. The characteristics of the flat-topped cone frustum are presented in Fig. 9.

2.2.7 Circular Cylinder

The circular cylinder is a special case of the cylindrical leading edge ($\Lambda = 90 \text{ deg}$) and the cone frustum ($\delta = 0$ and $\xi = 1$). Letting $\Lambda = 90 \text{ deg}$ in Eqs. (38), (42), (43), (49), (50), and (55) gives

$$C_N \frac{S}{K L R} = \frac{4}{3} \sin^2 \alpha \quad (155)$$

$$C_A = 0 \quad (156)$$

$$C_m = C_N \frac{L}{2 l} \quad (157)$$

$$C_{Y\beta} \frac{S}{K L R} = - \frac{4}{3} \sin \alpha \quad (158)$$

$$C_{n\beta} = C_{Y\beta} \frac{L}{2 l} \quad (159)$$

$$C_{l\beta} = 0 \quad (160)$$

where the moment coefficients are referenced to the base of the cylinder. The characteristics of the circular cylinder are presented in Figs. 4 and 8. The Eqs. (155) through (160) also apply to the flat-topped circular cylinder.

2.3 COMPOSITE CONFIGURATIONS

The Newtonian analysis is based on the local flow deflection angle and assumes that the only interference between components is that due to shielding. Therefore, the configuration being analyzed can be broken into independent elements corresponding to the components described in the previous sections. From the equations and charts, the aerodynamic characteristics of each component can be determined based on the reference area and length of the complete configuration. The contributions of the individual components are added together to give the total coefficients of the configuration. When this method is used to obtain the characteristics of a composite configuration, one component may be in a position where it shields another component from the flow, and the effects of this shielding must be considered.

The summation of moment coefficients and their derivatives requires a moment transfer from each component reference point to a common reference point. Let X_T and Z_T be the moment transfer distances, positive as shown in Fig. L.

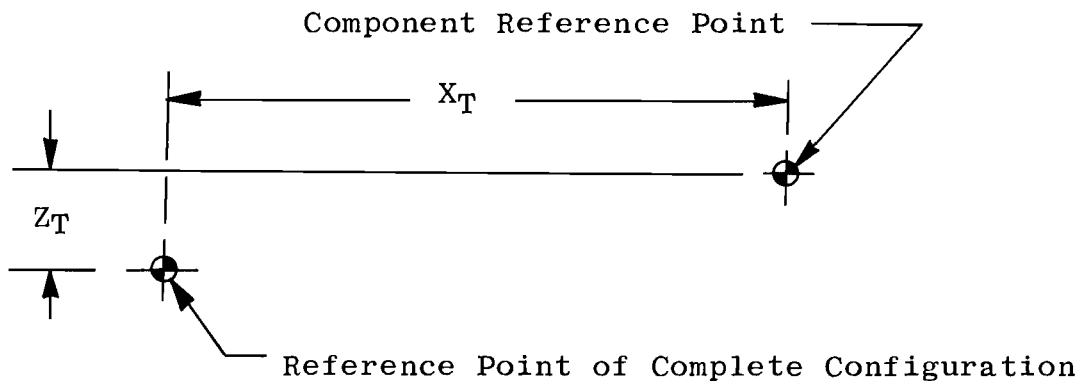


Fig. L Moment Transfer Lengths

Then,

$$C_{m_{\text{configuration}}} = C_{m_{\text{component}}} - C_N \frac{X_T}{l} + C_A \frac{Z_T}{l} \quad (161)$$

$$C_{n\beta_{\text{configuration}}} = C_{n\beta_{\text{component}}} - C_{Y\beta} \frac{X_T}{l} \quad (162)$$

$$C_{l\beta_{\text{configuration}}} = C_{l\beta_{\text{component}}} + C_{Y\beta} \frac{Z_T}{l} \quad (163)$$

The characteristics of a typical composite configuration are evaluated in the Appendix.

AEDC-TDR-64-25

REFERENCES

1. Penland, Jim A. "Aerodynamic Force Characteristics of a Series of Lifting Cone and Cone-Cylinder Configurations at a Mach Number of 6.83 and Angles of Attack up to 130°." NASA TN D-840, June 1961.
2. Ladson, Charles L. and Blackstock, Thomas A. "Air-Helium Simulation of the Aerodynamic Force Coefficients of Cones at Hypersonic Speeds." NASA TN D-1473, October 1962.
3. Neal, Luther, Jr. "Aerodynamic Characteristics at a Mach Number of 6.77 of a 9° Cone Configuration, with and without Spherical Afterbodies, at Angles of Attack up to 180° with Various Degrees of Nose Blunting." NASA TN D-1606, March 1963.
4. Fohrman, Melvin J. "Static Aerodynamic Characteristics of a Short Blunt 10° Semivertex Angle Cone at a Mach Number of 15 in Helium." NASA TN D-1648, February 1963.
5. Wells, William R. and Armstrong, William O. "Tables of Aerodynamic Coefficients Obtained from Developed Newtonian Expressions for Complete and Partial Conic and Spheric Bodies at Combined Angles of Attack and Sideslip with Some Comparisons with Hypersonic Experimental Data." NASA TR R-127, 1962.
6. Penland, Jim A. "Aerodynamic Characteristics of a Circular Cylinder at Mach Number 6.86 and Angles of Attack up to 90°." NACA TN 3861, January 1957.
7. Julius, Jerome D. "Experimental Pressure Distributions over Blunt Two- and Three-Dimensional Bodies Having Similar Cross Sections at a Mach Number of 4.95." NASA TN D-157, September 1959.
8. Bertram, Mitchel H. and Henderson, Arthur, Jr. "Recent Hypersonic Studies of Wings and Bodies." ARS Journal, Vol. 31, No. 8, August 1961, pp. 1129-1139.
9. Fisher, Lewis R. "Equations and Charts for Determining the Hypersonic Stability Derivatives of Combinations of Cone Frustums Computed by the Newtonian Impact Theory." NASA TN D-149, November 1959.
10. Rainey, Robert W. "Working Charts for Rapid Prediction of Force and Pressure Coefficients on Arbitrary Bodies of Revolution by Use of Newtonian Concepts." NASA TN D-176, December 1959.

11. Gray, J. Don. "Drag and Stability Derivatives of Missile Components According to the Modified Newtonian Theory." AEDC-TN-60-191, November 1960.
12. Margolis, Kenneth. "Theoretical Evaluation of the Pressures, Forces, and Moments at Hypersonic Speeds Acting on Arbitrary Bodies of Revolution Undergoing Separate and Combined Angle-of-Attack and Pitching Motions." NASA TN D-652, June 1961.
13. Malvestuto, Frank S., Jr., Sullivan, Phillip J., Marcy, William L., et al. "Study to Determine Aerodynamic Characteristics on Hypersonic Re-Entry Configurations: Analytical Phase, Design Charts." WADD-TR-61-56, Part II, Vol. 2, August 1962.
14. McDevitt, John B. and Rakich, John V. "The Aerodynamic Characteristics of Several Thick Delta Wings at Mach Numbers to 6 and Angles of Attack to 50°." (Title Unclassified) NASA TM X-162, March 1960. (Confidential)
15. Seaman, D. J. and Dore, F. J. "Force and Pressure Coefficients of Elliptic Cones and Cylinders in Newtonian Flow." Consolidated Vultee Aircraft Corporation, San Diego, California, ZA-7-004, May 16, 1952.
16. Jackson, Charlie M., Jr. "A Semigraphical Method of Applying Impact Theory to an Arbitrary Body to Obtain the Hypersonic Aerodynamic Characteristics at Angle of Attack and Side-slip." NASA TN D-795, May 1961.
17. Hayes, Wallace D. and Probstein, Ronald F. Hypersonic Flow Theory. Academic Press, New York, 1959.
18. Busemann, A. "Flüssigkeits-und-Gasbewegung." Handwörterbuch der Naturwissenschaften, Vol. IV, 2nd Edition, pp. 276-277, Gustav Fischer, Jena, 1933.
19. Love, Eugene S., Henderson, Arthur, Jr., and Bertram, Mitchel H. "Some Aspects of Air-Helium Simulation and Hypersonic Approximations." NASA TN D-49, October 1959.
20. Lees, Lester. "Hypersonic Flow." Fifth International Aeronautical Conference (Los Angeles, California, June 20-23, 1955), Institute of the Aeronautical Sciences, pp. 241-276.

APPENDIX

APPLICATION OF METHOD TO A TYPICAL DELTA WING

As an example of the use of the equations and charts given in this report, the aerodynamic characteristics of a typical delta wing were computed. The configuration which was analyzed is shown in Fig. 10, and the lengths, angles, and areas used in the calculations are given below:

(I) Spherical-wedge nose component

$$R = 0.0212 L_D \quad \Lambda = 75 \text{ deg}$$

$$X_T = -0.518 L_D$$

$$Z_T = 0$$

(II) Swept-cylinder leading edge component

$$R = 0.0212 L_D \quad \Lambda = 75 \text{ deg}$$

$$L = 0.950 L_D \quad \phi' = 74.5 \text{ deg}$$

$$X_T = 0.40 L_D$$

$$Z_T = 0$$

(III) Swept-wedge wing component

$$c = 0.940 L_D \quad \Lambda = 75 \text{ deg} \quad A_p/S = 0.888$$

$$t = 0.0675 L_D \quad \Gamma = 15 \text{ deg} \quad A_b/S = 0.064$$

$$h = 0.0205 L_D \quad \epsilon = 4.11 \text{ deg} \quad A_s/S = 0.119$$

$$X_T = 0.40 L_D$$

$$Z_T = 0$$

The coefficients were based on the planform area ($S = 0.267 L_D^2$), with the mean aerodynamic chord as reference length ($\ell = 0.667 L_D$) for the pitching-moment coefficient and the span as reference length ($\ell = 0.536 L_D$) for the yawing- and rolling-moment coefficients. For all angles of attack it was assumed that the base of the delta wing contributed no axial force, i. e., $C_{p_{base}} = 0$. The modified form of the pressure coefficient given by Eq. (2) was used with $K = 2$.

AEDC-TDR-64-25

The characteristics of the nose component were determined from Fig. 2 and the moment transfer equations, Eqs. (161), (162), and (163). Since ϕ' was not equal to 90 deg, it was necessary to use the equations of Section 2.1.3 and the moment-transfer equations to evaluate the leading-edge component. The wing component was evaluated with the equations of Section 2.1.5 and the moment-transfer equations.

The aerodynamic coefficients of each component and of the complete delta wing are presented in Fig. 11. To provide a comparison of the theory with hypersonic experimental results for this delta wing, data obtained in the 50-in. Mach 8 Gas Dynamic Wind Tunnel, Hypersonic (B) of the von Kármán Gas Dynamics Facility, Arnold Engineering Development Center, are also given. The data were obtained at a Mach number of 8.1 and free-stream Reynolds numbers of 1.3 to 5.2×10^6 based on model length. The theory predicts the experimental results with good accuracy at angles of attack up to about 57 deg, where the shock wave becomes detached. Above this angle of attack, the theory will give better agreement with the experimental data if $K = C_{p_{max}} = 1.83$ is used.

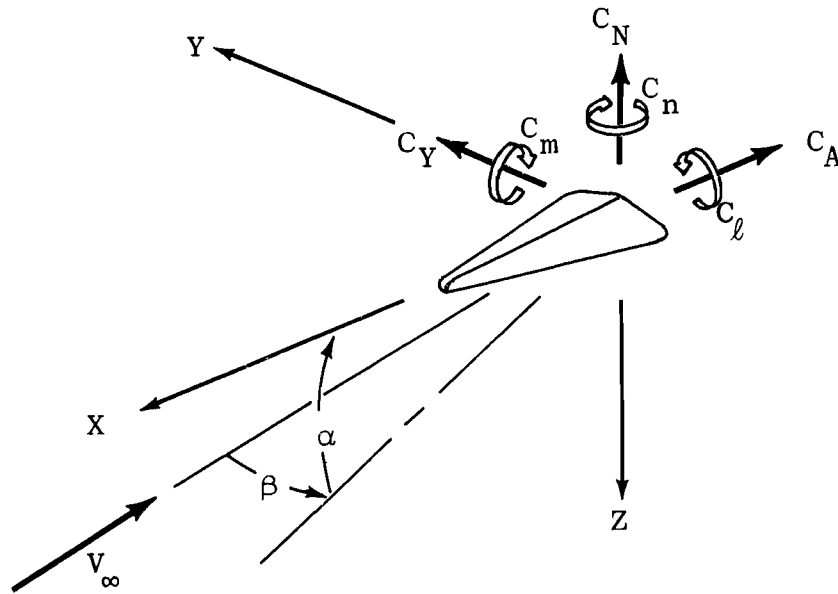
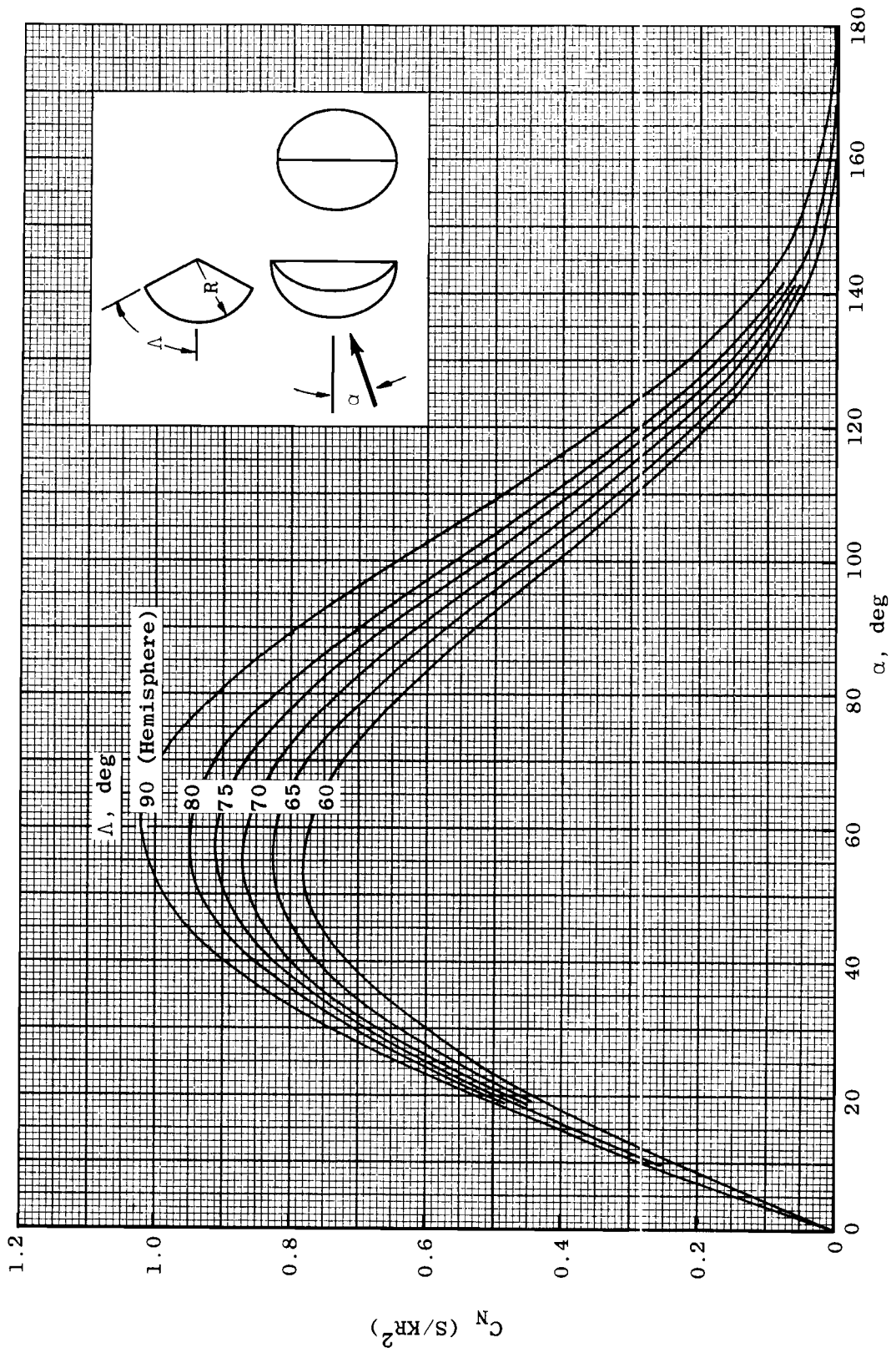
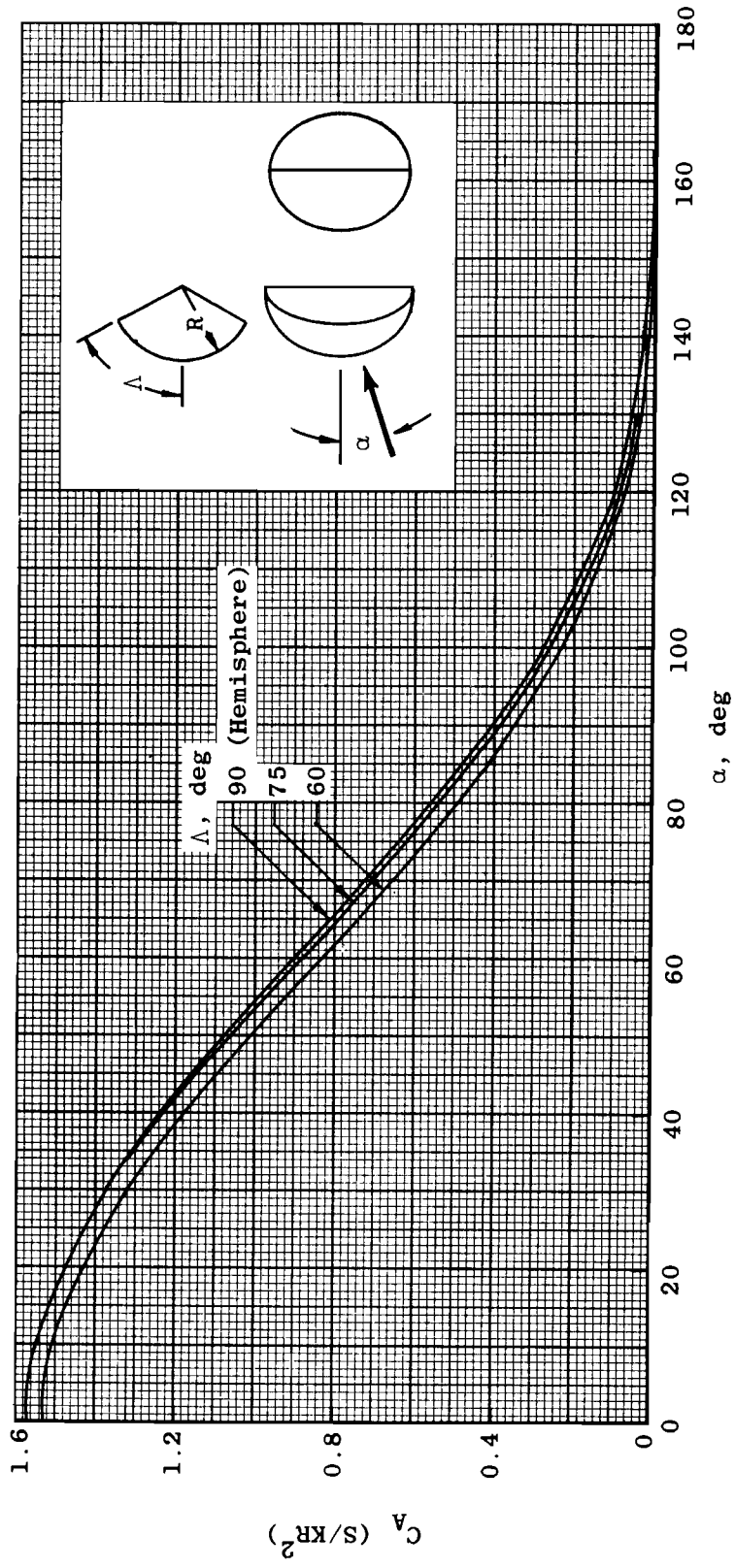


Fig. 1 Axis and Coefficient Nomenclature



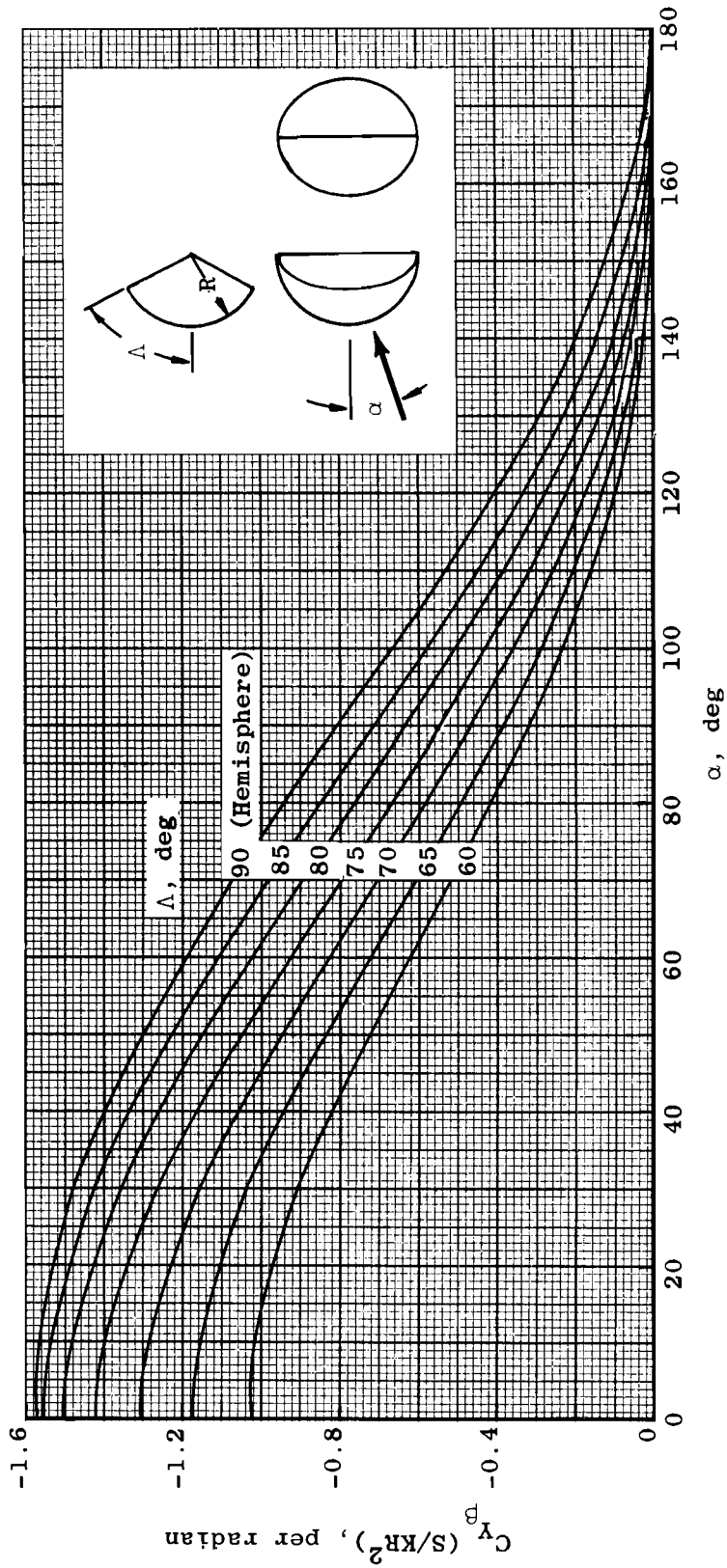
a. Normal Force
Fig. 2 Aerodynamic Characteristics of Spherical-Wedge Noses



b. Axial Force

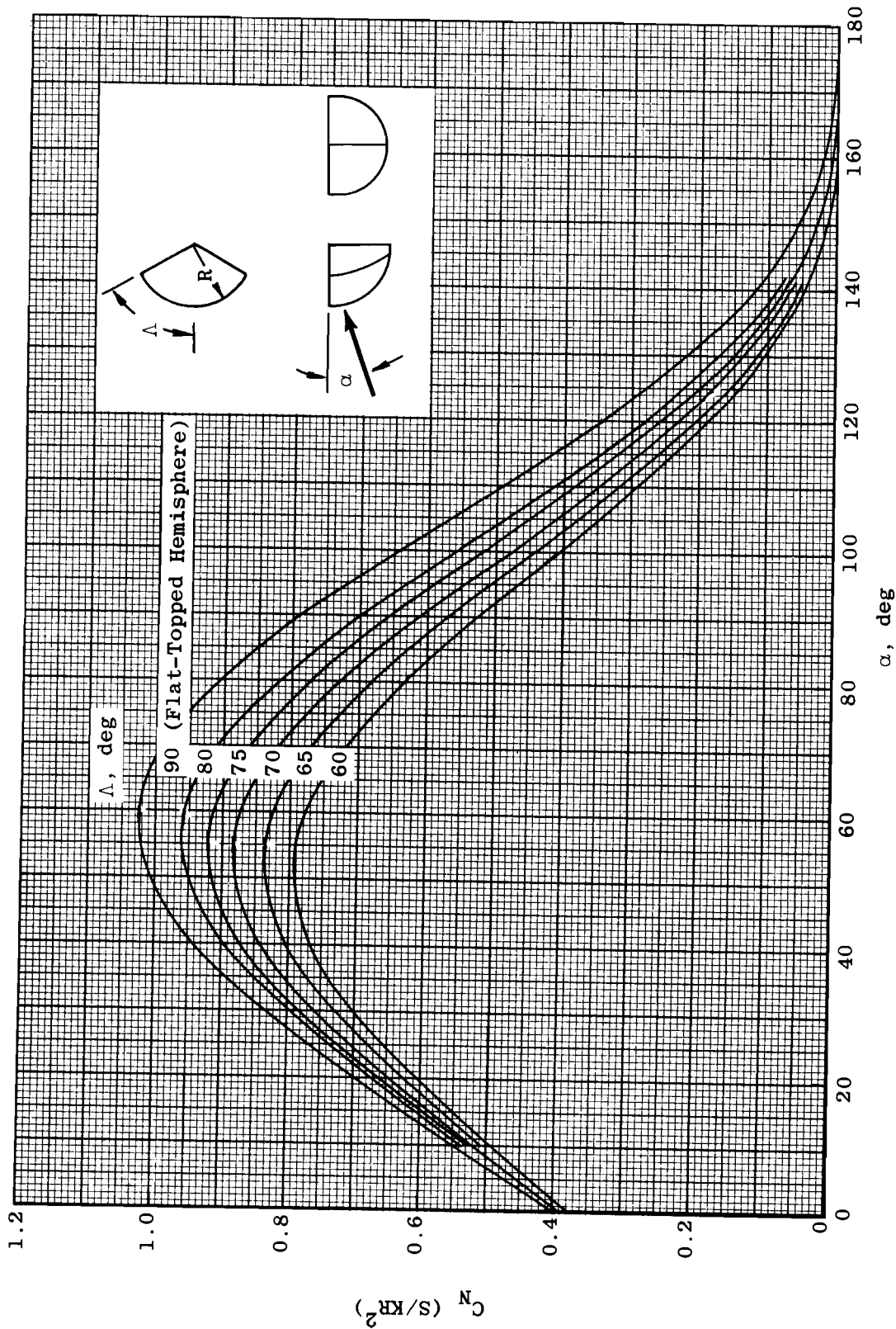
Fig. 2 Continued

AEDC-TDR-64-25



c. Side-Force Derivative, $\beta = 0$

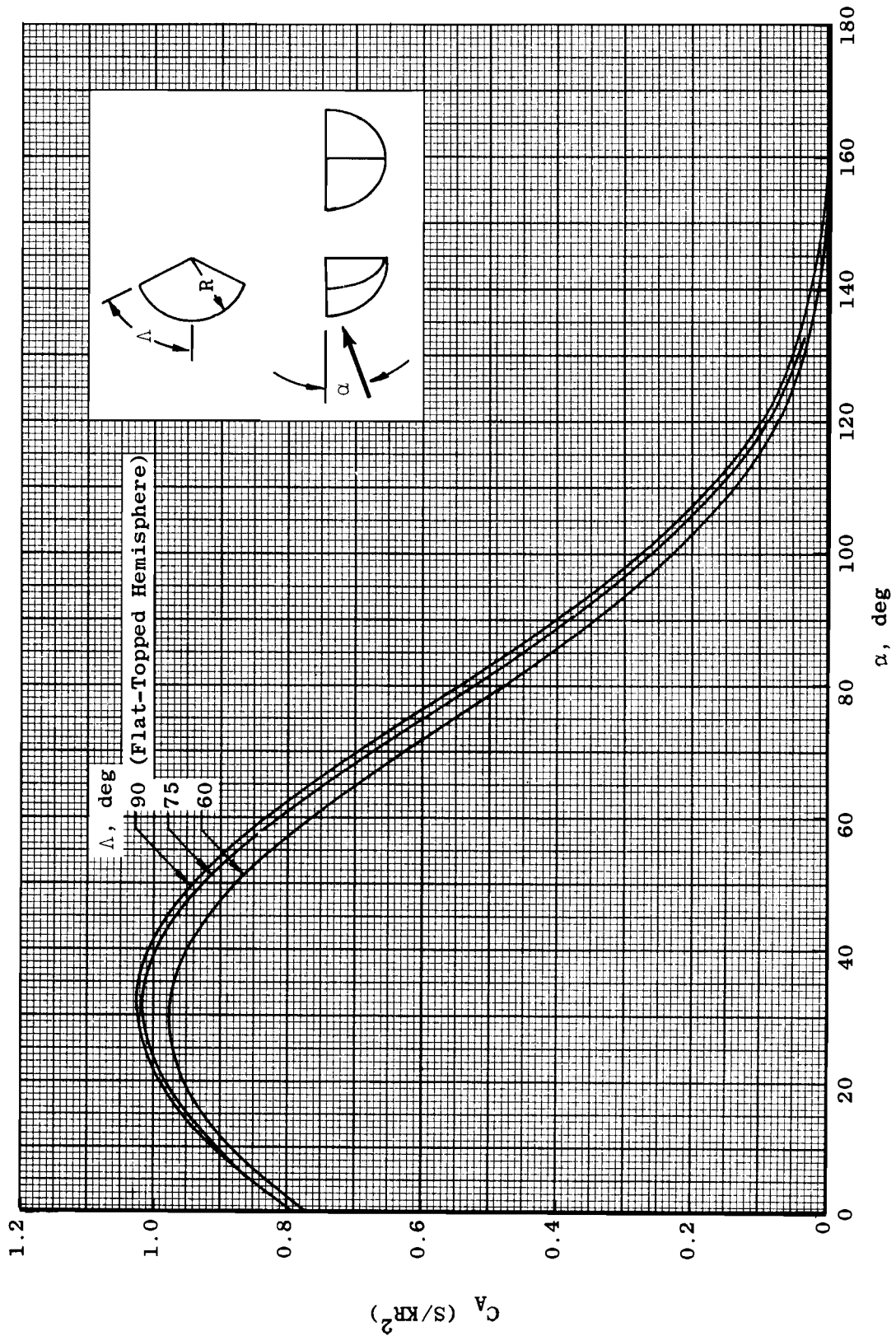
Fig. 2 Concluded



a. Normal Force

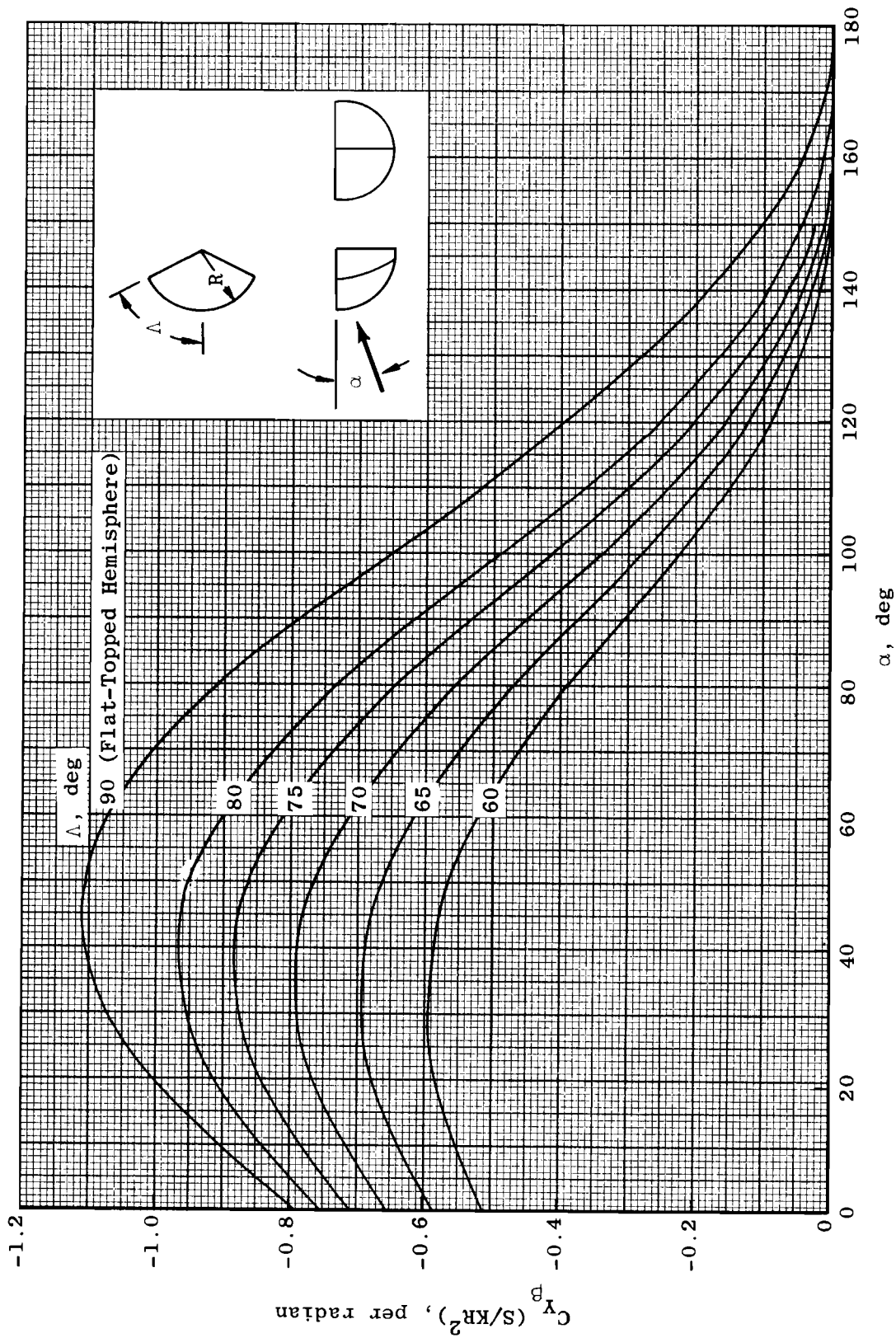
Fig. 3 Aerodynamic Characteristics of Flat-Topped Spherical-Wedge Noses

AEDC-TDR-64-25



b. Axial Force

Fig. 3 Continued



c. Side-Force Derivative, $\beta = 0$

Fig. 3 Concluded

AEDC-TDR-64-25

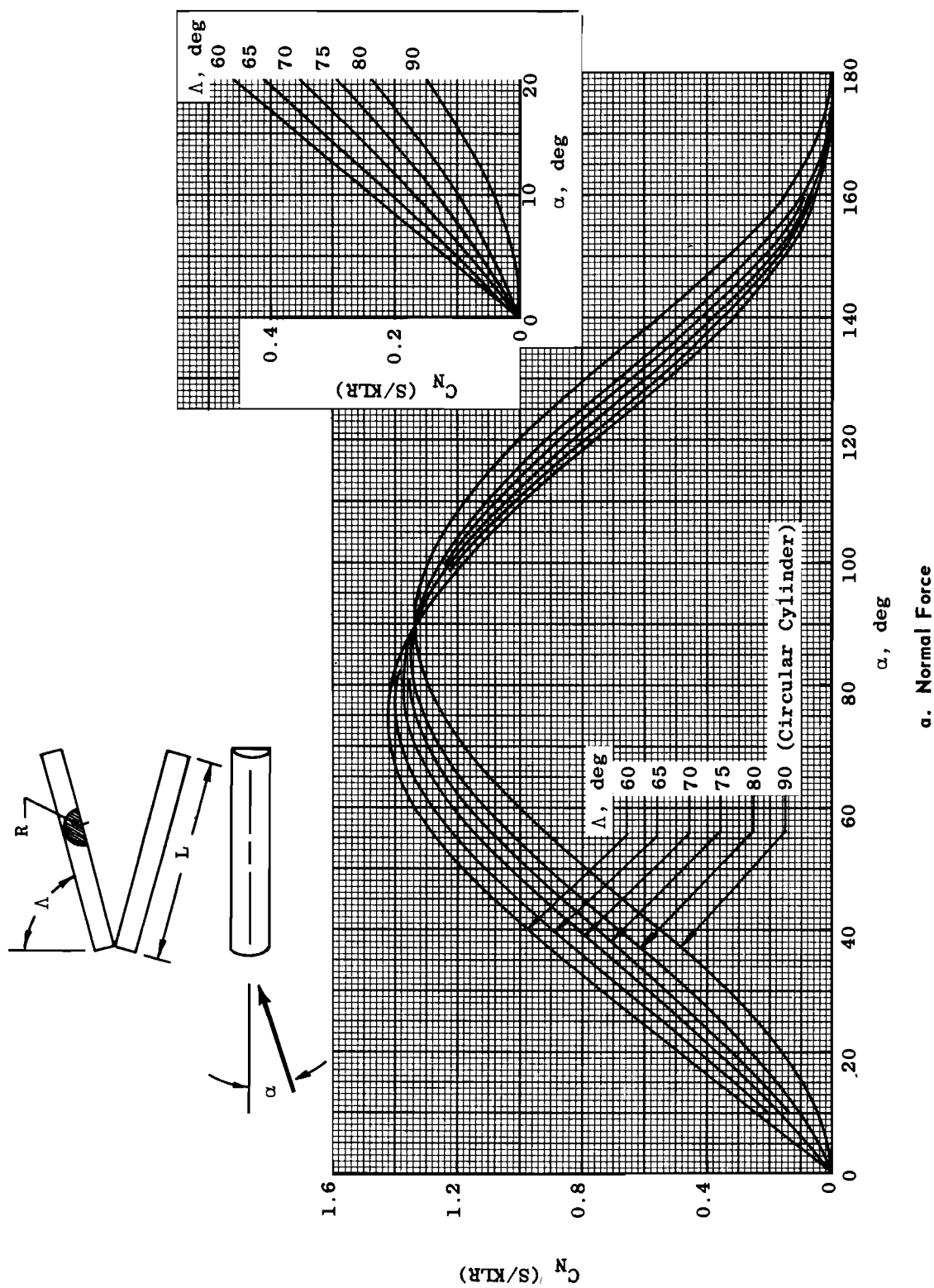
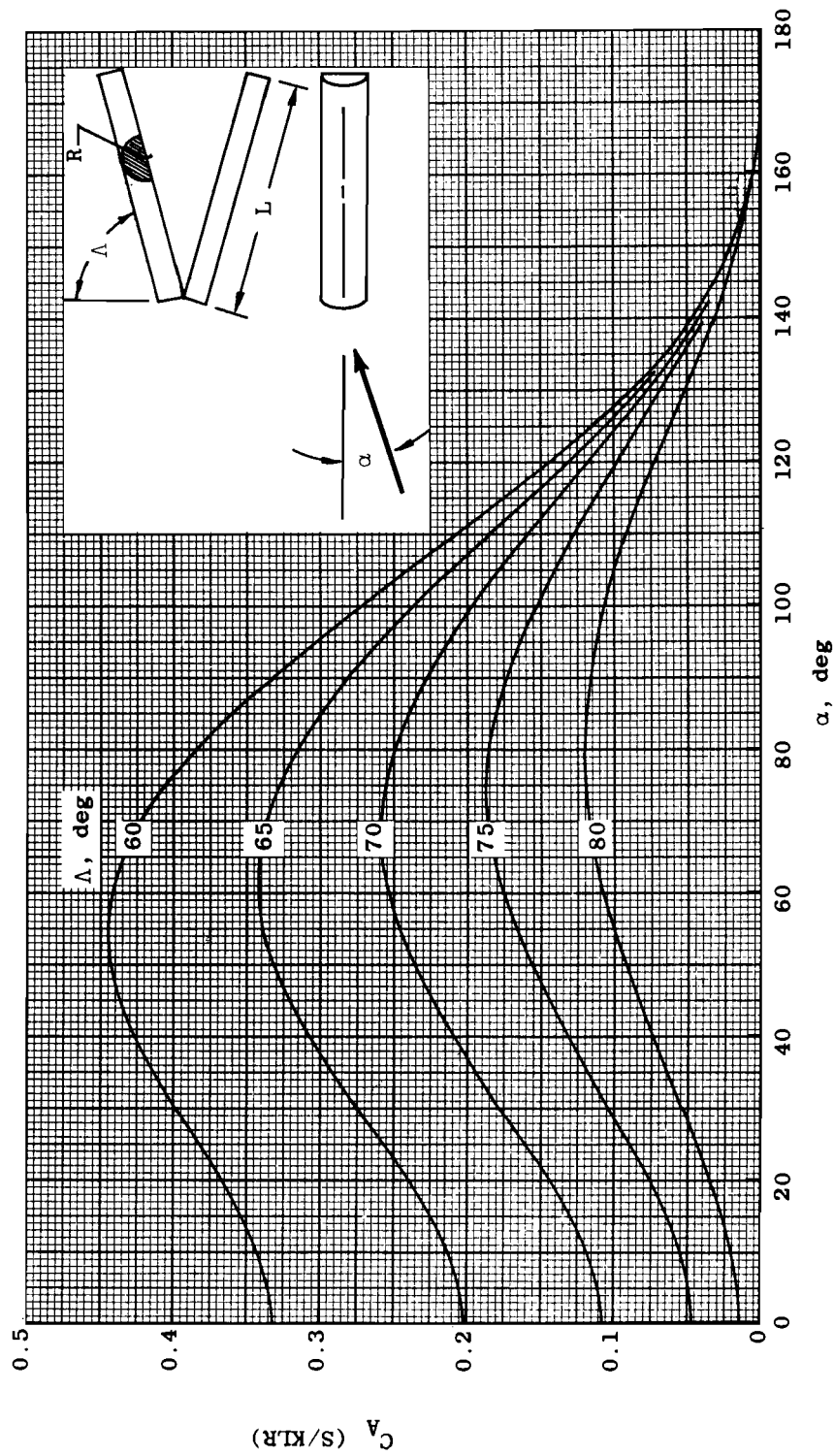


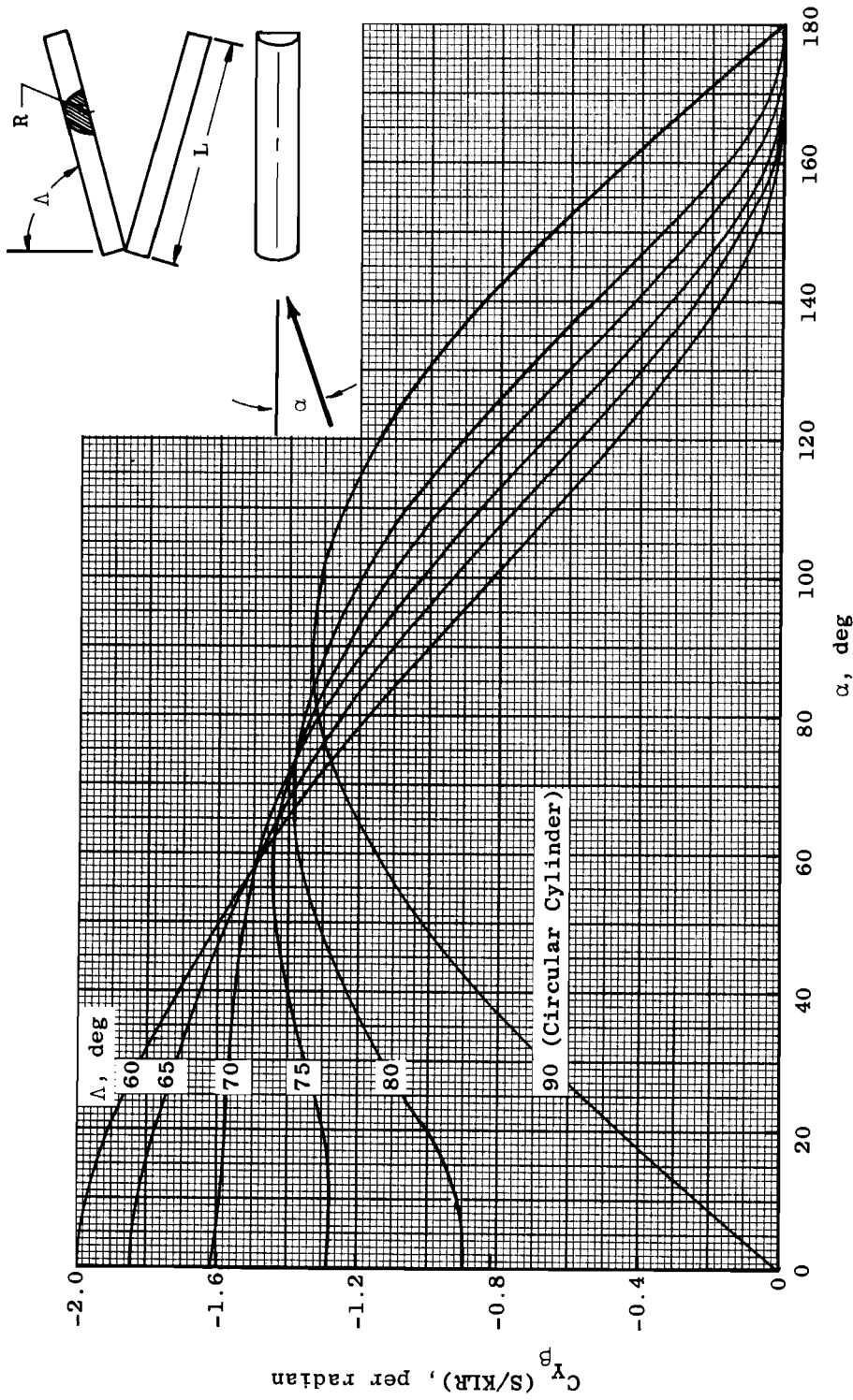
Fig. 4 Aerodynamic Characteristics of Swept-Cylinder Leading Edges ($\phi' = \pi/2$)

α . Normal Force



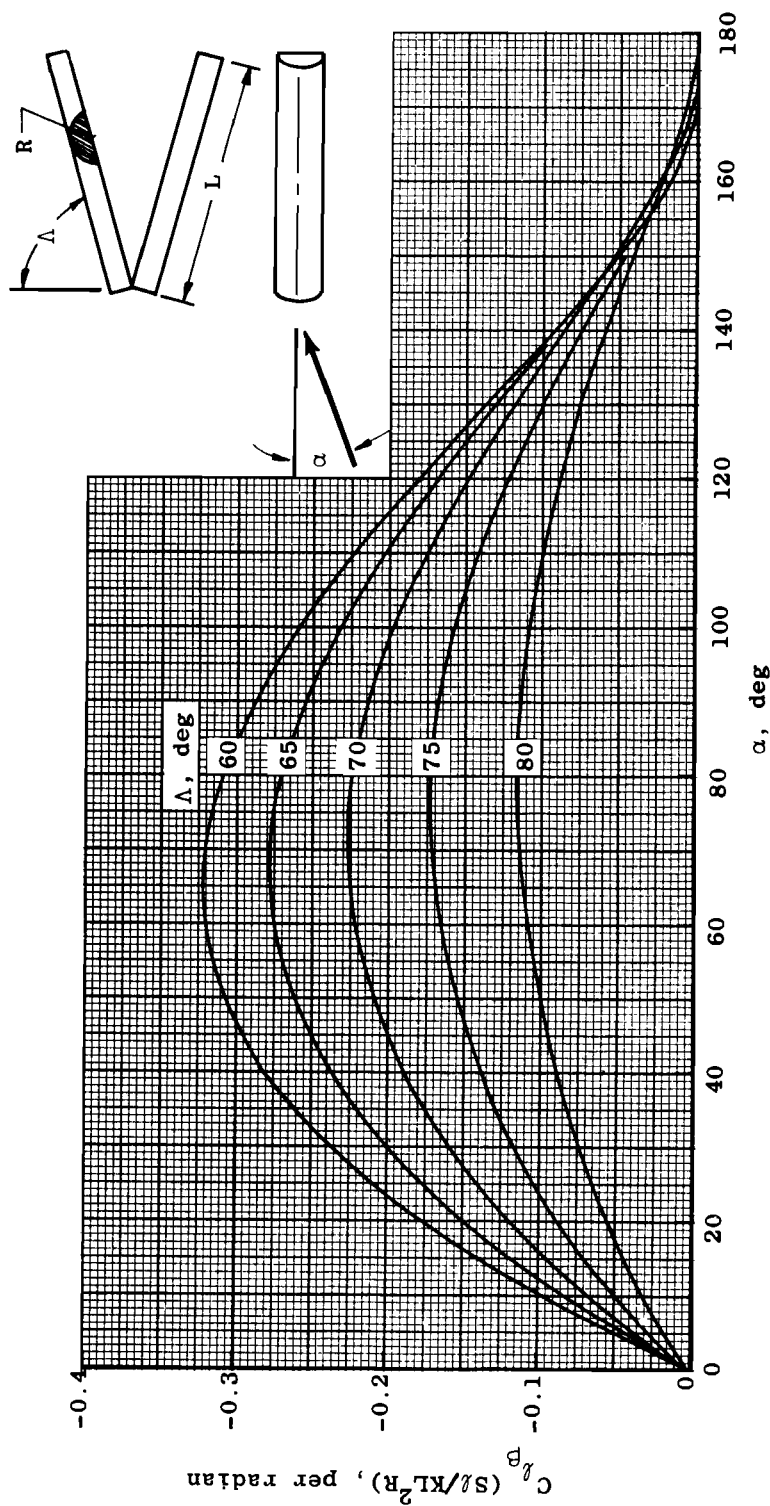
b. Axial Force
Fig. 4 Continued

AEDC-TDR-64-25



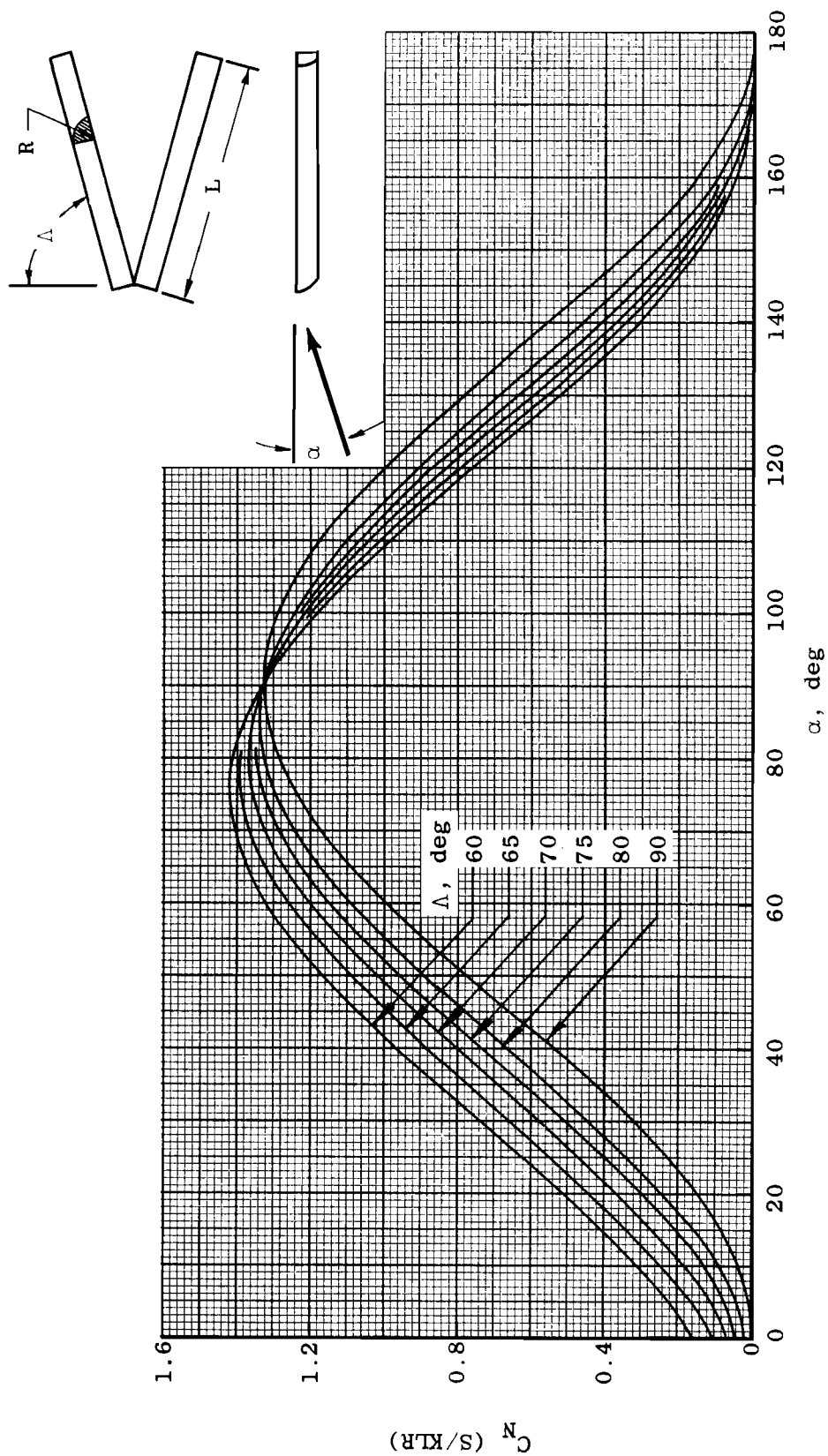
c. Side-Force Derivative, $\beta = 0$

Fig. 4 Continued

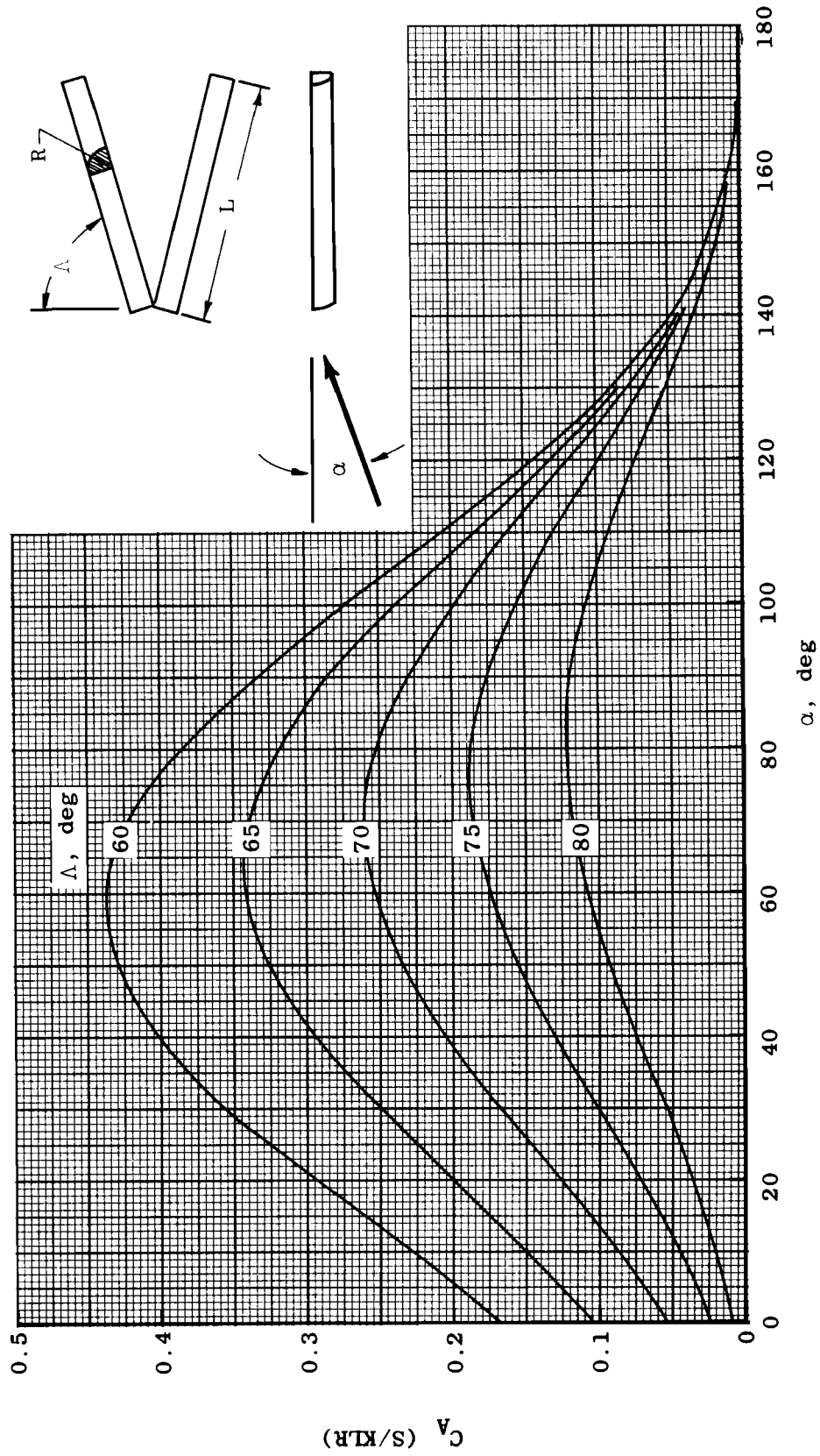


d. Rolling-Moment Derivative, $\beta = 0$

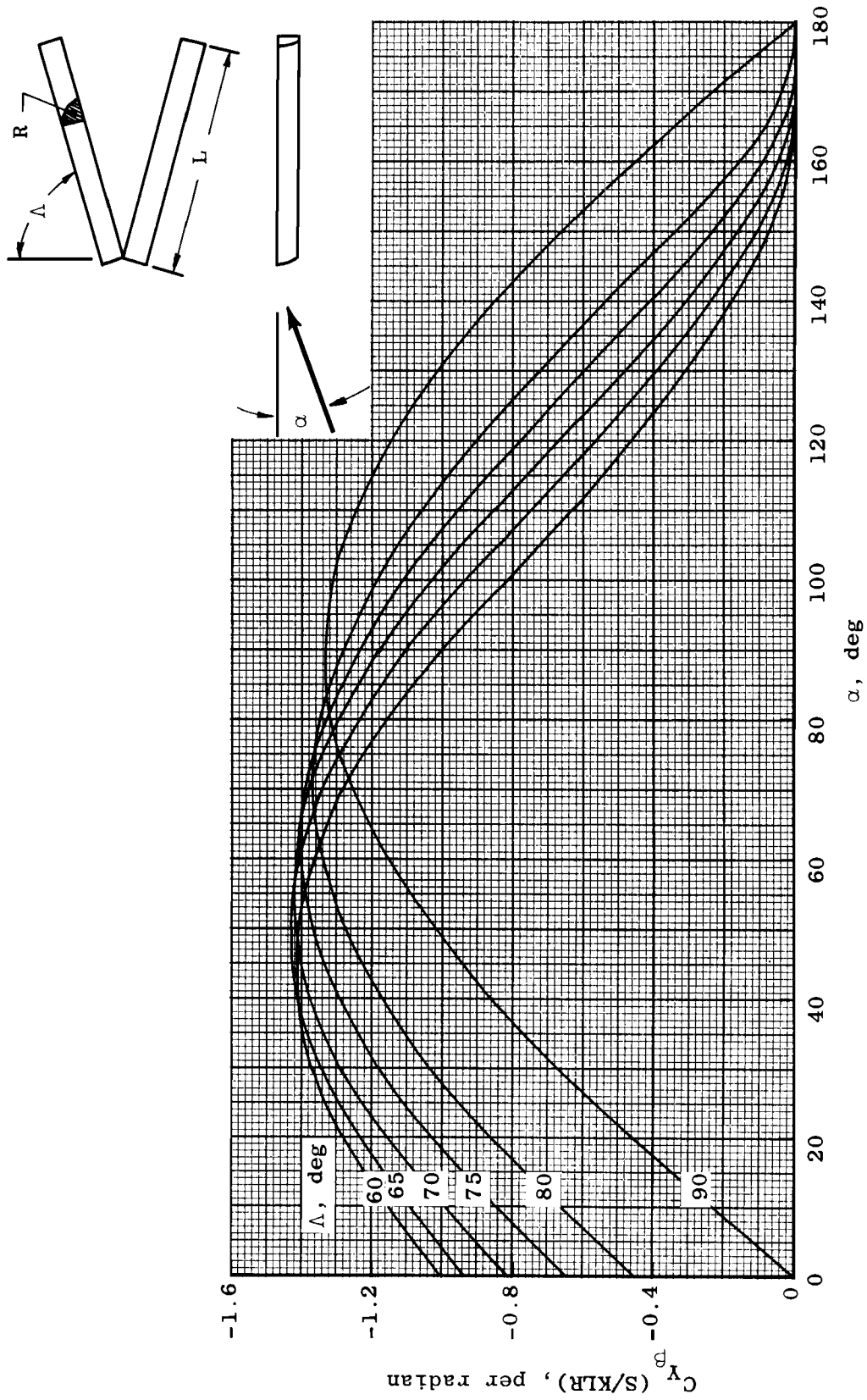
Fig. 1 Concluded



a. Normal Force
Fig. 5 Aerodynamic Characteristics of Flat-Topped Swept-Cylinder Leading Edges ($\phi' = \pi/2$)

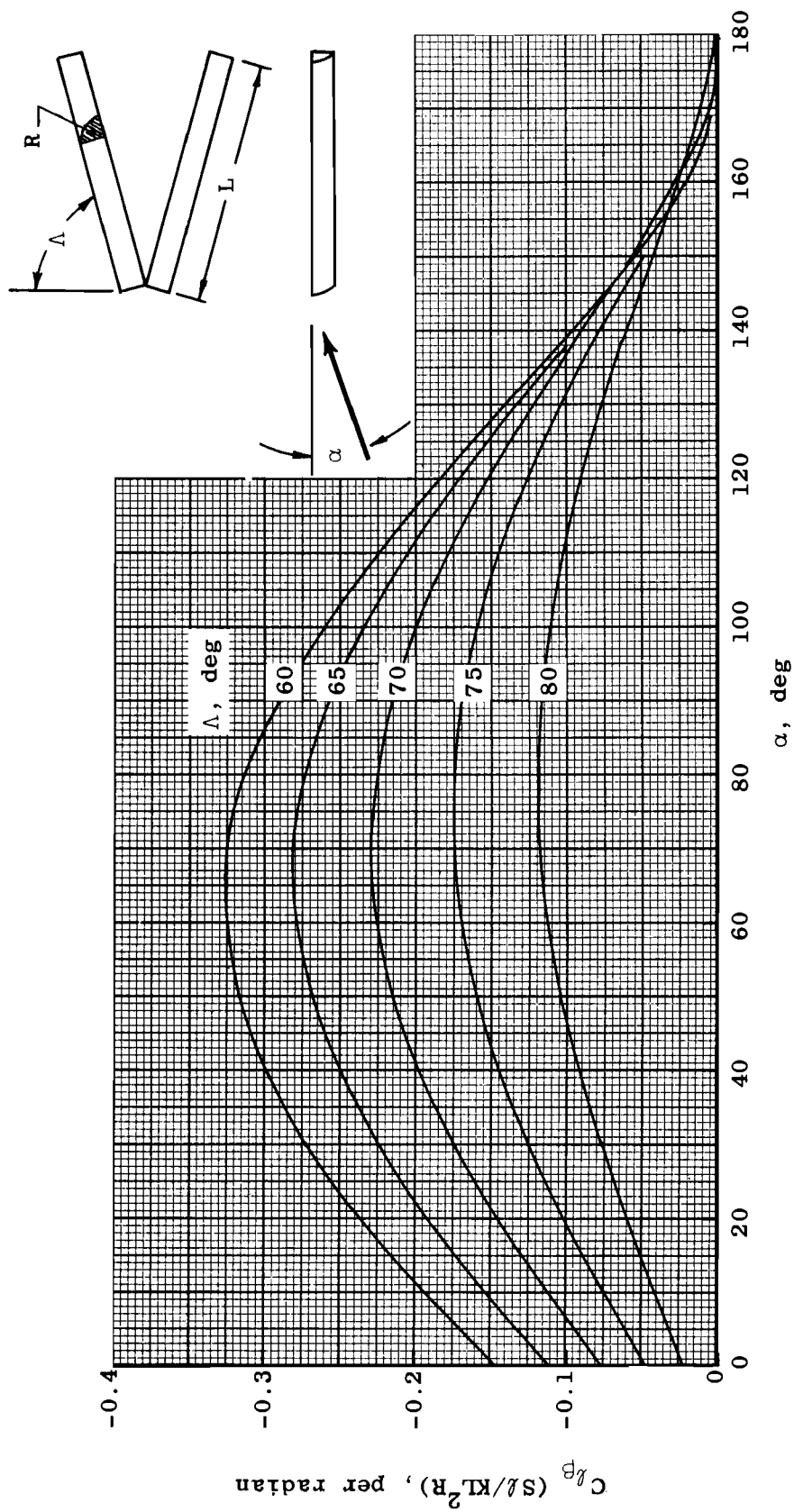


b. Axial Force
Fig. 5 Continued



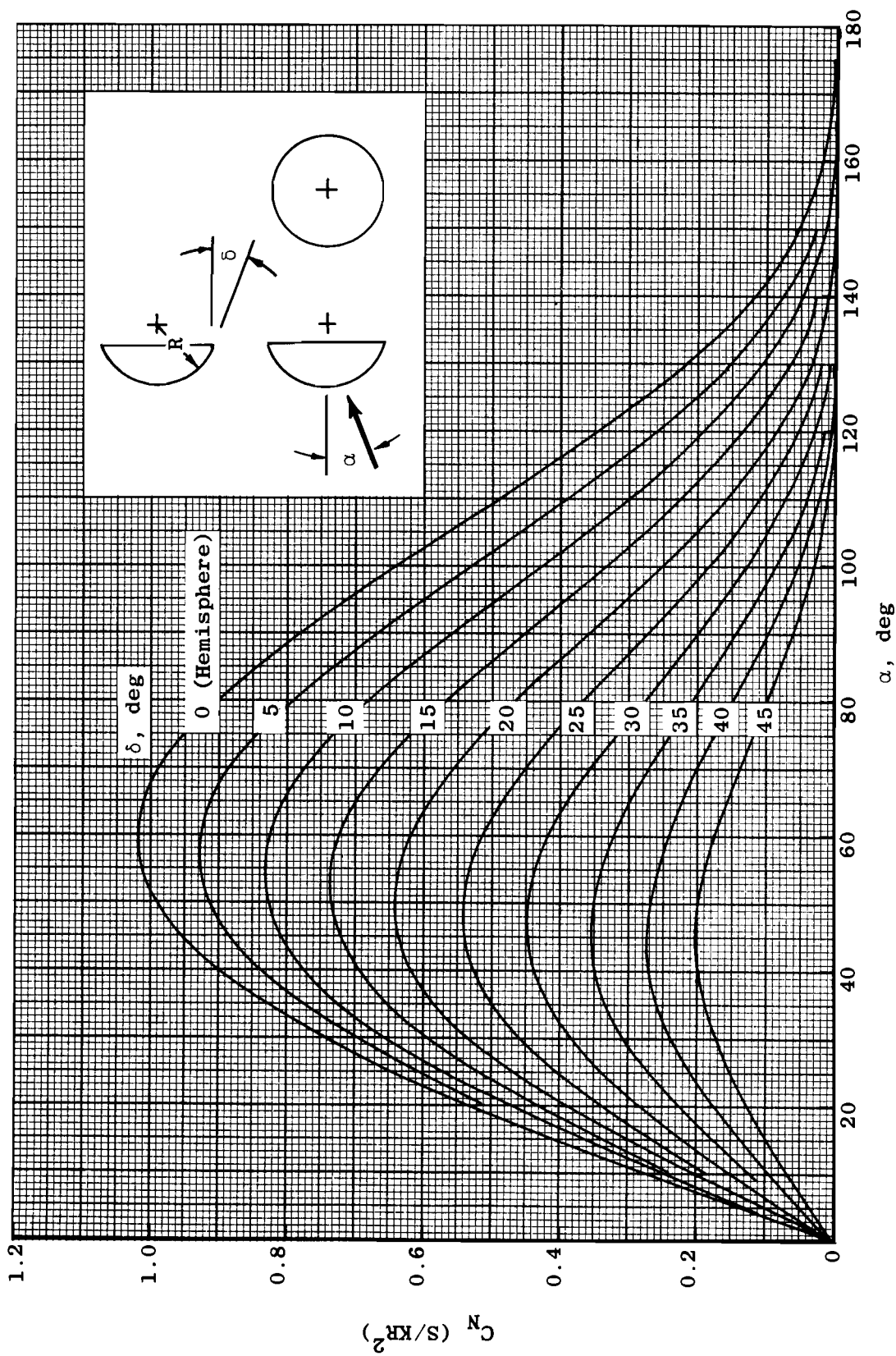
c. Side-Force Derivative, $\beta = 0$

Fig. 5 Continued



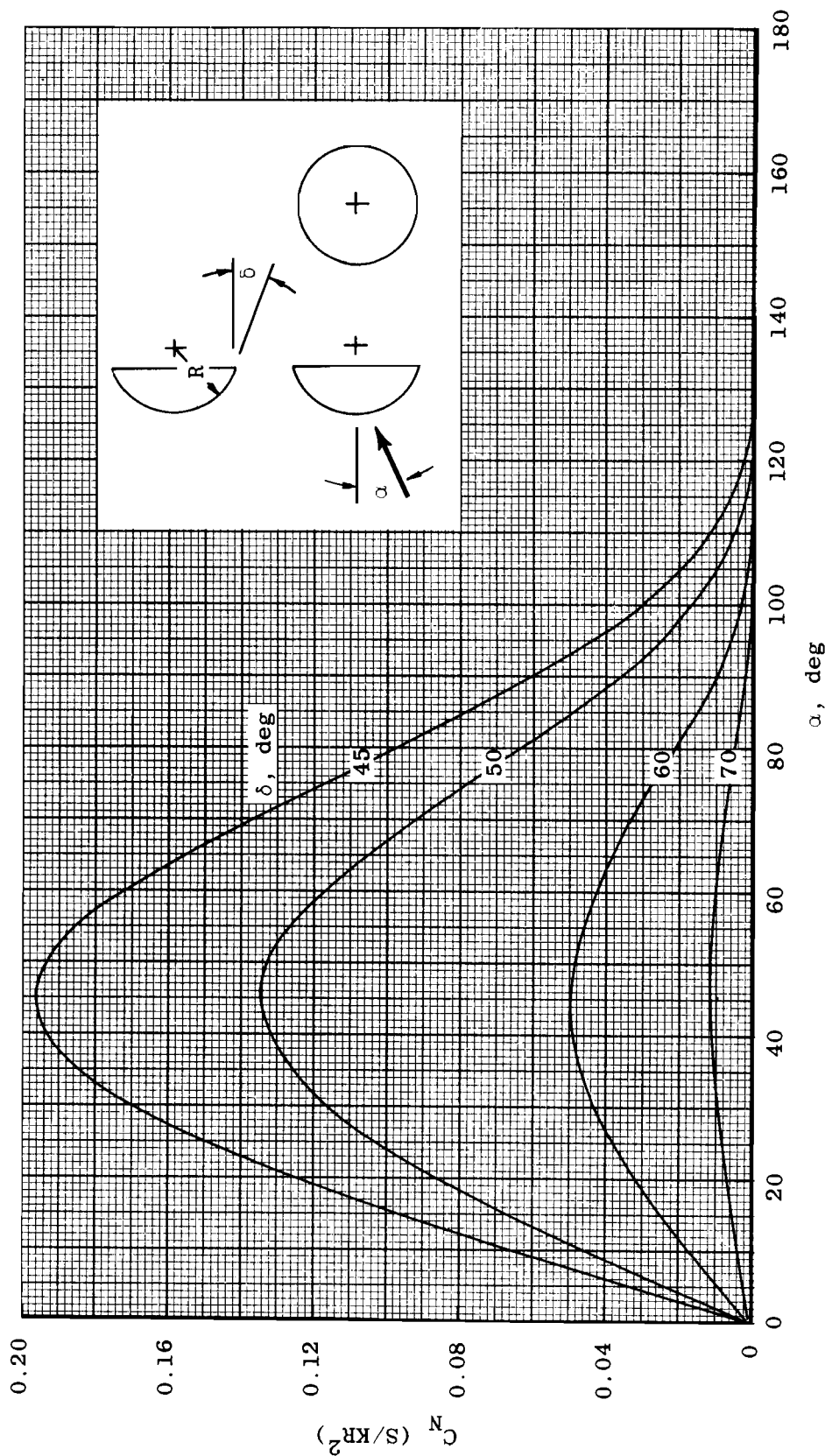
d. Rolling-Moment Derivative, $\beta = 0$

Fig. 5 Concluded



a. Normal Force, $\delta = 0$ to 45 deg

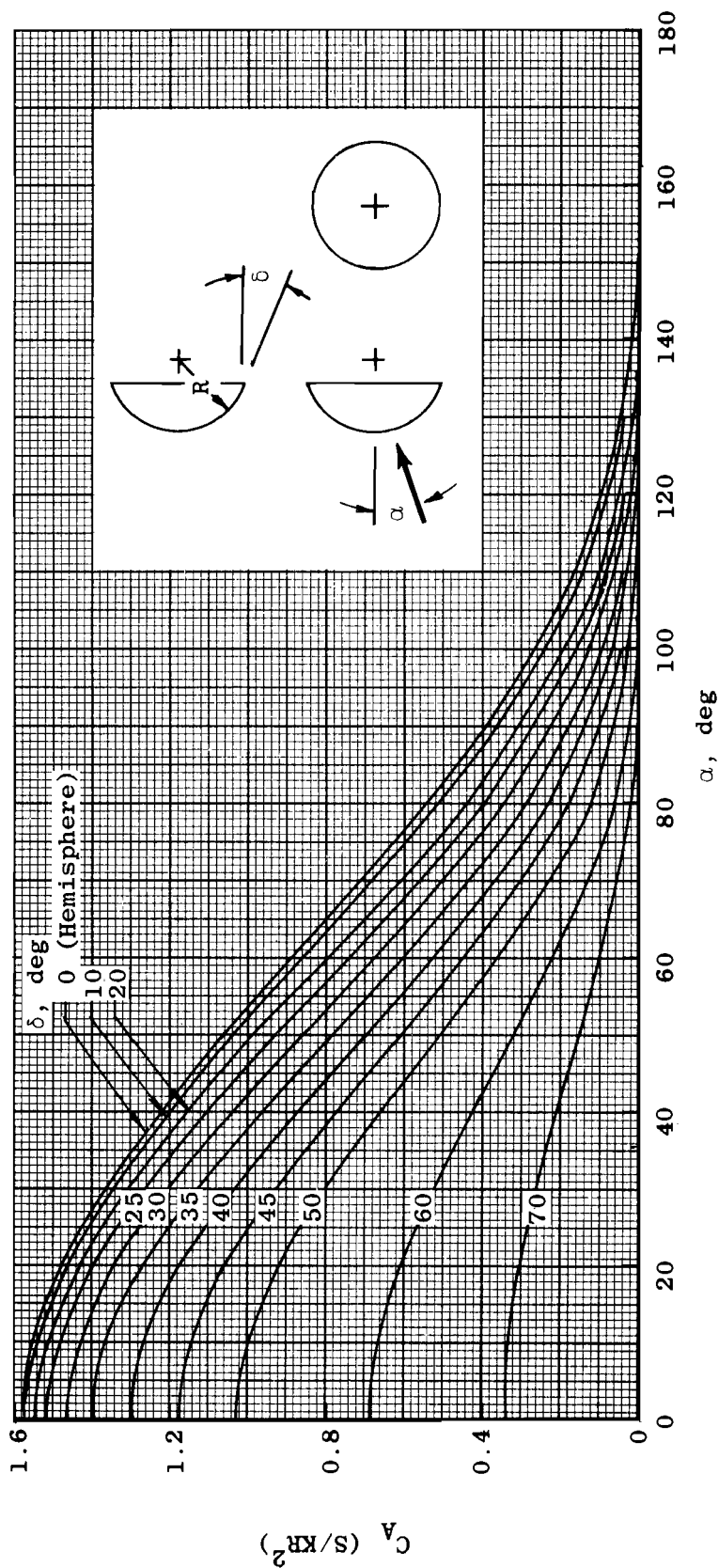
Fig. 6 Aerodynamic Characteristics of Spherical Segments



b. Normal Force, $\delta \approx 45$ to 70 deg

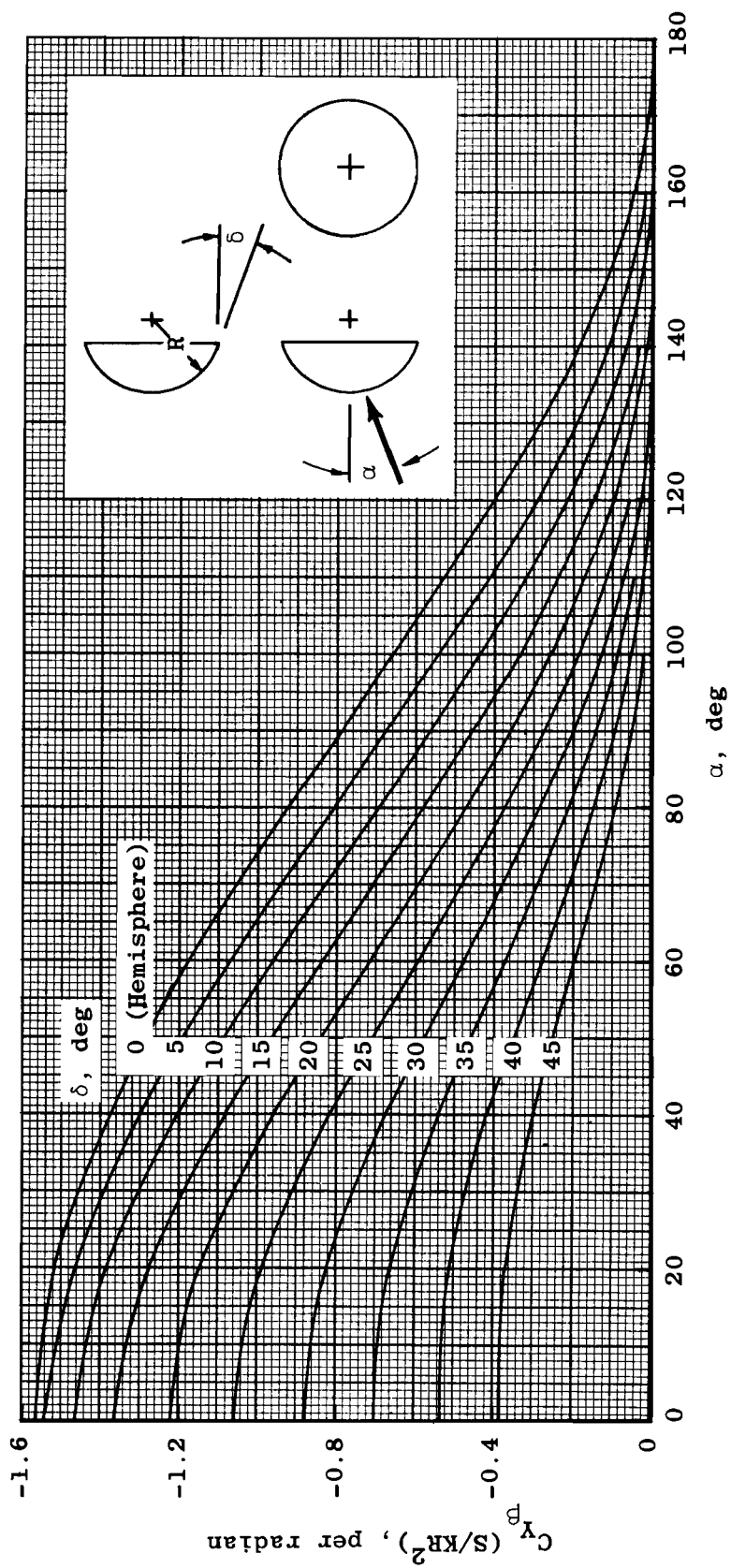
Fig. 6 Continued

AEDC-TDR-64-25



c. Axial Force

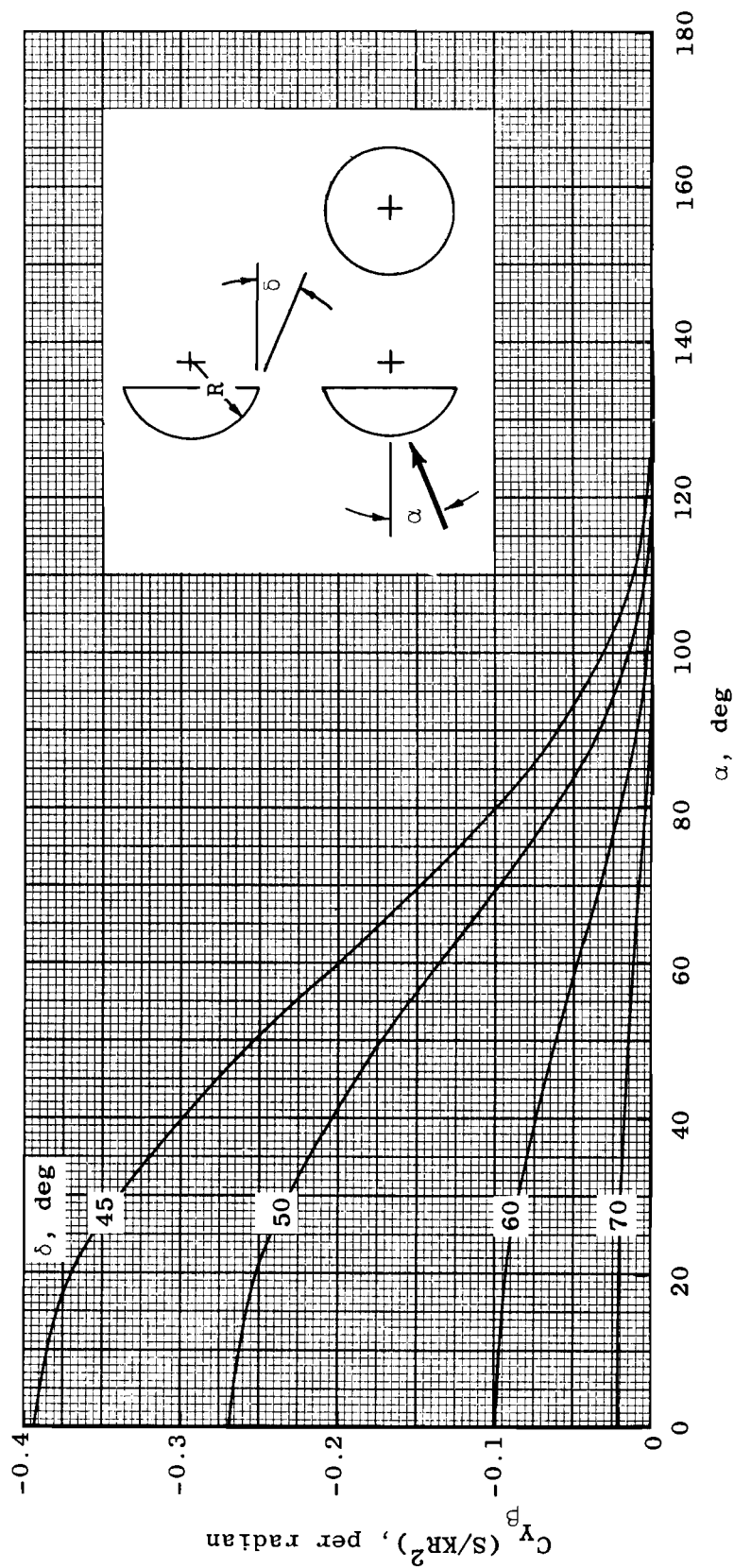
Fig. 6 Continued



d. Side-Force Derivative ($\beta = 0$), $\delta = 0$ to 45 deg

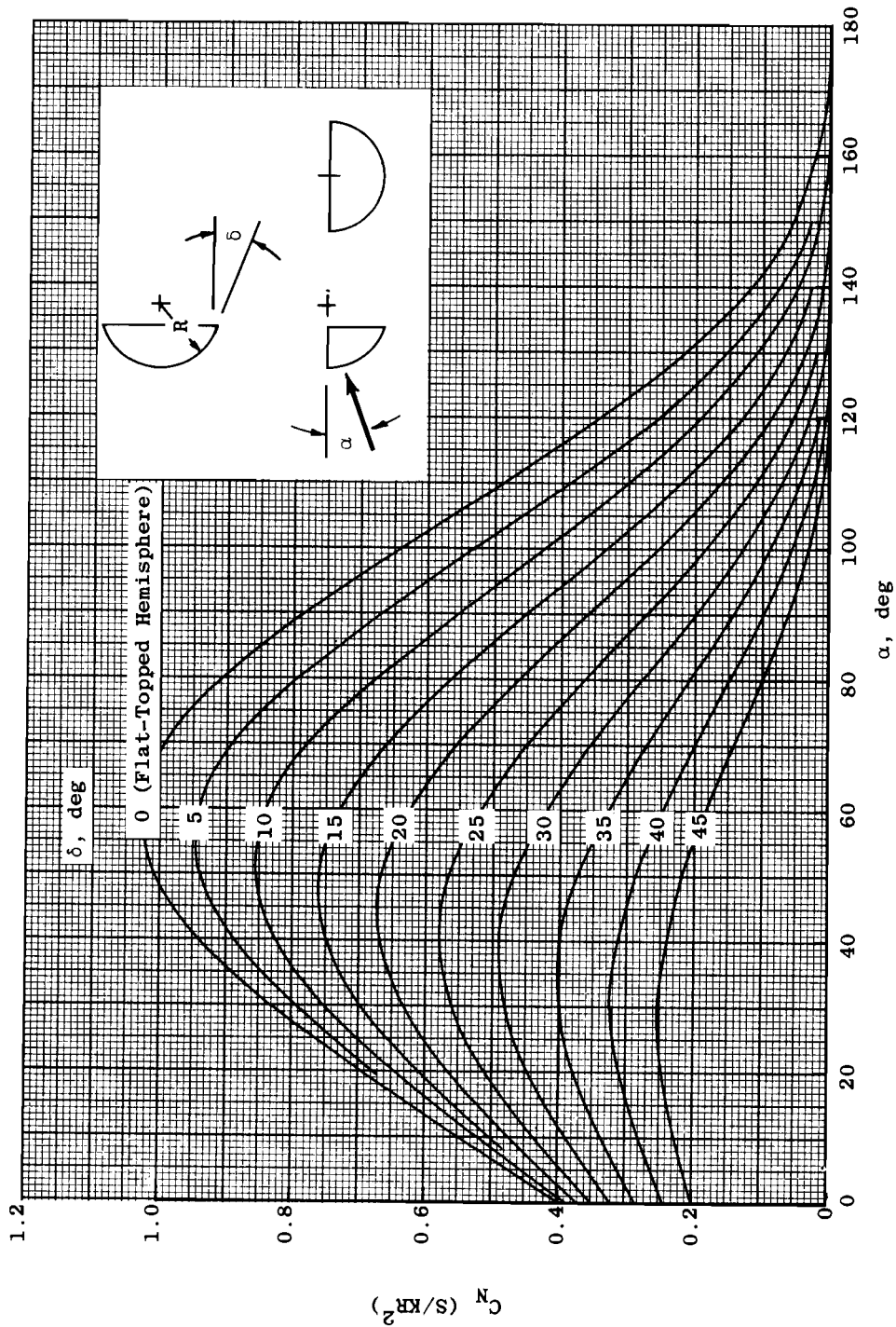
Fig. 6 Continued

AEDC-TDR-64-25



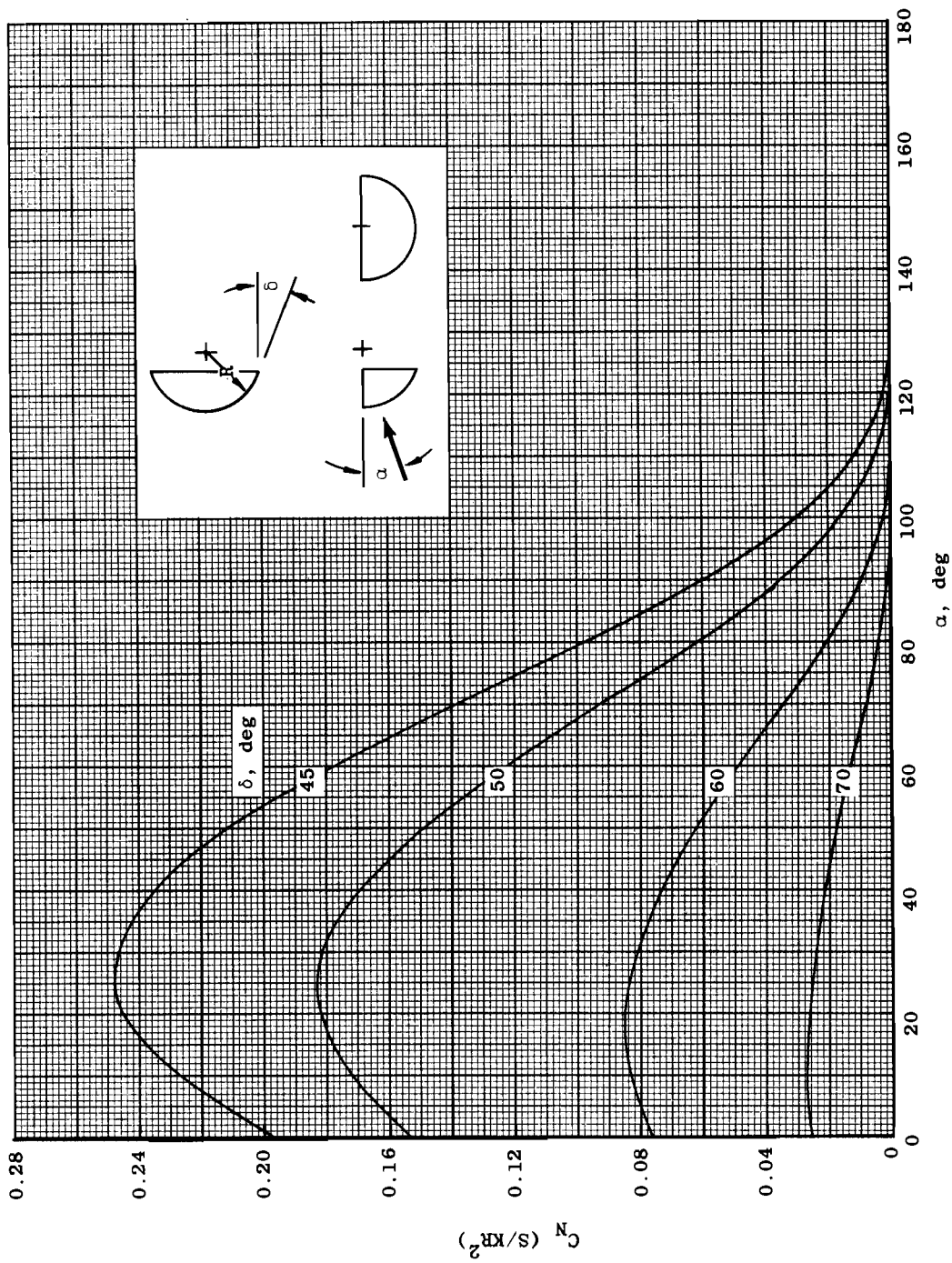
e. Side-Force Derivative ($\beta = 0$), $\delta = 45$ to 70 deg

Fig. 6 Concluded



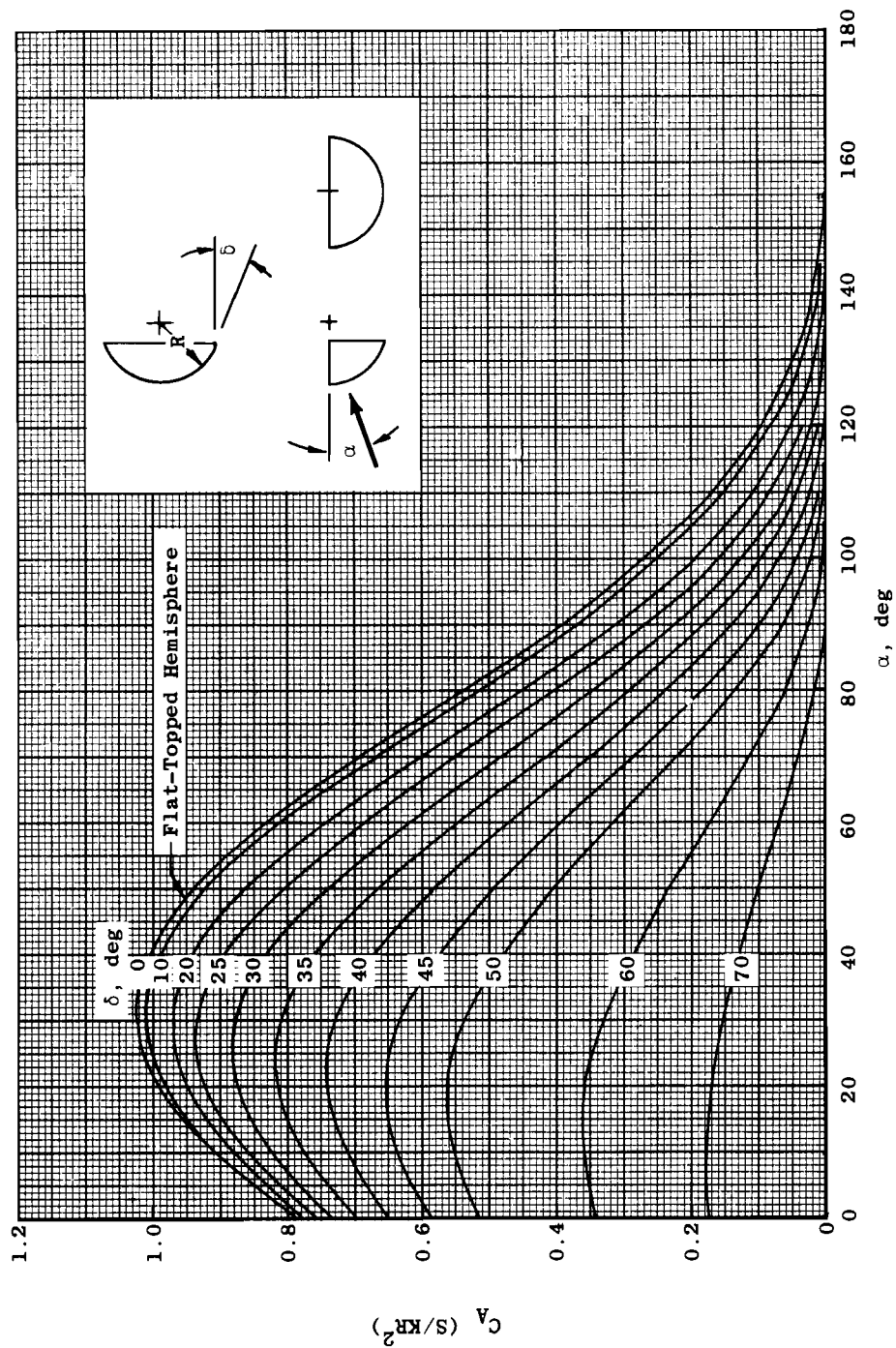
a. Normal Force, $\delta = 0$ to 45 deg
 Fig. 7 Aerodynamic Characteristics of Flat-Topped Spherical Segments

AEDC-TDR-64-25



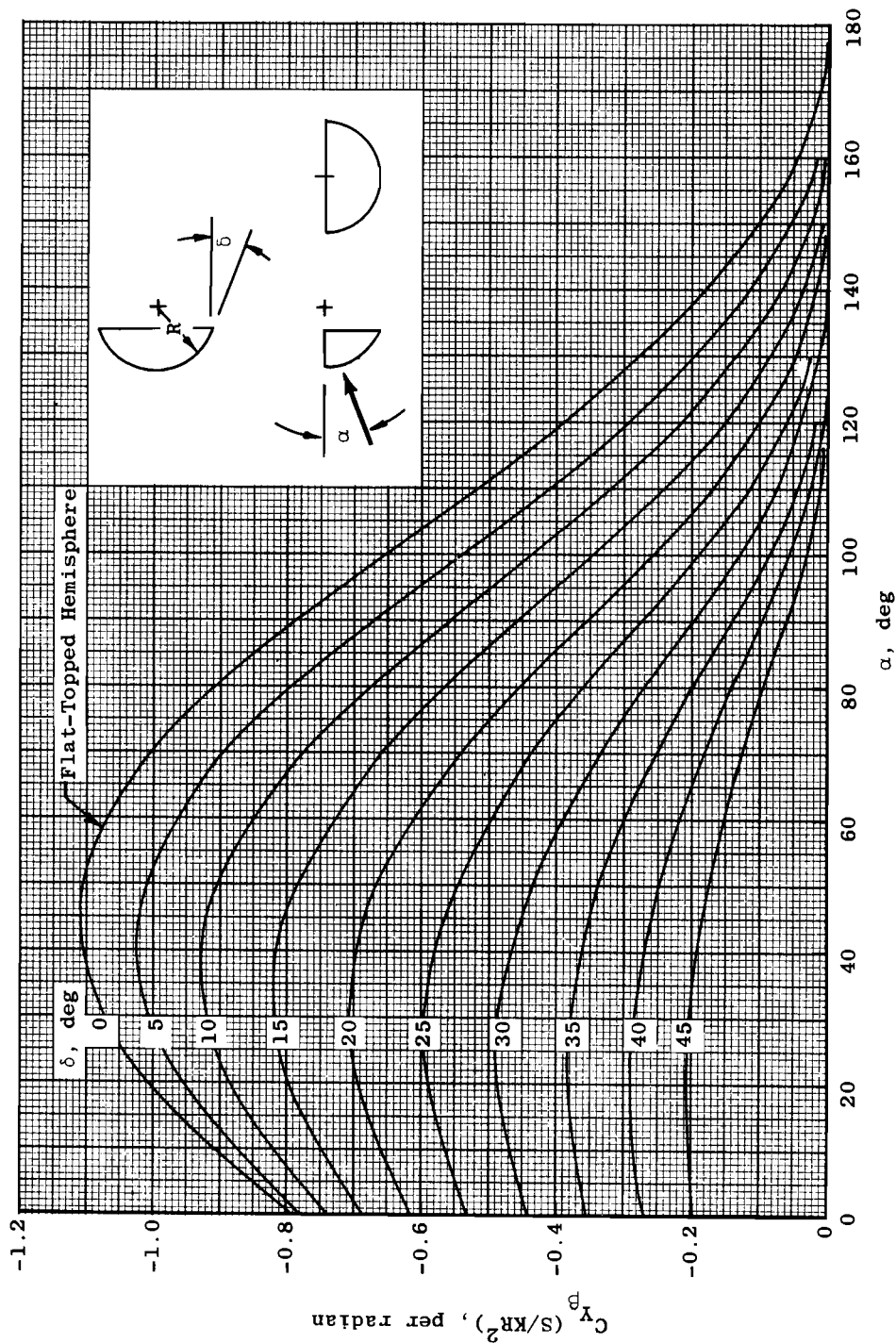
b. Normal Force, $\delta = 45$ to 70 deg

Fig. 7 Continued



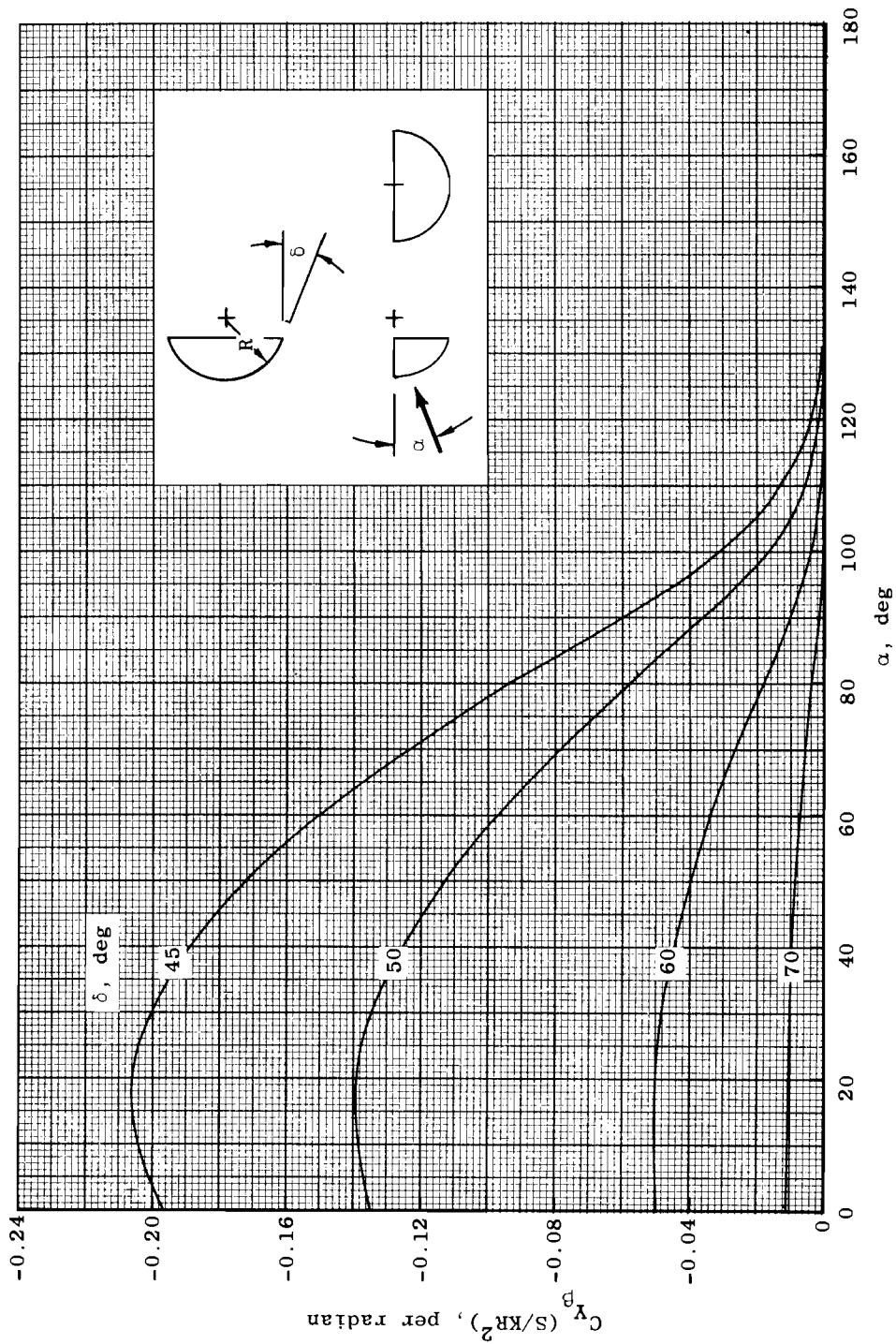
c. Axial Force

Fig. 7 Continued



d. Side-Force Derivative ($\beta = 0$), $\delta = 0$ to 45 deg

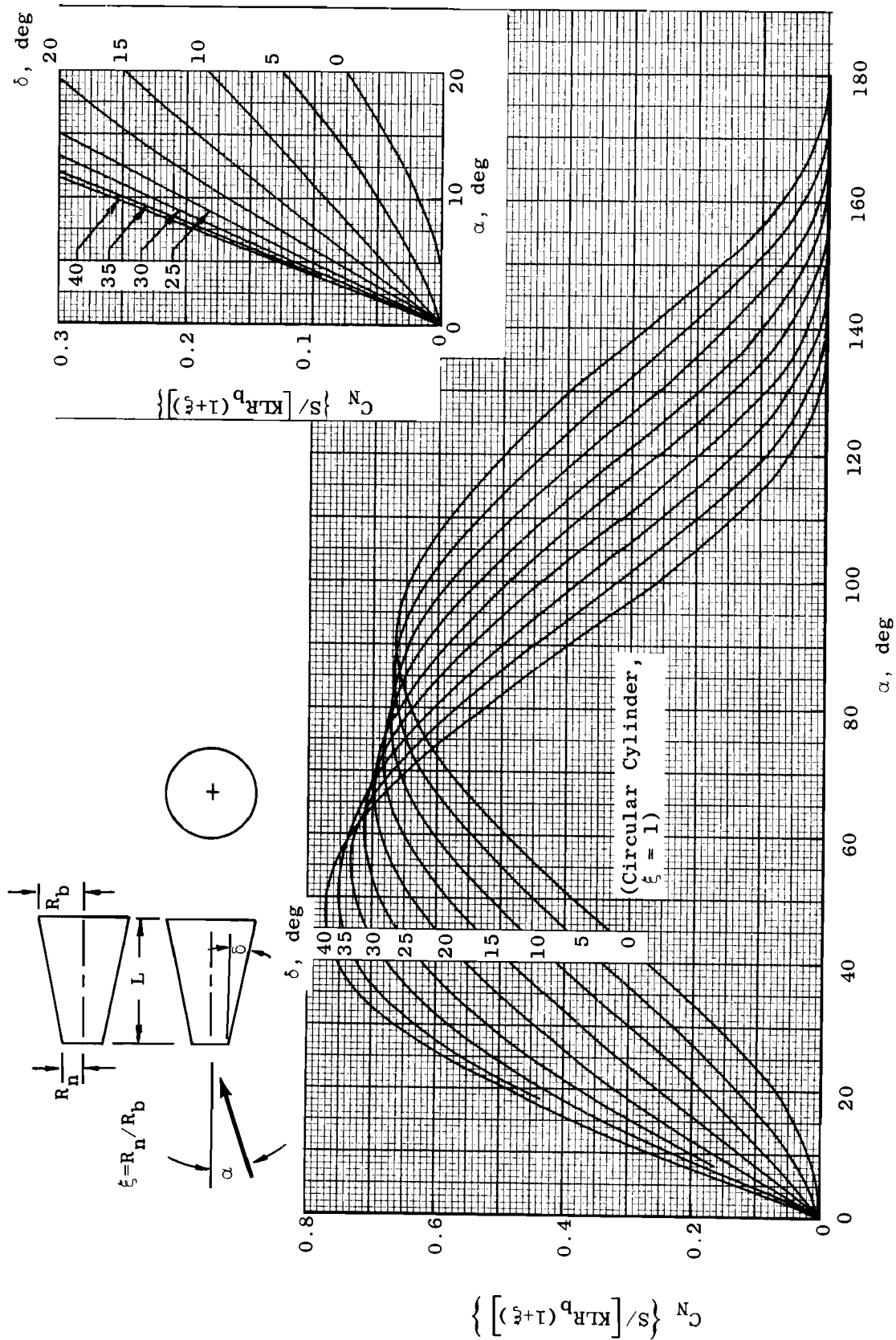
Fig. 7 Continued



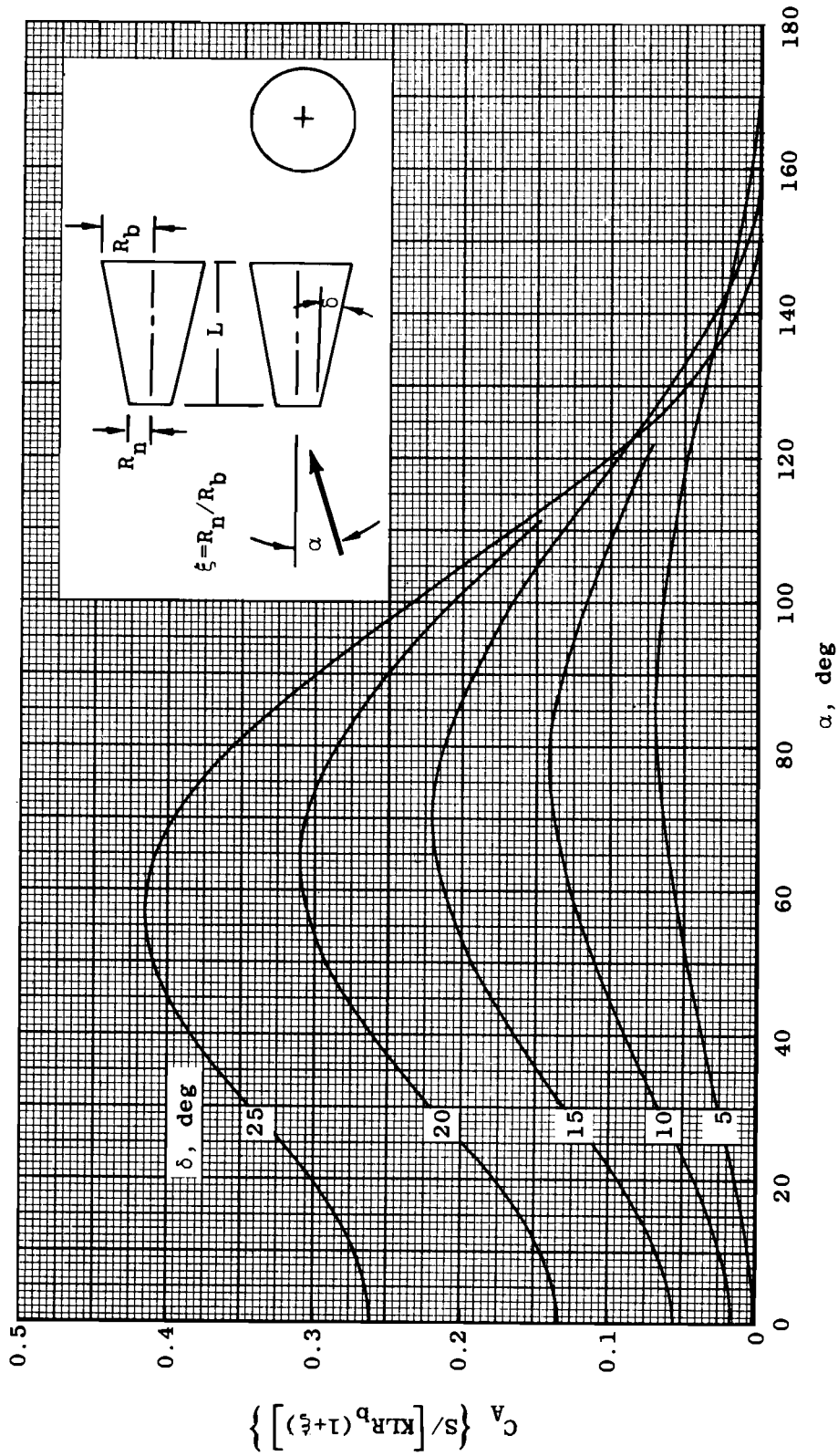
e. Side-Force Derivative ($\beta = 0$), $\delta = 45$ to 70 deg

Fig. 7 Concluded

AEDC-TDR-64-25

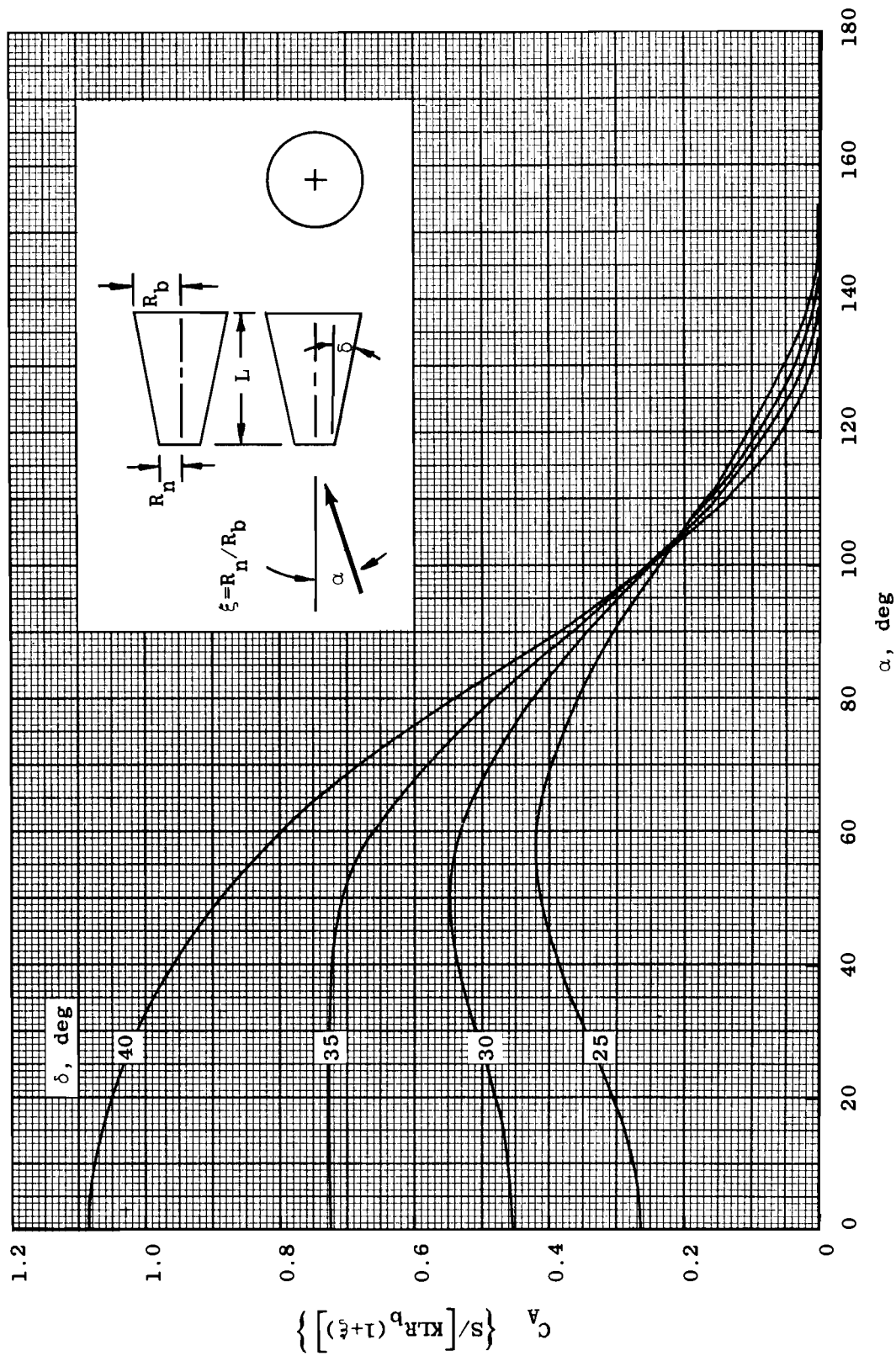


a. Normal Force
 Fig. 8 Aerodynamic Characteristics of Cone Frustums



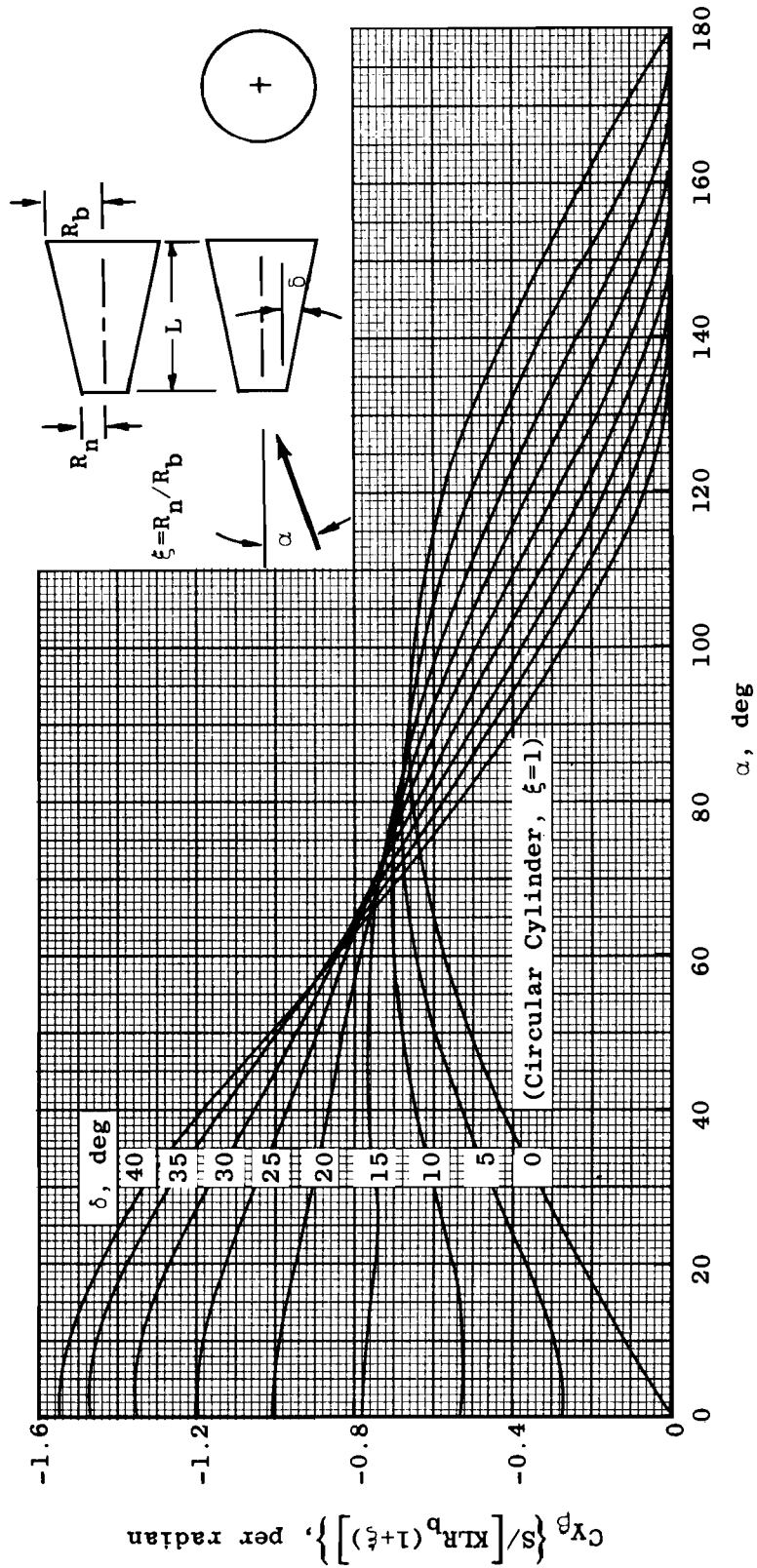
b. Axial Force, $\delta = 5$ to 25 deg

Fig. 8 Continued



c. Axial Force, $\delta = 25$ to 40 deg

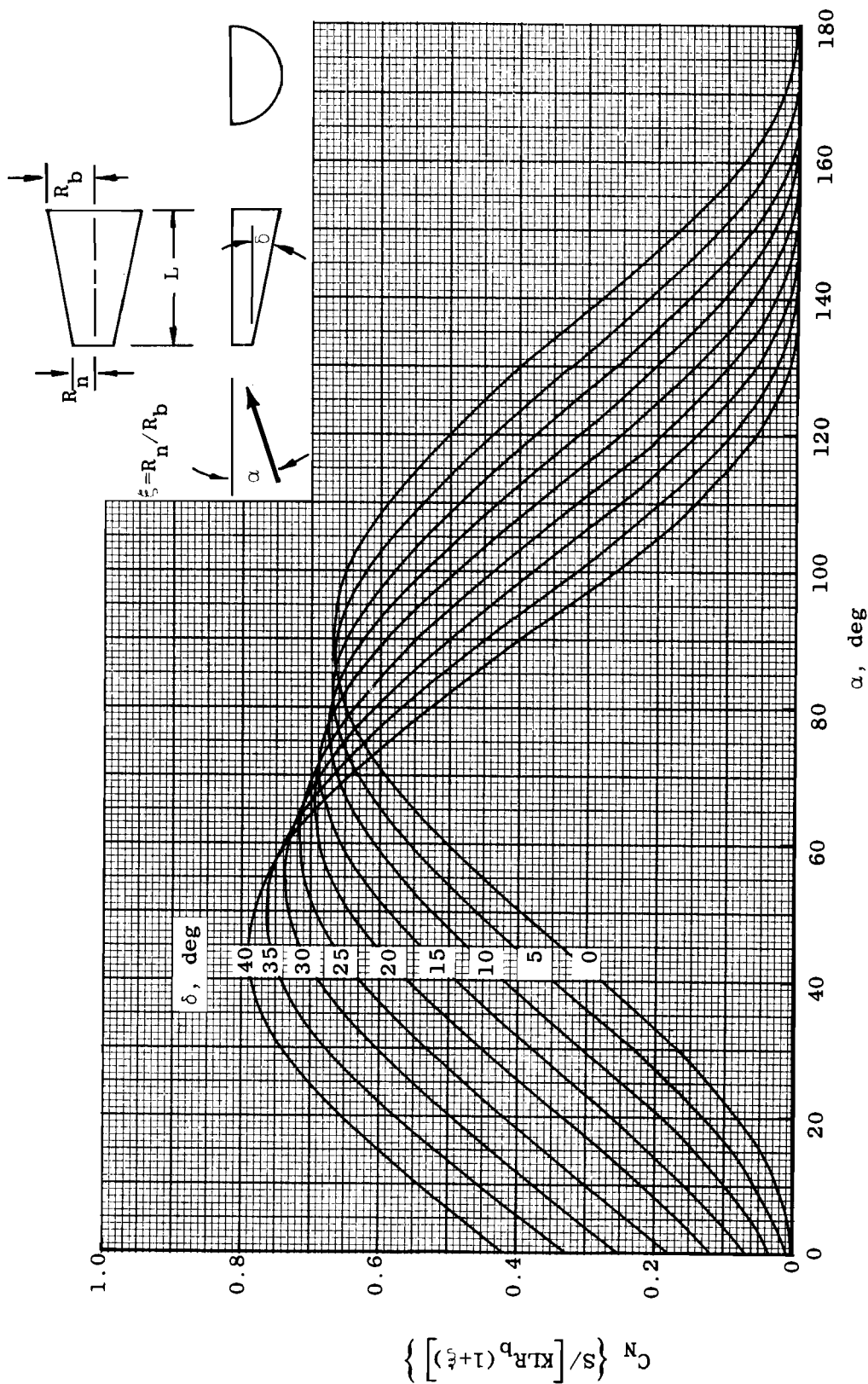
Fig. 8 Continued



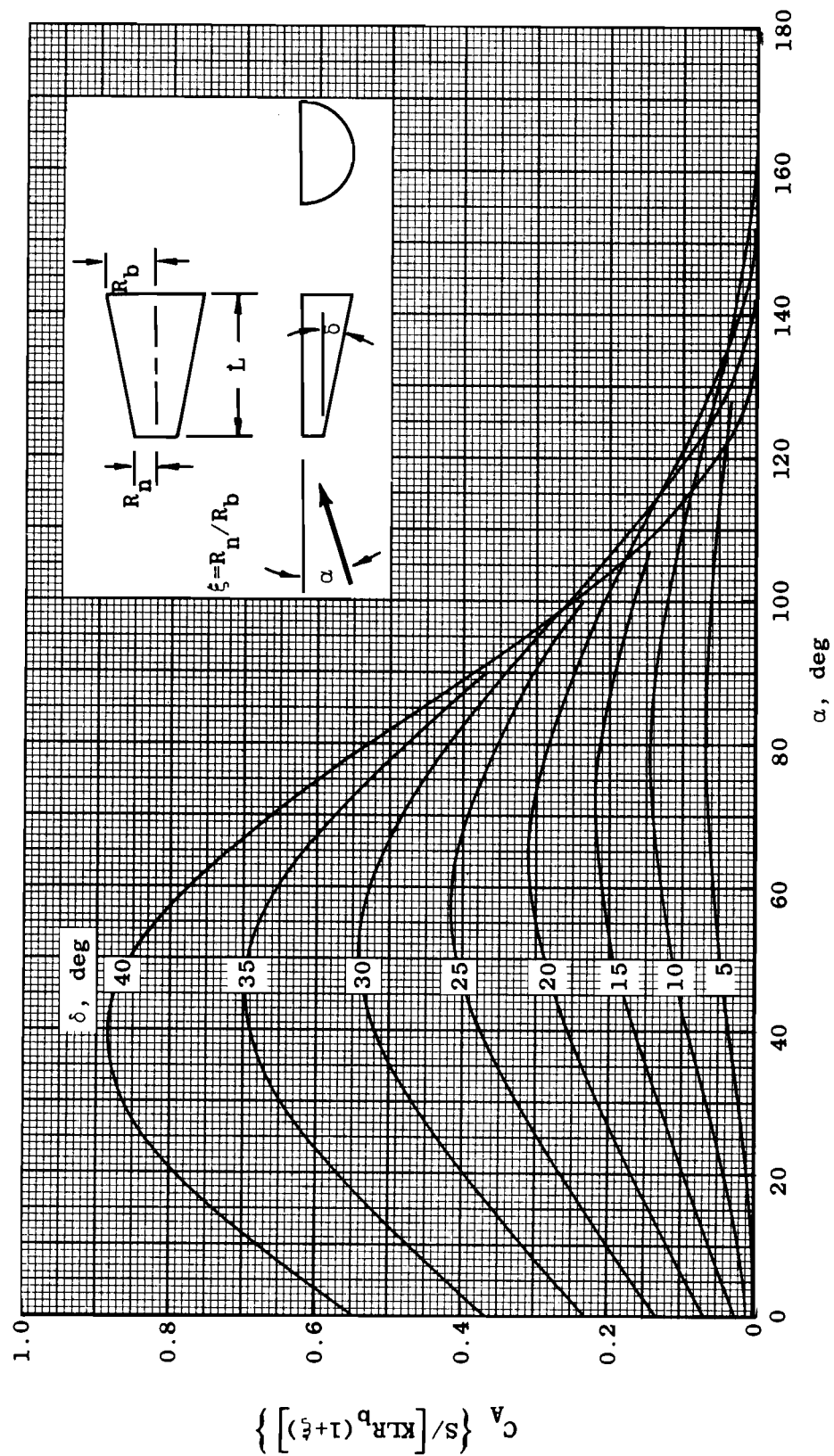
d. Side-Force Derivative, $\beta \approx 0$

Fig. 8 Concluded

AEDC-TDR-64-25

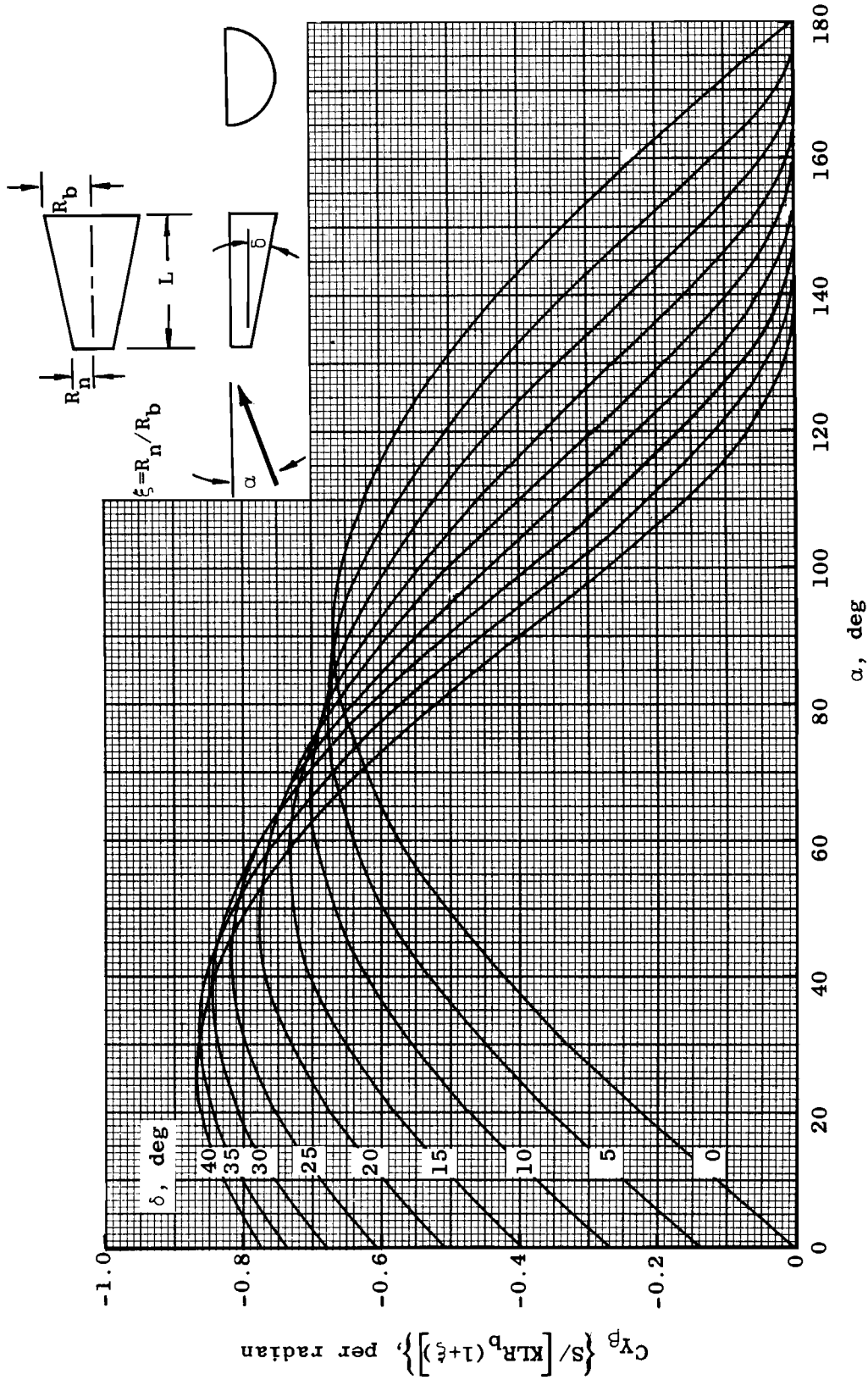


a. Normal Force
 Fig. 9 Aerodynamic Characteristics of Flat-Topped Cone Frustums



b. Axial Force
Fig. 9 Continued

AEDC-TDR-64-25



c. Side-Force Derivative, $\beta = 0$

Fig. 9 Concluded

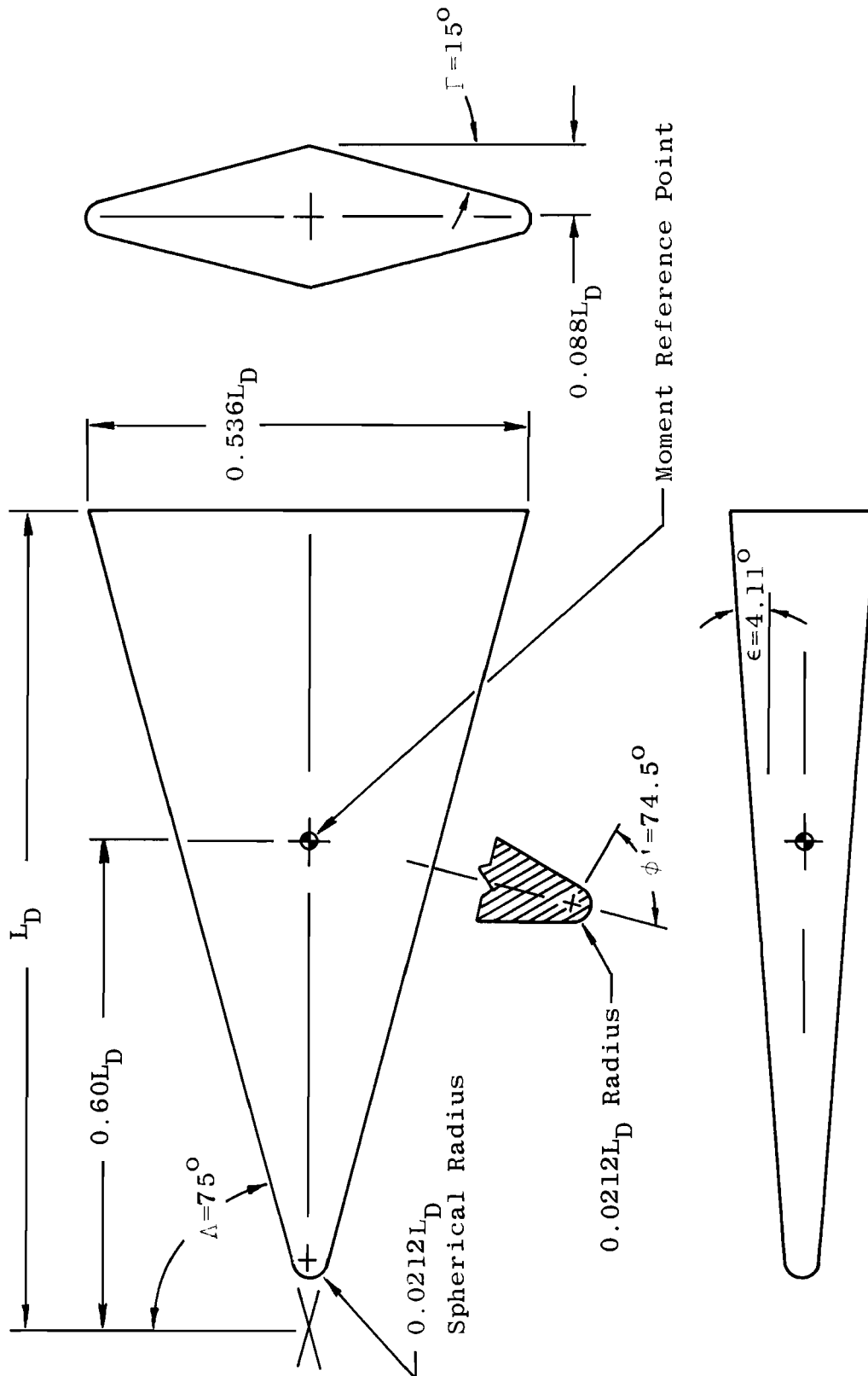
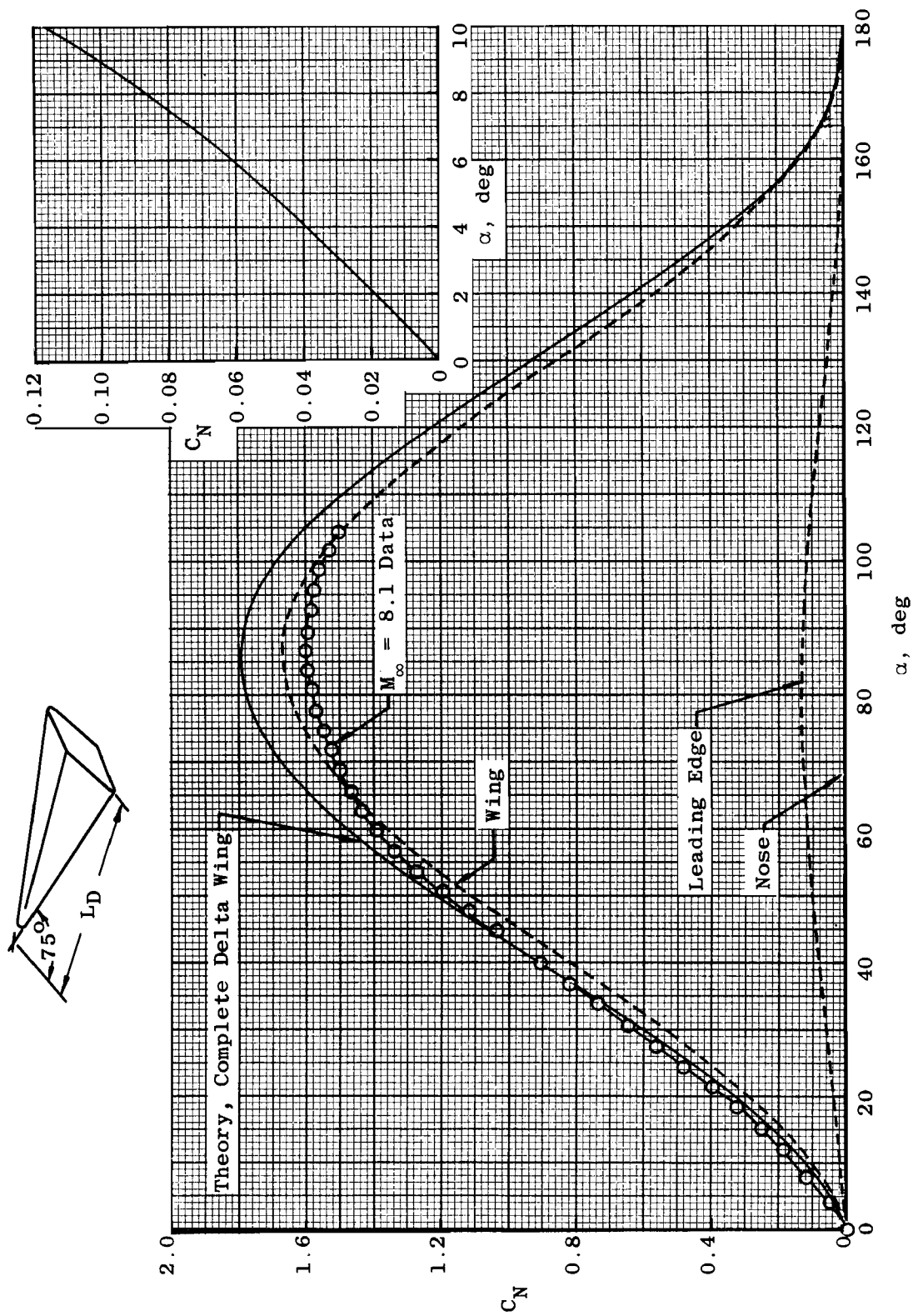
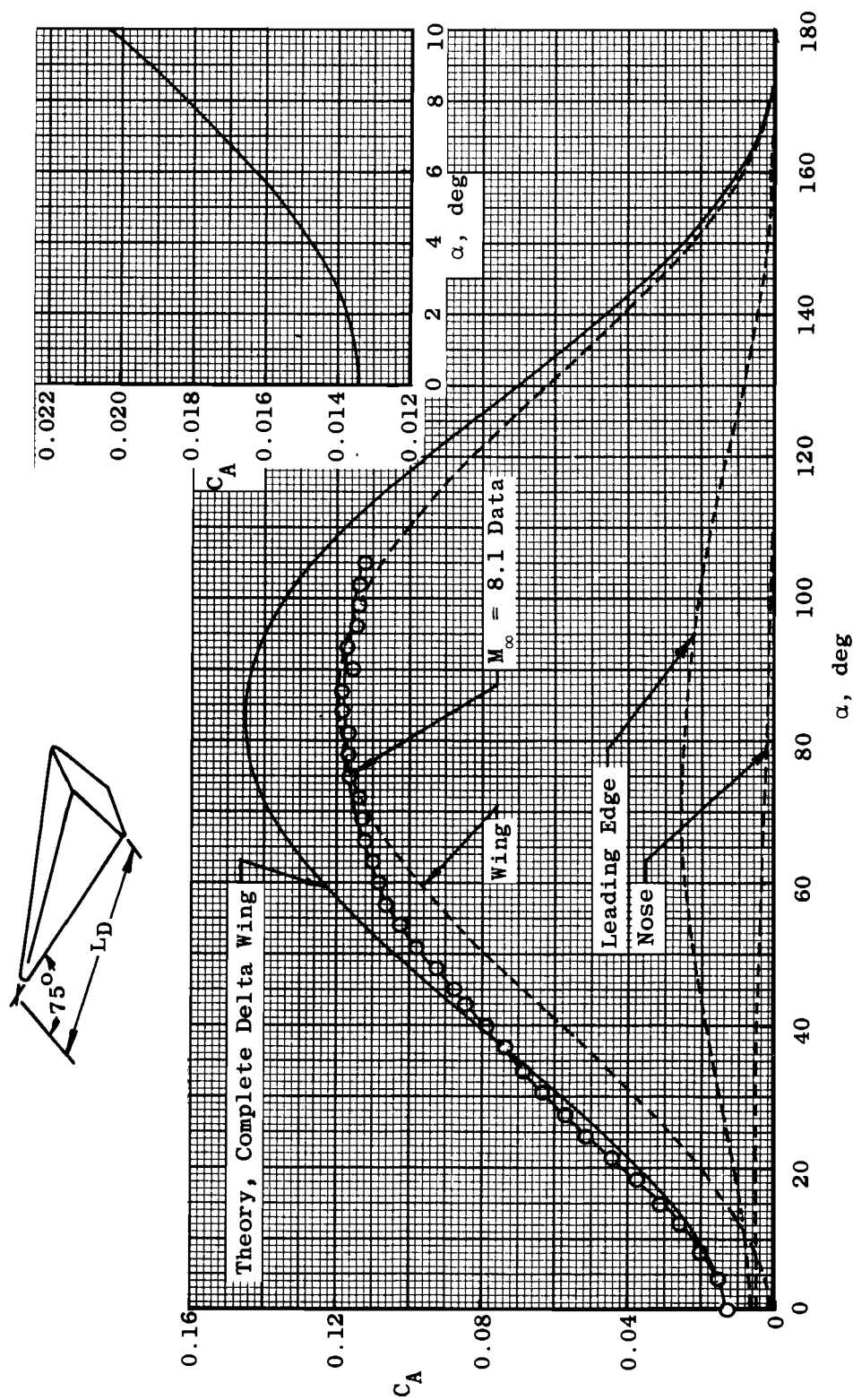


Fig. 10 Details of 75-deg Swept Delta Wing

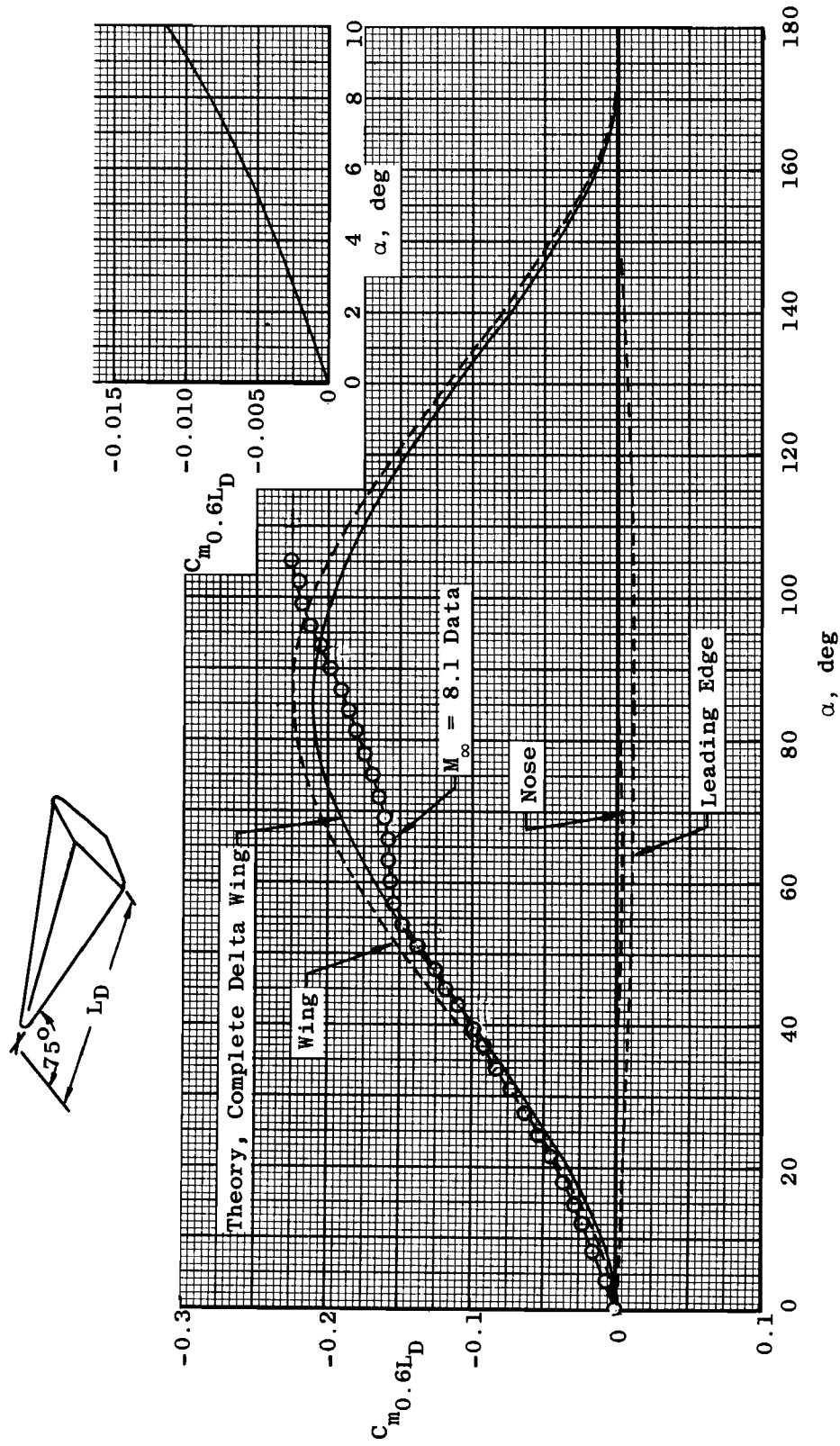
AEDC-TDR-64-25



a. Normal Force
 Fig. 11 Aerodynamic Characteristics of a 75-deg Delta Wing

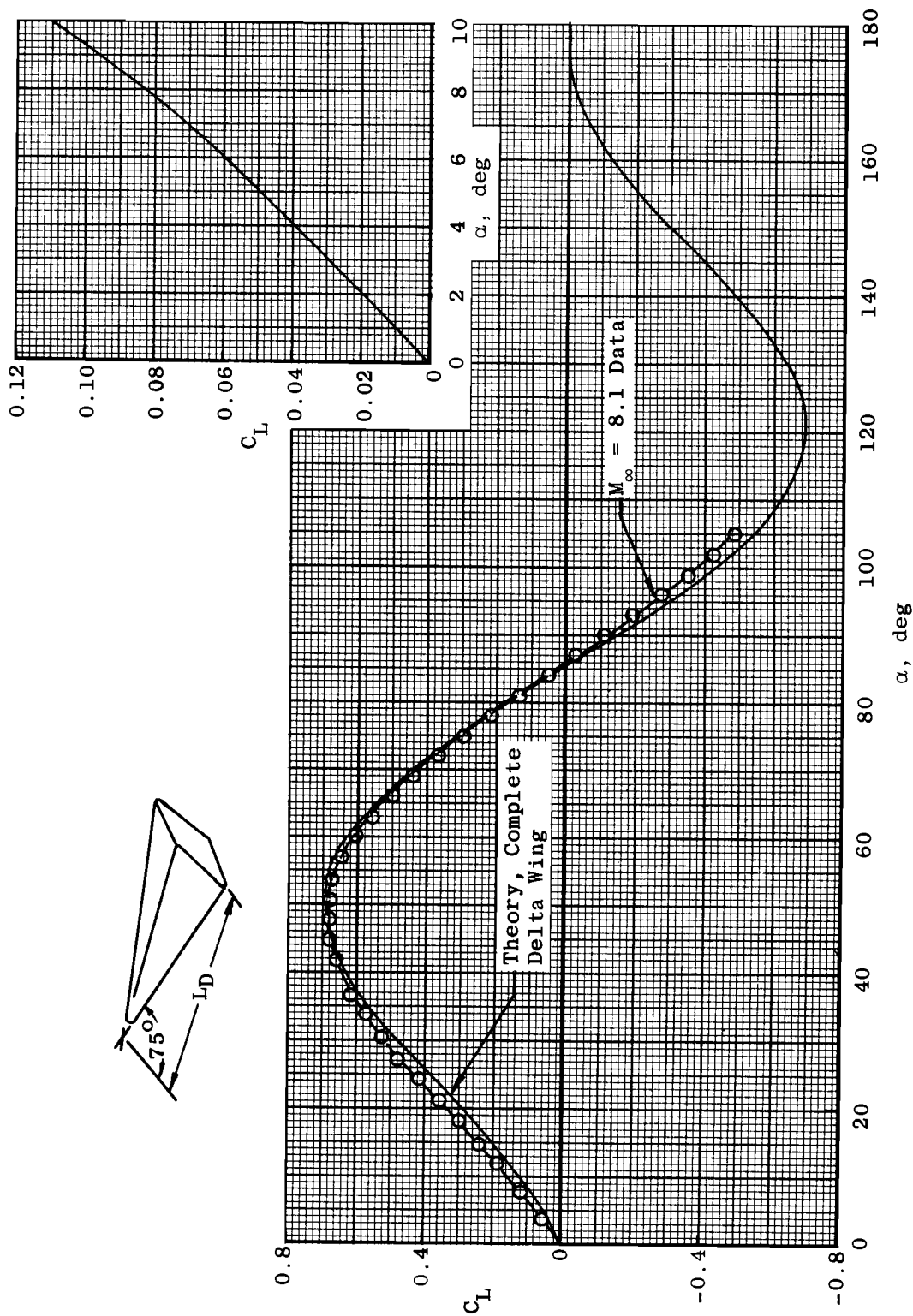


b. Axial Force
Fig. 11 Continued



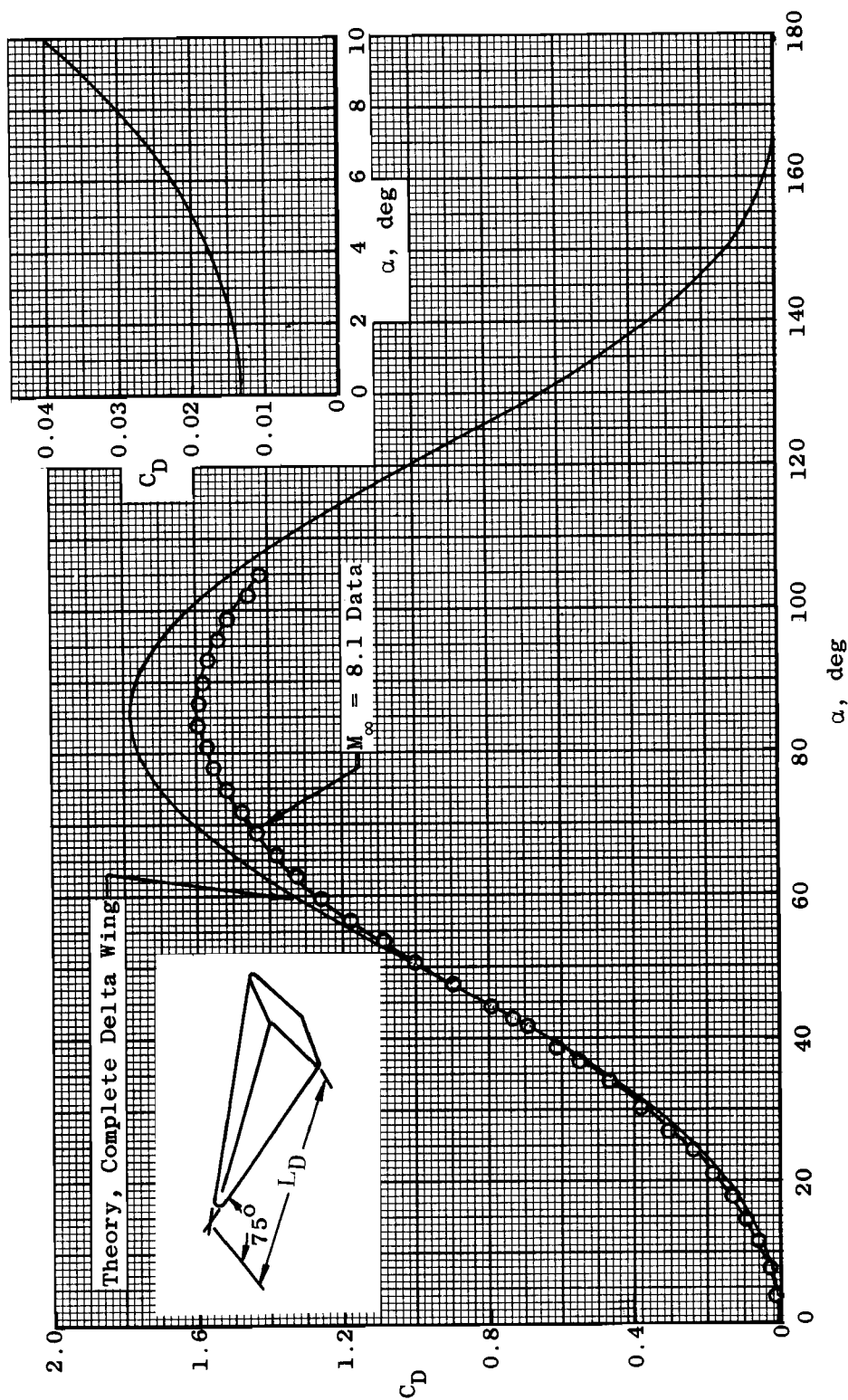
c. Pitching Moment, Referenced to $0.6 L_D$

Fig. 11 Continued



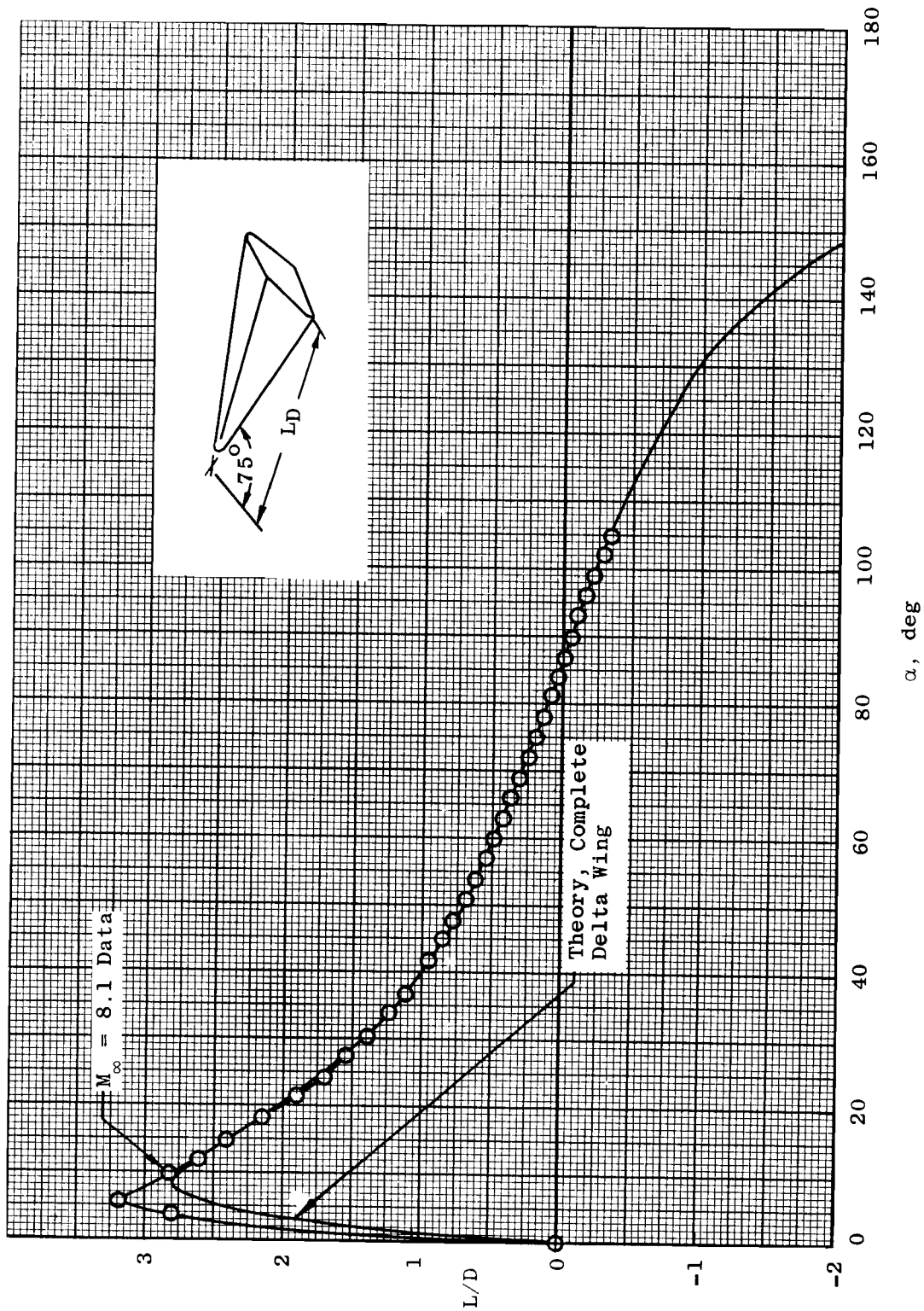
d. Lift

Fig. 11 Continued



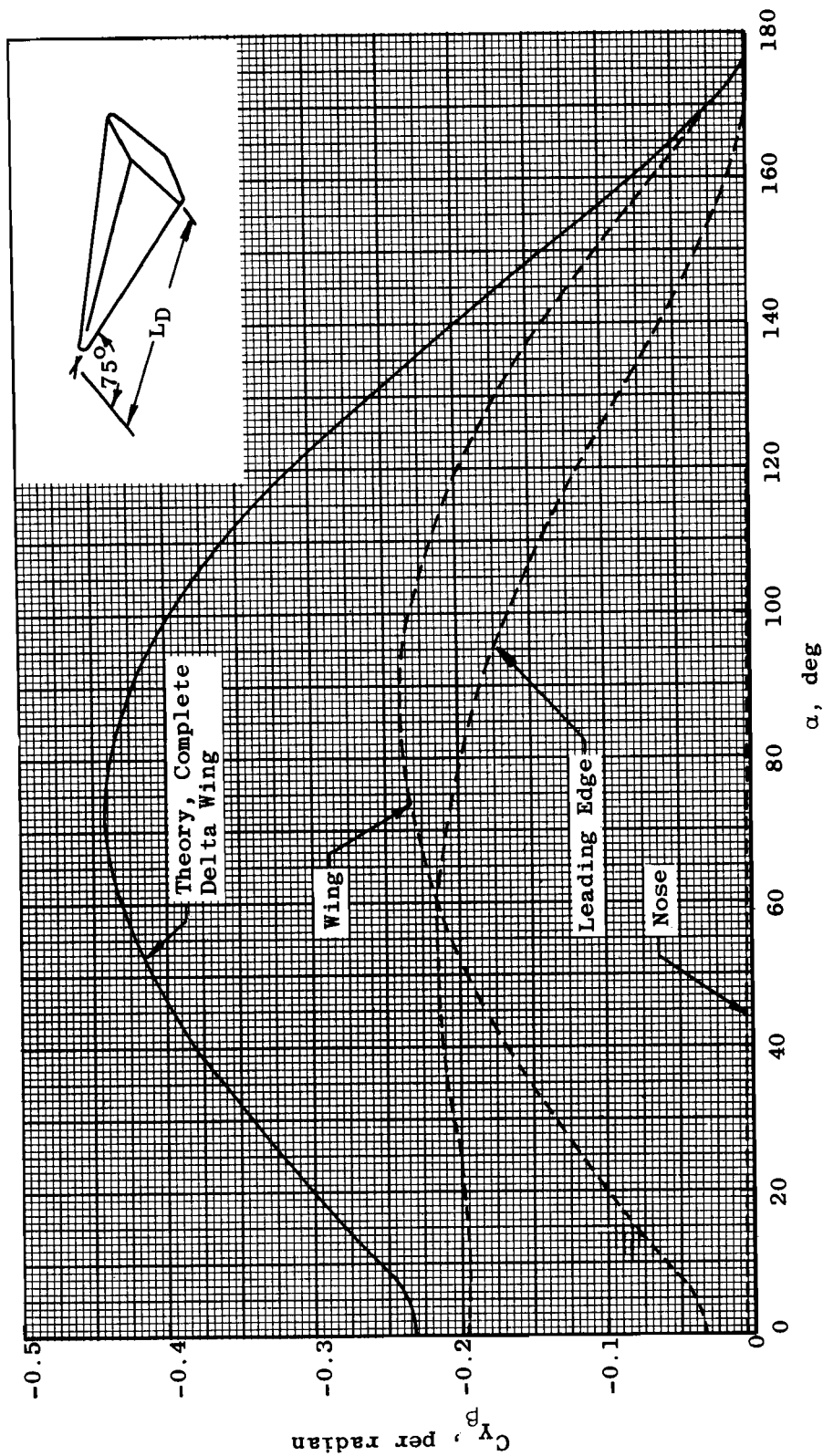
e. Drag

Fig. 11 Continued



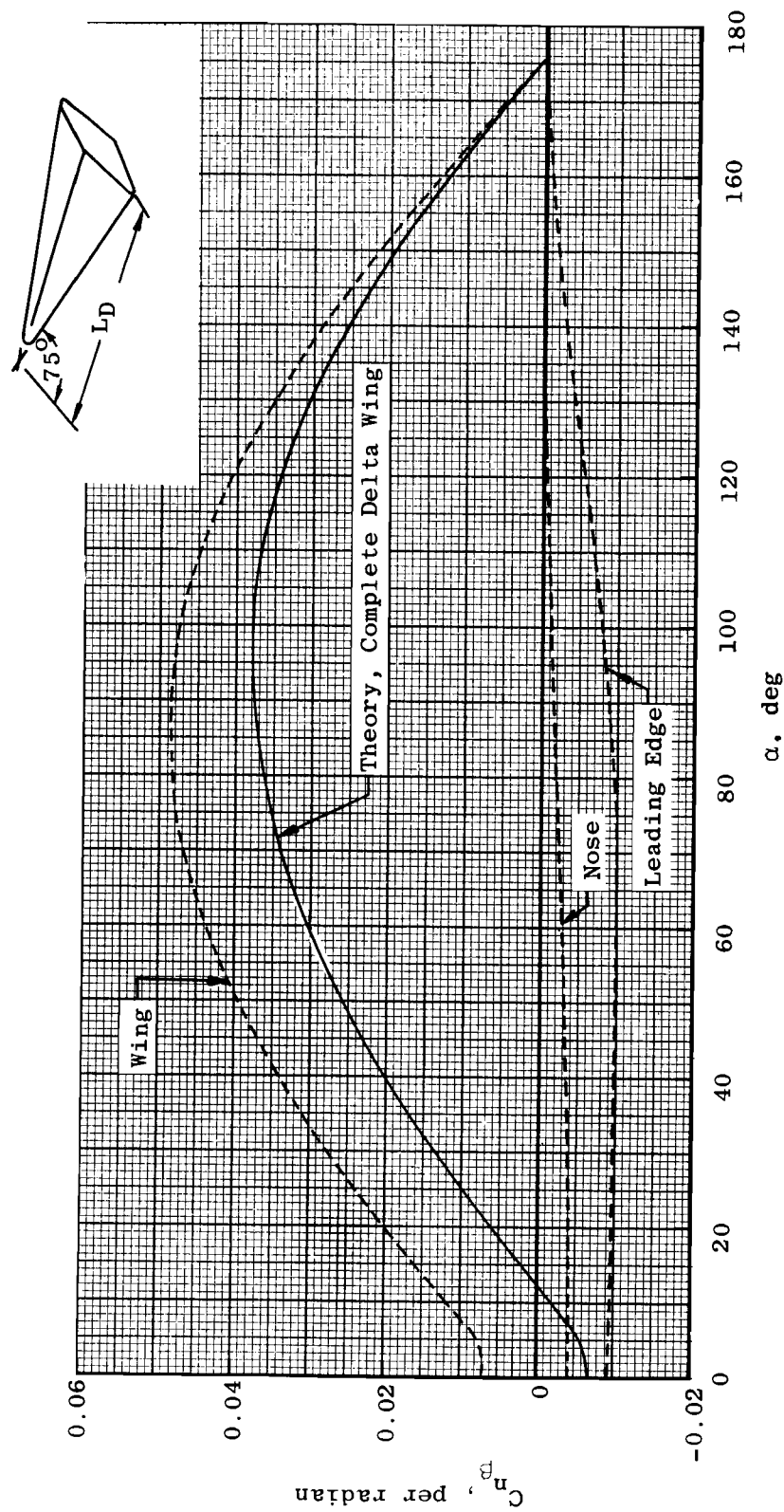
f. Lift-to-Drag Ratio

Fig. 11 Continued



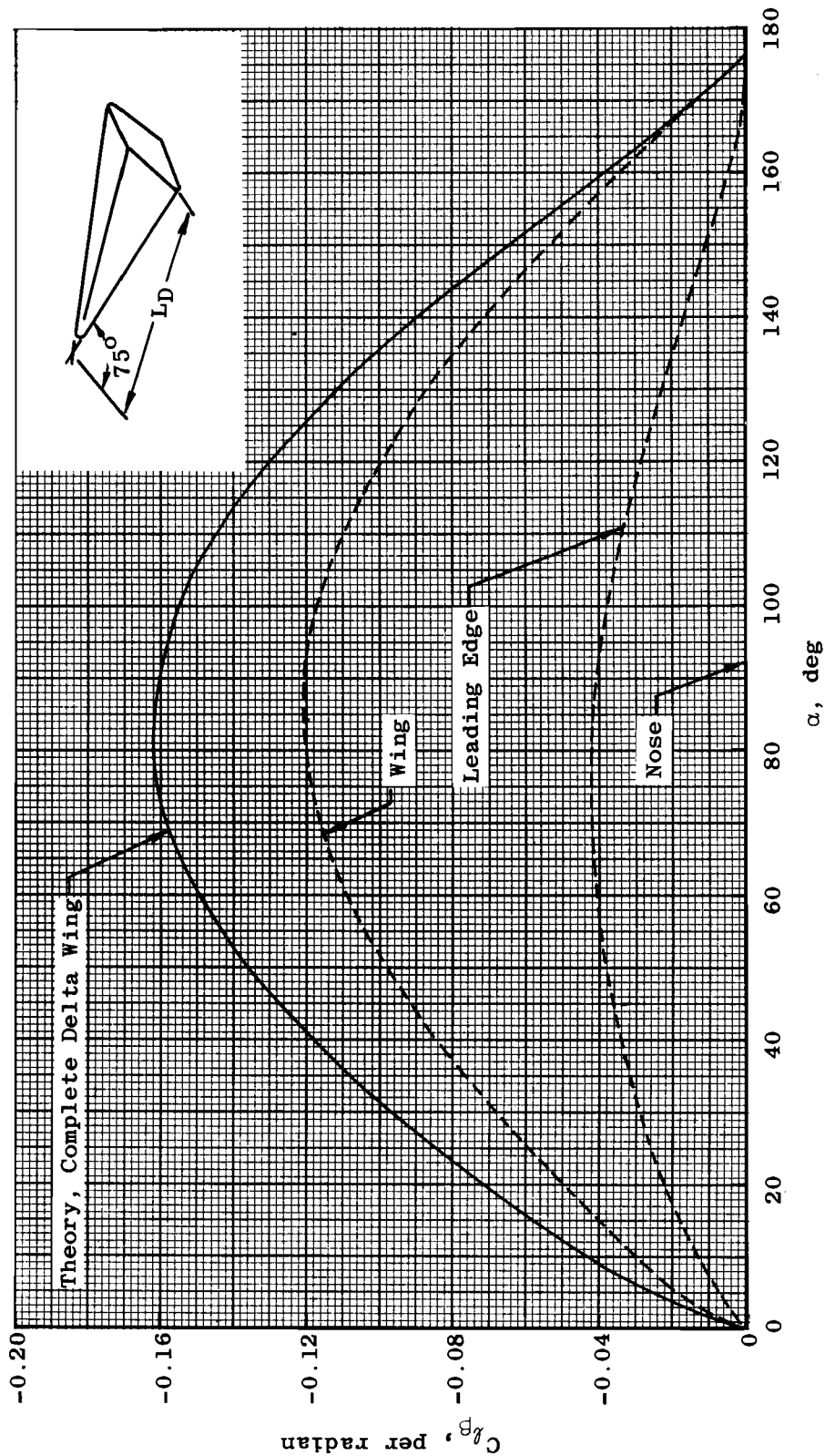
g. Side-Force Derivative, $\beta = 0$

Fig. 11 Continued



h. Yawing-Moment Derivative, $\beta = 0$, Referenced to $0.6 L/D$

Fig. 11 Continued



i. Rolling-Moment Derivative, $\beta = 0$

Fig. 11 Concluded